PART I. EARTHQUAKE SOURCE MODELS, MAGNITUDES AND SCALING RELATIONS

PART II. AMPLITUDES OF ROTATIONALLY SPLIT NORMAL MODES FOR THE 1960 CHILEAN AND 1964 ALASKAN EARTHQUAKES

Thesis by

Robert James Geller

In Partial Fulfillment of the Requirements

for the Degree of

Doctor of Philosophy

California Institute of Technology

Pasadena, California

1977

(Submitted May 17, 1977)

ACKNOWLEDGEMENTS

David G. Harkrider has been a continual source of encouragement and advice, both professionally and personally. As my thesis advisor, he has offered valuable comments at every stage of the preparation of this thesis. His guidance has been extremely helpful in setting the direction of my research.

Hiroo Kanamori has had a profound influence in my development as a geophysicist. I have benefited immensely from our frequent informal discussions. He has encouraged my interest in a broad range of geophysical phenomena, which he has never been too busy to discuss. Chapter 3 of Part I was written jointly with Hiroo, and is in press in the BSSA.

I have been very fortunate to have had Seth Stein as a partner in my work on split normal modes, which comprises Part II of this thesis. Seth and I have shared countless hours of debugging algebra and codes, and puzzling over data. The work in Part II will all be published jointly by Geller and Stein or Stein and Geller.

All of the faculty of the Caltech Seismological Lab have been extremely kind during my stay here. In particular, Don L. Anderson has critically read my papers, answered innumerable questions at "coffee" and "lunch" and encouraged me in my work. Don Helmberger, in his teaching and in informal discussions, gave me a sense of the excitement of working with data. Charles B. Archambeau and Jerry Frazier helped me get started and encouraged me to pursue my own research ideas.

My work has been continually shaped by the atmosphere of informal communication at the Seismo Lab. I am indebted to all of my colleagues at the Lab for their contribution to my development. I especially want to thank, in addition to the people listed above, Yoshio Fukao, Bob Hart, Dan Kosloff, Emile Okal, Kunihiko Shimazaki and Seiya Uyeda.

I have benefited greatly from the critical review of all or part of this thesis by Don L. Anderson, Jerry Frazier, Yoshio Fukao, David G. Harkrider, Don Helmberger, Hiroo Kanamori, Dan Kosloff, Emile Okal, Paul Richards, C. F. Richter, Kunihiko Shimazaki and Seth Stein. Don L. Anderson, Bob Hart and Hiroo Kanamori kindly made their work available prior to publication.

Several friends have made great contributions to my life during the period of this research. Werner Erhard contributed extraordinary value at a time of very rapid personal growth. The support and love of Jonell Polansky were an inspiration throughout this work.

I thank my family for their support, encouragement and love throughout my residence at Caltech.

Marla Turner and Laszlo Lenches did superbly professional typing and drafting work.

At various times during this research I was partially supported by the National Science Foundation under Grants EAR74-22489 and EAR76-14262 and the Advanced Research Projects Agency as monitored by the Air Force Office of Scientific Research under Contracts F44620-72-C-0078 and F44620-77-C-0022.

ABSTRACT

In Part I several fundamental concepts in seismology are examined in detail. The different teleseismic seismic magnitude scales are studied on the basis of Gutenberg and Richter's original notepads. The "revised magnitudes" presented by Richter and Duda are shown to be basically body wave magnitudes which are converted to the surface wave basis. These revised magnitudes are systemically higher (by an average of 0.22) than the magnitudes published by Gutenberg and Richter in Seismicity of the Earth, which are basically surface wave magnitudes. Use of the revised magnitudes has led to substantial over-estimates of the moment of great earthquakes. Fault area, rather than magnitude, should be used for moment estimates when the moment is unavailable.

A dataset of 41 moderate and large earthquakes is used to derive scaling laws relating kinematic fault parameters such as magnitudes, moment and fault dimensions. If effective stress and static stress drop are equal, then fault rise time, τ, and fault area, S, are related by $\tau = 16S^{1/2}/(7\pi^{3/2}\beta)$, where β is shear velocity. Fault length (parallel to strike) and width (parallel to dip) are empirically related by L = 2W. Observed data agree well with the predicted scaling relations. Fault width (i.e. the two dimensionality of faults) must not be neglected. Inclusion of width leads to different average source spectra for surface waves and body waves. The m_b versus M_s relation from this study differs significantly from the Gutenberg-Richter relation, because the Gutenberg-Richter equation was derived for body waves with a predominant period of about 5 sec

and thus does not apply to modern 1 sec m_b determinations. Previous investigators who assumed that the Gutenberg-Richter relation was derived from 1 sec data were in error.

In Part II, the theory necessary to calculate the amplitudes of the earth's rotationally and elliptically split free oscillations is developed. The amplitude of each singlet is explicitly given as the product of factors for fault geometry, seismic moment, source depth, earth structure and the geographic coordinates of the source and receiver. These results are applicable for the synthesis of either spectra or time domain records for which splitting is an important factor.

The splitting of the earth's normal modes was observed for both the 1960 Chilean and 1964 Alaskan earthquakes. The theoretical results for the excitation of singlets are used to predict the relative amplitude of observed split peaks. Good agreement is obtained for thrust fault source models derived from long period surface waves. However, other mechanisms, such as a slow isotropic volume change, are also consistent with the split mode relative amplitudes, and are excluded only by additional data.

The split modes are observed for the 1960 Chilean earthquake by analysis in the time domain. One hundred fifty hours of the Isabella, California strain record are filtered to isolate individual multiplets. Synthetic seismograms with and without splitting are used to confirm the splitting of ${}_0S_2$ and ${}_0S_3$ and to demonstrate the splitting of ${}_0S_4$, ${}_0S_5$, ${}_0T_3$ and ${}_0T_4$. Different techniques for measuring the Q

of split modes are studied. It is concluded that Q determinations from comparison of time domain synthetics to data give much more stability than frequency domain techniques. Uncertainties in the calibration of the instrumental absolute amplitudes rule out a direct determination of the moment of the Chilean earthquake. However, by comparing Isabella records for Chile and Alaska, the long-period moment of the Chilean earthquake is found to be 3.3 times that of the Alaskan event. By using the moment estimated for Alaska from long period surface waves, the moment of the Chilean earthquake is estimated to be 2.4×10^{30} dyne cm.

TABLE OF CONTENTS

PART I.

EARTHQUAKE SOURCE MODELS, MAGNITUDES AND SCALING RELATIONS

Chapter 1

INTRODUCTION

The first fundamental understanding of earthquake sources was achieved by Reid (1910) after the 1906 San Francisco earthquake. Reid realized that the dislocation along a fault could be considered as an "elastic rebound." The earth, which had been subjected to a strain by some tectonic forces, released that strain by slipping at a preexisting zone of weakness. The elastic rebound theory, and the recognition of the fundamental role of faults, allowed the first real understanding of the earthquake process.

Despite the early recognition of faulting, a long controversy persisted about the physical and mathematical nature of the earthquake source. It was proposed that earthquake sources could be modeled as single couples, double couples or "cone-type" mechanisms. The "cone-type" mechanism (equivalent to the compensated linear vector dipole) fell into disfavor, as it was recognized that the observed P wave first motions for well-constrained events always had a quadrantal distribution. However, the couple and double couple both have quadrantal P wave radiation patterns. Honda (1962) presented conclusive evidence for the double couple mechanism by studying S wave polarization angles.

In recent years, the "cone-type" mechanism was revived by Knopoff and Randall (1970). Gilbert (1970) presented a general formalism, the moment tensor, which can represent double couples, "cone-type" mechanisms and explosions.

The elucidation of the mechanism of earthquakes is one of the most important fundamental problems in seismology. Another equally important problem is the specification of the "size" of an earthquake. Ideally we wish to describe the "size" in terms of energy, or some other fundamental physical quantity. However, in practice the simplest measurements involve the amplitude and period of various body and surface wave phases, which may then be converted into a magnitude on the scales defined by Gutenberg and Richter. Several different magnitude scales exist, and although earthquake "magnitudes" may be given on any of several different scales, frequently the description of which scale was used is lacking. As is shown in Chapter 2, serious errors can result when Richter's (1958) "revised magnitudes," which are basically body wave magnitudes converted to the surface wave basis, are treated as surface wave magnitudes. For example, large overestimates of seismic strain release, have been caused by using the revised magnitudes to obtain moment estimates.

Magnitude is one parameter describing the "size" of an earthquake, but is not directly related to physical dimensions such as fault length, rise time, etc. A class of scaling relations has been developed to relate the magnitude, which is assumed to be related to a particular part of the seismic source spectrum, to physical fault

parameters. The classic example of scaling relations is the work of Aki (1967).

Scaling relations are presented in Chapter 3 which differ from Aki's in two important ways. 1) Aki (1967) did not consider the effect of fault width (i.e. the two dimensionality of faults), while this is included in the present model. 2) Aki constrained his model to fit Gutenberg and Richter's $m_b - M_s$ relation, and assumed that the m_b was measured at a period of 1 sec. However, because it is shown in Chapter 2 that Gutenberg and Richter actually measured m_b at a period of about 6-12 sec, Aki's assumption was inappropriate.

The scaling relations in Chapter 3 fit a variety of data, including $m_b - M_s$, $\log M_o - M_s$, $\log S - M_s$ and spectral ratios of similar events. Major conclusions are 1) There are upper limits on m_b and M_s caused by the saturation of the source spectrum. 2) The inclusion of width leads to different average spectra for teleseismic surface and body waves.

REFERENCES

Aki, K. (1967). Scaling law of seismic spectrum, J. Geophys. Res., 72, 1217-1231.

Gilbert, F. (1970). Excitation of the normal modes of the Earth by earthquake sources, Geophys. J., 22, 223-226.

Honda, H. (1962). Earthquake mechanism and seismic waves, Geophysical notes (supplement), Geophysical Institute, Faculty of Science, Tokyo University, Tokyo, Japan, 15, 1-97.

Knopoff, L. and M. J. Randall (1970). The compensated linear vector dipole: a possible mechanism for deep earthquakes, J. Geophys. Res., 75, 4957-4963.

Reid, H. F. (1910). The mechanics of the earthquake, The California Earthquake of April 18, 1906, Report of the State Investigation Commission, Vol. 2, Carnegie Institution, Washington, D. C.

Richter, C. F. (1958). Elementary Seismology, W. H. Freeman, San Francisco.

Chapter 2

MAGNITUDES OF GREAT SHALLOW EARTHQUAKES FROM 1904 TO 1952

ABSTRACT

The "revised magnitudes", M, converted from Gutenberg's unified magnitude, m, and listed by Richter (1958) and Duda (1965) are systematically higher than the magnitudes listed by Gutenberg and Richter (1954) in Seismicity of the Earth. This difference is examined on the basis of Gutenberg and Richter's unpublished original worksheets for Seismicity of the Earth. It is concluded that (1) the magnitudes of most shallow "class a" earthquakes in Seismicity of the Earth are essentially equivalent to the 20 sec surface-wave magnitude, M_s; (2) the revised magnitudes, M, of most great shallow (less than 40 km) earthquakes listed in Richter (1958) (also used in Duda, 1965) heavily emphasize body-wave magnitudes, m_b, and are given by $M = \frac{1}{4} M_s + \frac{3}{4} \cdot (1.59\ m_b - 3.97)$. For earthquakes at depths of 40-60 km, M is given by $M = (1.59\ m_b - 3.97)$. M and M_s are thus distinct and should not be confused. Because of the saturation of the surface-wave magnitude scale at $M_s \simeq 8.0$, use of empirical moment vs. magnitude relations for estimating the seismic moment results in large errors. Use of the fault area, S, is suggested for estimating the moment.

INTRODUCTION

In spite of its imperfections, magnitude is still the most commonly used parameter in describing the size of an earthquake. However, one frequently hears references to "the" magnitude of an earthquake without any specification of which scale is being used. Actually there are many different magnitude scales, and a magnitude is much less useful if it is not accompanied by a description of how it was determined.

The proliferation of magnitude scales is particularly insidious because sometimes two different magnitude scales have the same name. For example, the teleseismic body wave magnitude, m_b, was determined from broad band instruments by Gutenberg and Richter, but currently is determined from short-period, narrow-band, WWSSN instruments by the USGS. Thus there really are two completely different scales for teleseismic body-wave magnitudes, one for periods of about 6 to 12 sec and another for periods of 1 sec, but they go by the same name, in spite of their radically different characteristics.

The present state of knowledge of the background of the magnitude scales seems to warrant a re-examination of the magnitude scales for body waves, m_b, and for surface waves, M_s, both as developed by Gutenberg and Richter and as defined in modern practice. M_s is particularly worth examining because M_s values have been used with various empirical relations to estimate the energy and the seismic moment of earthquakes. Earthquake energy and seismic moment are important in the discussion of various global problems, such as heat flow, the Chandler Wobble and plate motion. For earthquakes from 1904 to 1952,

three magnitude catalogs are most commonly used: Gutenberg and Richter (1954), Richter (1958) and Duda (1965). However, there are significant differences between the magnitude values listed in these catalogs. In view of the fundamental importance of the earthquake magnitude in various geophysical problems, we examine these differences and the meaning of the magnitude scale adopted in each of these catalogs.

MAGNITUDE SCALES

The magnitude of an earthquake was the first source parameter to be defined and is still the most directly measurable. As originally defined by Richter (1935), magnitudes for local earthquakes, M_L, were calculated from amplitudes on Wood-Anderson torsion instruments. Gutenberg and Richter (1936, 1941, 1942) published several intermediate reports on amplitudes and magnitudes. Gutenberg (1945a, b, c) defined surface wave magnitudes, M_s, and body wave magnitudes, m_b. The final versions of the body wave and surface wave scales were given by Gutenberg and Richter (1956). The details of Gutenberg and Richter's body-wave and surface-wave magnitudes, as well as later definitions, are discussed in the Appendix to this chapter.

Although M_s and m_b are measured at different periods, Gutenberg and Richter viewed M_s and m_b as parameters representing the same quantity, namely energy (Gutenberg, 1945c). This view led Gutenberg and Richter (1956) and Gutenberg (1957) to the concept of "unified magnitude." To facilitate the construction of a "unified magnitude" scale, they obtained empirical relations between m_b and M_s:

$$m_b = 0.63\ M_s + 2.5 \tag{2.1a}$$

$$M_s = 1.59\ m_b - 3.97. \tag{2.1b}$$

These relations were then used to define the body-wave basis and surface-wave basis for magnitudes. Magnitudes are converted by using the relations

$$m(M) = 0.63\ M + 2.5 \tag{2.2a}$$

$$M(m) = 1.59\ m - 3.97 \tag{2.2b}$$

where M is a magnitude on the surface-wave basis and m(M) is the corresponding magnitude on the body-wave basis. Similarly, if m is a magnitude on the body-wave basis then M(m) is the computed magnitude on the surface-wave basis. $m_s \equiv m(M_s)$ is the magnitude on the body-wave basis calculated from the observed surface-wave magnitude, M_s. Also $M_b \equiv M(m_b)$ is the magnitude on the surface-wave basis calculated from the observed body-wave magnitude.

The unified magnitude, m, was obtained by taking a weighted average of m_b and m_s (Gutenberg and Richter, 1956 ; Gutenberg, 1957)

$$m = \alpha m_b + \beta m_s \tag{2.3}$$

with $\alpha + \beta = 1$. It is equally possible to define the unified magnitude on the surface-wave basis:

$$M = \alpha M_b + \beta M_s \tag{2.4}$$

Richter prefers this to m. In his book (Richter, 1958), he converted

Gutenberg's unified magnitudes, m, to M by using equation (2.2b). (As a result of roundoff the M values differ slightly from those obtained directly from equation (2.4).)

GREAT EARTHQUAKE MAGNITUDES FROM 1904 TO 1952

Four primary data sets for magnitudes of large shallow earthquakes from 1904 to 1952 are displayed in Table 2.1. Gutenberg and Richter (1954) listed all of the 109 events (in Table 2.1) in their Table 13, "class a shallow shocks." (Their Table 13 contained events having $M \geq 7.75$.) The earthquake locations and origin times are also from Gutenberg and Richter. Richter (1958) listed "revised magnitudes" for the class a shocks with magnitudes greater than 7 3/4 in his Table XIV-2. Duda (1965) listed magnitudes for all of the events in Table 2.1. Each of these references lists "magnitudes" without any description of the scales used to derive them. The revised magnitudes denoted by M given by Richter (1958) are on the average 0.22 higher than the magnitudes in Seismicity of the Earth. The largest difference is 0.6. The magnitudes listed by Duda (1965) are taken from Richter's catalog if an event is listed there - otherwise the value from Seismicity of the Earth is used. Thus the differences between Duda's magnitudes and the Gutenberg-Richter (G-R) catalog reflect only the differences between Richter's catalog and the G-R values. We will explore the difference between the Richter (1958) magnitudes and the G-R (1954) magnitudes, to clarify the differences between the magnitude scales.

The best source of data for reexamining the magnitudes is the

TABLE 2.1 EARTHQUAKE DATA

NO.	DATE	TIME	LOCATION	Published Magnitudes			Gutenberg-Richter		Notes
				SEIS. OF EARTH (1954)	DUDA (1965)	RICHTER (1958)	M_s	m_b	$\overline{T}$
1	1904, Jan. 20	14:52.1	7 N 79 W	7 3/4	7.9	7.9	7.7	7.6	12
2	June 25	14:45.6	52 N 159 E	8.0	8.3	8.3	7.9	7.8	8
3	June 25	21:00.5	52 N 159 E	8.1	8.1	8.1	8.0	7.7	6
4	June 27	00:09.0	52 N 159 E	7.9	7.9	7.9	7.9	7.5	7
5	Aug. 24	20:59.9	30 N 130 E	7 3/4	7.9	7.9	7.7	7.7	9
6	Aug. 27	21:56.1	64 N 151 W	7 3/4	8.3	8.3	7.7	7.8	7
7	Dec. 20*	05:44.3	8 1/2 N 83 W	7 3/4	8.3	8.3	7.6	7.8	11
8	1905, Feb. 14	08:46.6	53 N 178 W	7 3/4	7.9	7.9	7.9	7.5	12
9	April 4	00:50.0	33 N 76 E	8	8.6	8.6	---	---	--
10	July 6	16:21.0	39 1/2 N 142 1/2 E	7 3/4	7.9	7.9	7.8	7.5	--
11	July 9	09:40.4	49 N 99 E	8 1/4	8.4	8.4	7.9(1)	---	--
12	July 23	02:46.2	49 N 98 E	8 1/4	8.7	8.7	8.2(1)	---	--
13	1906, Jan. 31	15:36.0	1 N 81 1/2 W	8.6	8.9	8.9	8.7	8.2	9
14	April 18	13:12.0	38 N 123 W	8 1/4	8.3	8.3	8.3	7.4	13
15	Aug. 17	00:10.7	51 N 179 E	8.0	8.3	8.3	8.2	7.8	7

TABLE 2.1 EARTHQUAKE DATA (Cont'd)

NO.	DATE	TIME	LOCATION	Published Magnitudes SEIS. OF EARTH (1954)	DUDA (1965)	RICHTER (1958)	Gutenberg-Richter Notes M_s	m_b	$\overline{T}$
16	Aug. 17	00:40.0	33 S 72 W	8.4	8.6	8.6	8.4	---	--
17	Sept. 14	16:04.3	7 S 149 E	8.1	8.4	8.4	---	---	--
18	Nov. 19*	07:18.3	22 S 109 E	7 3/4	7 3/4	---	7.5	7.5	10
19	Dec. 22	18:21.0	43 1/2 N 85 E	7.9	8.3	8.3	7.7	7.5	9
20	1907, April 15	06:08.1	17 N 100 W	8.1	8.3	8.3	8.0	7.9	14
21	Sept. 2	16:01.5	52 N 173 E	7 3/4	7 3/4	---	7.8	7.3	13
22	Oct. 21	04:23.6	38 N 69 E	8.0	8.1	8.1	7.6	7.6	11
23	1909, July 30*	10:51.9	17 N 100 1/2 W	7 3/4	7 3/4	---	7.4	7.4	10
24	1911, Jan. 3	23:25:45	43 1/2 N 77 1/2 E	8.4	8.7	8.7	8.4	8.1	14
25	Feb. 18	18:41:03	40 N 73 E	7 3/4	7 3/4	---	7.6	7.3	8
26	June 7*	11:02.7	17 1/2 N 102 1/2 W	7 3/4	7.9	7.9	7.7	7.5	8
27	July 12*	04:07.6	9 N 126 E	7 3/4	7 3/4	---	7.7	7.6	8
28	Aug. 16	22:41.3	7 N 137 E	7.9	8.1	8.1	7.8	7.6	9
29	1912, May 23	02:24.1	21 N 97 E	8.0	7.9	7.9	8.0	7.3	13
30	Aug. 9	01:29.0	40 1/2 N 27 E	7 3/4	7 3/4	---	7.7	7.0	10

TABLE 2.1 EARTHQUAKE DATA (Cont'd)

NO.	DATE	TIME	LOCATION	Published Magnitudes			Gutenberg-Richter Notes		
				SEIS. OF EARTH (1954)	DUDA (1965)	RICHTER (1958)	M_s	m_b	$\overline{T}$
31	1913, Mar. 14*	08:45:00	4 1/2 N 126 1/2 E	7.9	8.3	8.3	7.9	7.7	4
32	1913, Aug. 6	22:14.4	17 S 74 W	7 3/4	7.9	7.9	---	---	--
33	1914, May 26	14:22.7	2 S 137 E	7.9	7.9	---	8.0	7.3	6
34	1915, May 1	05:00:0	47 N 155 E	7.9	8.1	8.1	8.0	7.7	11
35	July 31	01:31.4	54 N 162 E	7 3/4	7 3/4	---	7.6	7.5	7
36	Oct. 3	06:52.8	40 1/2 N 117 1/2 W	7 3/4	7 3/4	---	7.7	7.3	7
37	1916, Jan. 1	13:20.6	4 S 154 E	7 3/4	7.9	7.9	---	---	--
38	Jan. 13	08:20.8	3 S 135 1/2 E	7.8	8.1	8.1	7.7	7.6	7
39	1917, Jan. 30	02:45.6	56 1/2 N 163 E	7 3/4	8.1	8.1	7.8	7.7	9
40	May 1*	18:26.5	29 S 177 W	8	8.6	8.6	7.9	7.9	8
41	June 26	05:49.7	15 1/2 S 173 W	8.3	8.7	8.7	8.4	8.0	11
42	1918, Aug. 15	12:18.2	5 1/2 N 123 E	8 1/4	8.3	8.3	8.0	7.6	7
43	Sept. 7	17:16:13	45 1/2 N 151 1/2 E	8 1/4	8.3	8.3	---	---	--
44	Nov. 8	04:38.0	44 1/2 N 151 1/2 E	7 3/4	7.9	7.9	7.7	7.5	6
45	Dec. 4*	11:47.8	26 S 71 W	7 3/4	7 3/4	---	7.6	7.3	9

TABLE 2.1 EARTHQUAKE DATA (Cont'd)

NO.	DATE	TIME	LOCATION	Published Magnitudes SEIS. OF EARTH (1954)	DUDA (1965)	RICHTER (1958)	Gutenberg-Richter Notes M_s	m_b	$\overline{T}$
46	1919, April 30	07:17:05	19 S 172 1/2 W	8.3	8.4	8.4	---	---	--
47	May 6	19:41:12	5 S 154 E	7.9	8.1	8.1	---	---	--
48	1920, June 5	04:21:28	23 1/2 N 122 E	8	8.3	8.3	---	---	--
49	Sept. 20	14:39:00	20 S 168 E	8	8.3	8.3	7.9	7.8	7
50	Dec. 16	12:05:48	36 N 105 E	8 1/2	8.6	8.6	---	---	--
51	1922, Nov. 11	04:32.6	28 1/2 S 70 W	8.3	8.4	8.4	---	---	--
52	1923, Feb. 3	16:01:41	54 N 161 E	8.3	8.4	8.4	8.3	7.7	7
53	Sept. 1	02:58:36	35 1/4 N 139 1/2 E	8.2	8.3	8.3	8.2 (2)	7.7	--
54	1924, April 14	16:20:23	6 1/2 N 126 1/2 E	8.3	8.3	8.3	8.3	7.7	5
55	* June 26	01:37:34	56 S 157 1/2 E	7.8	8.3	8.3	7.7	7.9	8
56	1927, March 7	09:27:36	35 3/4 N 134 3/4 E	7 3/4	7.9	7.9	7.6	7.6	4
57	May 22	22:32:42	36 3/4 N 102 E	8.0	8.3	8.3	7.9	7.9	7
58	1928, June 17	03:19:27	16 1/4 N 98 W	7.8	7.9	7.9	7.8	7.6	9
59	Dec. 1	04:06:10	35 S 72 W	8.0	8.3	8.3	8.0	7.7	8
60	1929, March 7	01:34:39	51 N 170 W	8.1	8.6	8.6	7.7 (3)	7.7 (3)	9 (3)

TABLE 2.1 EARTHQUAKE DATA (Cont'd)

NO.	DATE	TIME	LOCATION	Published Magnitudes			Gutenberg-Richter Notes		
				SEIS. OF EARTH (1954)	DUDA (1965)	RICHTER (1958)	M_s	m_b	$\overline{T}$
61	June 27	12:47:05	54 S 29 1/2 W	7.8	8.3	8.3	---	---	--
62	1931, Jan. 15	01:50:41	16 N 96 3/4 W	7.8	7.9	7.9	7.8	7.6	13
63	Feb. 2	22:46:42	39 1/2 S 177 E	7 3/4	7.9	7.9	7.8	7.6	10
64	Aug. 10	21:18:40	47 N 90 E	8.0	7.9	7.9	7.9	7.6	9
65	1931, Oct. 3	19:13:13	10 1/2 S 161 3/4 E	7.9	8.1	8.1	7.9	7.7	7
66	1932, May 14	13:11:00	1/2 N 126 E	8.0	8.3	8.3	8.0	7.8	13
67	June 3	10:36:50	19 1/2 N 104 1/4 W	8.1	8.1	8.1	8.2	7.6	12
68	June 18	10:12:10	19 1/2 N 103 1/2 W	7.8	7.9	7.9	7.8	7.4	11
69	1933, March 2	17:30:54	39 1/4 N 144 1/2 E	8.5	8.9	8.9	$8.3^{(4)}$	$8.2^{(4)}$	$11^{(4)}$
70	1934, Jan. 15	08:43:18	26 1/2 N 86 1/2 E	8.3	8.4	8.4	8.3	7.8	10
71	July 18	19:40:15	11 3/4 S 166 1/2 E	8.2	8.1	8.1	8.1	6.8	10
72	1935, Sept. 20	01:46:33	3 1/2 S 141 3/4 E	7.9	7.9	7.9	---	---	--
73	Dec. 28	02:35:22	0 N 98 1/4 E	7.9	8.1	8.1	7.7	7.7	8
74	1938, Feb. 1	19:04:18	5 1/4 S 130 1/2 E	8.2	8.6	8.6	8.2	8.0	6
75	Nov. 10	20:18:43	55 1/2 N 158 W	8.3	8.7	8.7	8.3	8.2	13

TABLE 2.1 EARTHQUAKE DATA (Cont'd)

NO.	DATE	TIME	LOCATION	Published Magnitudes			Gutenberg-Richter Notes		
				SEIS. OF EARTH (1954)	DUDA (1965)	RICHTER (1958)	M_s	m_b	$\overline{T}$
76	1939, Jan. 25	03:32:14	36 1/4 S 72 1/4 W	7 3/4	8.3	8.3	---	---	--
77	Jan. 30	02:18:27	6 1/2 S 155 1/2 E	7.8	7.9	7.9	7.8	---	--
78	April 30*	02:55:30	10 1/2 S 158 1/2 E	8.0	8.1	8.1	8.0	7.4	7
79	Dec. 26	23:57:21	39 1/2 N 38 1/2 E	8.0	7.9	7.9	7.8	7.7	8
80	1940, May 24*	16:33:57	10 1/2 S 77 W	8	8.4	8.4	7.9	7.9	8
81	1941, June 26*	11:52:03	12 1/2 N 92 1/2 E	8.1	8.7	8.7	7.7	8.0	8
82	Nov. 18	16:46:22	32 N 132 E	7.8	7.9	7.9	7.8	7.5	8
83	Nov. 25	18:03:55	37 1/2 N 18 1/2 W	8.3	8.4	8.4	8.2	7.8	8
84	1942, May 14	02:13:18	3/4 S 81 1/2 W	7.9	8.3	8.3	7.9	7.7	8
85	Aug. 6*	23:36:59	14 N 91 W	7.9	8.3	8.3	7.9	7.7	5
86	Aug. 24*	22:50:27	15 S 76 W	8.1	8.6	8.6	8.2	7.9	11
87	Nov. 10	11:41:27	49 1/2 S 32 E	7.9	8.3	8.3	7.9	7.7	11
88	1943, April 6*	16:07:15	30 3/4 S 72 W	7.9	8.3	8.3	7.9	7.6	9
89	May 25	23:07:36	7 1/2 N 128 E	7.9	8.1	8.1	7.7	7.8	7
90	July 29	03:02:16	19 1/4 N 67 1/2 W	7 3/4	7.9	7.9	7.7	7.5	8

TABLE 2.1 EARTHQUAKE DATA (Cont'd)

NO.	DATE	TIME	LOCATION	Published Magnitudes			Gutenberg-Richter Notes		
				SEIS. OF EARTH (1954)	DUDA (1965)	RICHTER (1958)	M_s	m_b	$\overline{T}$
91	Sept. 6	03:41:30	53 S 159 E	7.8	7.9	7.9	7.7	7.5	11
92	1944, Dec. 7	04:35:42	33 3/4 N 136 E	8.0	8.3	8.3	8.0	7.8	15
93	1945, Nov. 27	21:56:50	24 1/2 N 63 E	8 1/4	8.3	8.3	8.0	7.7	9
94	Dec. 28	17:48:45	6 S 150 E	7.8	7.8	---	7.7	7.3	9
95	1946, Aug. 4	17:51:05	19 1/4 N 69 W	8.1	8.1	8.1	8.0	7.6	10
96	Sept. 12	15:20:20	23 1/2 N 96 E	7 3/4	7 3/4	---	7.8	7.4	8
97	Sept. 29	03:01:55	4 1/2 S 153 1/2 E	7 3/4	7 3/4	---	7.7	7.4	8
98	Dec. 20	19:19:05	32 1/2 N 134 1/2 E	8.2	8.4	8.4	8.2	7.8	9
99	1948, Jan. 24	17:46:40	10 1/2 N 122 E	8.2	8.3	8.3	8.2	7.7	13
100	Sept. 8	15:09:11	21 S 174 W	7.8	7.9	7.9	7.8	7.5	6
101	1949, Aug. 22	04:01:11	53 3/4 N 133 1/4 W	8.1	8.1	8.1	8.1	7.5	8
102	Dec. 17	06:53:30	54 S 71 W	7 3/4	7 3/4	---	7.7	7.4	7
103	Dec. 17	15:07:55	54 S 71 W	7 3/4	7 3/4	---	7.7	7.4	6
104	1950, Aug. 15	14:09:30	28 1/2 N 96 1/2 E	8.6	8.7	8.7	8.6	8.0	9
105	Dec. 2*	19:51:49	18 1/4 S 167 1/2 E	7 3/4	8.1	8.1	7.2	7.6	7

TABLE 2.1 EARTHQUAKE DATA (Cont'd)

NO.	DATE	TIME	LOCATION	Published Magnitudes SEIS. OF EARTH (1954)	DUDA (1965)	RICHTER (1958)	Gutenberg-Richter Notes M_s	m_b	$\overline{T}$
106	1951, Nov. 18	09:35:47	30 1/2 N 91 E	8.0	7.9	7.9	8.0	7.3	10
107	1952, Mar. 4	01:22:43	42 1/2 N 143 E	8.3	8.6	8.6	8.3	8.0	9
108	Mar. 19	10:57:12	9 1/2 N 127 1/4 E	7 3/4	7.9	7.9	7.6	7.6	8
109	Nov. 4	16:58:26	52 3/4 N 159 1/2 E	8 1/4	8.4	8.4	8.2	7.9	8

(1) Okal (1977).

(2) Kanamori and Miyamura (1970)

(3) Kanamori (1972).

(4) Kanamori (1971)

*Hypocentral depth 40 - 60 km

original work of Gutenberg and Richter. Fortunately, most of their original worksheets for Seismicity of the Earth are still on file at Caltech. We found copies of their worksheets for 91 of the 109 events in Table 2.1. The surface-wave magnitudes (M_s) for these 91 events (and five others, from other sources) are listed in Table 2.1. (Sources for the other five events are given in footnotes.) The surface wave magnitudes were derived from the worksheets in a straightforward manner. Gutenberg and Richter's original single station M_s (often labeled M_{max}, for maximum amplitude, on their worksheets) values were numerically averaged for each event. On the whole, the surface-wave magnitudes from the notes differ only slightly from those in the Gutenberg-Richter catalog.

Magnitudes in Seismicity of the Earth were given to the nearest tenth when Gutenberg and Richter considered the value accurate to the nearest tenth, e.g. 8.0, 7.7; values which they considered to be less accurate are given only the the nearest quarter, e.g. 8, $7\frac{3}{4}$. The magnitudes in Seismicity of the Earth are an average of 0.06 higher than those from the notepads. Furthermore, the magnitudes of 74 of the 96 events differ by 0.1 or less. We therefore conclude that the magnitudes in Seismicity of the Earth are essentially equivalent to M_s for the events we have checked. Probably for nearly all the shallow events in the G-R catalog it is safe to treat their "magnitude" as being M_s.

We also obtained body-wave magnitudes from the notes. Because there were several different definitions of the body-wave magnitude, many of the worksheets have several different calculations in which a

body-wave magnitude is given. We list in Table 2.1 the value which appeared to us to be calculated according to the method in Gutenberg and Richter (1956). Although in some cases the value we have listed may be slightly in error, it seems important to list these previously unpublished m_b values. m_b values were given in the worksheets for 90 events, and are listed in Table 2.1, together with two from other sources. Apparently the station corrections given by Gutenberg (1945c) were used in making these m_b determinations.

Two other items are listed in Table 2.1. $\overline{T}$ is the average period used in determination of m_b from equation (2.15). Also, Gutenberg and Richter considered most of the events in Table 2.1 to be at normal depth, but some earthquakes were considered to be at depths of 40-60 km. The deeper events are indicated by an asterisk to the right of the date.

UNIFIED MAGNITUDES

Gutenberg and Richter never published the details of their methods of determining the unified magnitudes. However, Gutenberg (1957) stated that the unified magnitude was found primarily from body-wave magnitudes, with only supplemental use of surface-wave magnitudes. This suggests that m_b was emphasized in the weighted average of m_b and m_s to find m described by Gutenberg and Richter (1956). Our analysis, described below, supports this suggestion.

A preliminary examination of the data in Table 2.1 suggested that in most cases the weights used by Gutenberg and Richter in finding the

unified magnitudes were $\alpha = \frac{3}{4}$ and $\beta = \frac{1}{4}$ (in equations 2.3 and 2.4). In finding m they apparently used the magnitudes in Seismicity of the Earth as M_s. Therefore we have used the magnitudes from Seismicity of the Earth, rather than the M_s values we list in Table 2.1, in testing these weights. Also, for the deeper events (40-60 km) in Table 2.1 the weights apparently are $\alpha = 1$ and $\beta = 0$, i.e. only the body-wave magnitude was used in finding the unified magnitude of these events.

We have the m_b values from the worksheets for 77 events for which Richter (1958) gives a revised magnitude. Of these, 66 are at normal depth and 11 at depths of 40-60 km. We tested the relations

$$M = \frac{1}{4} M_s + \frac{3}{4} (1.59\ m_b - 3.97) \tag{2.5}$$

for events at normal depth and

$$M = (1.59\ m_b - 3.97) \tag{2.6}$$

for events at depths of 40-60 km. We then rounded the M value from equation (2.5) or (2.6) to the nearest tenth. 53 of our 66 M values for shallow earthquake were within 0.1 of the revised magnitude given by Richter, as were 8 of the 11 deep earthquake magnitudes. Furthermore, the scatter was basically symmetric about zero. We therefore conclude that equations (2.5) and (2.6) give the revised magnitude, M, of Richter (1958).

After the above text was written, a further examination of Gutenberg's notes uncovered additional typed worksheets with his values of "M_B", "M_s" and "m." Although these worksheets list body-wave

magnitudes for events which are missing from Table 2.1, they have not been added to the table, because it is not known how they were derived. An examination of the unified magnitudes suggests that the above interpretation is generally correct and that there may also have been a subjective weighting factor used in averaging m_b and m_s.

The revised magnitudes, M, in Richter's catalog are distinctly different from M_s in Seismicity of the Earth. The magnitudes which were given in these catalogs are on different scales. Errors have resulted from treating the revised magnitudes, M, as M_s. For illustration we now examine several earthquakes for which the magnitude is significantly larger in Richter's catalog than in Seismicity of the Earth.

The Tokachi-Oki earthquake of 4 March 1952 is a simple case. Gutenberg and Richter (unpublished notes) found $m_b = 8.0$ and $M_s = 8.3$. The "magnitude" in Seismicity of the Earth is given as 8.3. For $M_s = 8.3$, equation (2.2a) yields $m_s = 7.7$. The weighted average, from equation (2.3) of m_s and m_b (with $\alpha = 3/4$ and $\beta = 1/4$) gives $m = 7.9$, or through equation (2.2b), $M = 8.6$, which is the value given by Richter (1958).

Richter (1958, p. 350) gives some examples of calculating the unified magnitude in his Table 22-5. This table is misleadingly labeled. The column labeled "m from surface waves" is not an m_s value from equation (2.2a). Rather, it is the average of m_s and m_b. This may have resulted from the manner in which the table was constructed. Perhaps the M value had already been found and the other columns were added later. In any case, the unified magnitude found by taking an

unweighted average of the "m from body waves" and the "m from surface waves" still has the effect of weighting m_b three times as heavily.

The Aleutian earthquake of 7 March 1929 is a notable example of a large difference between M_s, from the G-R catalog, and M, from the Richter catalog. Kanamori (1972) found $m_b = 7.67$ and $M_s = 7.68$. The G-R catalog gives M = 8.1. Their magnitude may have been increased to compensate for the apparent focal depth of 50-60 km which was noted by Richter (1958); this is unclear, because we did not find the work-sheet for this event. Richter (1958) gave $m_b = 7.9$ and M = 8.6; apparently his unified magnitude was derived completely from m_b, using equation (2.6).

Despite its various imperfections, the magnitude scale provides important information concerning the source spectrum at the period where the magnitude is determined. In the light of recent earthquake source theories (e.g. Aki, 1967), the differences between the source spectra of different events are very important for understanding various source characteristics, such as source dimension, stress drop and ambient stress. As shown in Table 2.1, most body-wave magnitudes for large earthquakes from 1904 to 1952 were determined at periods of 6 to 12 seconds. However, the determinations of m_b used in the PDE Catalog are made at periods of 1 to 3 seconds. Thus the classical and modern m_b determinations represent different parts of the spectrum and should not be directly compared. It is important to note not only the magnitude but also the period at which the magnitude is determined. This point is discussed further in the appendix to this chapter.

ESTIMATES OF SEISMIC MOMENT

Besides being intrinsically significant, the magnitudes are frequently used to estimate other source parameters. For example, Gutenberg and Richter (1956) gave an empirical relation between log E, seismic energy, and m, unified magnitude. Later, Brune (1968), Davies and Brune (1971) and O'Connell and Dziewonski (1976) used the magnitudes from Duda's catalog, together with empirical relations between log M_o and M_s (treating Duda's magnitudes as M_s) to estimate seismic moment. The first two papers used the moment estimates to estimate the seismic slip rates between plates, while the last used the estimated moments to study the excitation of the Chandler Wobble by earthquakes.

Moment estimates from the magnitude of great earthquakes are very unreliable. Several recent papers (Kanamori and Anderson, 1975; Chinnery and North, 1975; Geller, 1976) point out that for any earthquake with $M_o \gtrsim 10^{28}$ dyne cm, M_s will be 8.3 ± 0.3. Thus for great earthquakes M_s is essentially constant, independent of further increase in M_o. Once the maximum magnitude is reached, estimates of M_o and M_s are extremely unreliable and almost meaningless.

More reliable estimates of M_o may be made by using the fault area S. Several studies have shown (Aki, 1972, Kanamori and Anderson, 1975; Abe, 1975) that a remarkably linear relation exists between log S and log M_o for very large earthquakes. In terms of a crack model, this relation suggests a constant stress drop, $\Delta\sigma$. For a circular crack,

$$M_o = \frac{16}{7} \Delta\sigma \left(\frac{S}{\pi}\right)^{3/2}.$$

The fault area, S, can be reliably estimated from the locations of aftershocks. Even for earthquakes in the early part of the century, S can be fairly reliably estimated from ISS data (e.g. Sykes, 1971). Abe (1975) proposed a relation

$$M_o = 1.23 \times 10^{22} S^{3/2} \text{ dyne-cm} \qquad (2.7)$$

(S in km^2)

for determining the moment from the fault area. This relation corresponds to a nearly circular geometry and a stress drop of about 30 bars. Although this relation does not apply to earthquakes having a stress drop very different from 30 bars, it should give much more reliable estimates of M_o for most large earthquakes than empirical moment-magnitude relations.

One of the most remarkable examples is the 7 March 1929 Aleutian Islands earthquake. Kanamori (1972) obtained a moment of 6.7×10^{27} dyne-cm. The result of Sykes (1971) suggests $S \sim 8 \times 10^3$ km^2. Relation (2.7) then gives $M_o = 8.8 \times 10^{27}$ dyne-cm, which is in good agreement with the measured moment. On the other hand Richter (1958) gave M = 8.6 for this event. If this value is considered as M_s and is used to estimate the moment through an empirical relation between M_o and M_s (e.g. $\log M_o = 8.8 + 2.5 M_s$; O'Connell and Dziewonski, 1976), $M_o = 2 \times 10^{30}$ dyne-cm is obtained. This value is more than 200 times too large and is equal to the largest seismic moment ever reliably determined (2×10^{30} dyne-cm for the 1960 Chilean earthquake; Kanamori and Cipar, 1974).

Recently Kanamori (1977) studied the energy release in great earthquakes, on the basis of the moment of great earthquakes, either as measured directly or as estimated from the aftershock area or 100-sec magnitude. Kanamori then used the relation

$$W = M_o/(2 \times 10^4) \ , \tag{2.8}$$

to estimate W, the minimum released strain energy. This relation gave much more satisfactory estimates of released seismic energy than those made from the Gutenberg-Richter energy-magnitude formula,

$$\log_{10} E = 1.5 M_s + 11.8 \ , \qquad E \text{ in ergs} \tag{2.9}$$

because the estimates based on moment are not affected by the saturation of the magnitude scale. In fact, equation (2.9) was inverted by Kanamori to find a new magnitude, M_W, from log W.

$$\begin{aligned} M_W &= 0.67 \ (\log_{10} W) - 7.9 \\ &= 0.67 \ (\log_{10} M_o) - 10.7 \quad M_o \text{ and } W \text{ in dyne-cm} \end{aligned} \tag{2.10}$$

M_W is not affected by the saturation of the surface-wave magnitude scale and gives a reliable estimate of the size of the greatest earthquakes.

CONCLUSION

We have given M_s values (for 96) and m_b values (for 92) of the 109 "class a" shallow earthquakes in Gutenberg and Richter's (1954) Seismicity of the Earth. Our values of M_s, taken from Gutenberg and Richter's unpublished notes, differ only slightly from the Gutenberg-

Richter magnitudes, which are significantly lower than the "revised magnitudes" of Richter (1958) and Duda (1965). This difference results from the fact that the Gutenberg-Richter magnitudes are basically M_s, while the revised magnitudes are "unified magnitudes" which heavily emphasize m_b.

For most shallow earthquakes Richter's (1958) M is related to the 20 sec surface-wave magnitude, M_s, and the body-wave magnitude m_b by

$$M = \frac{1}{4} M_s + \frac{3}{4} \left[1.59\ m_b - 3.97\right].$$

For events at depths of 40-60 km the revised magnitude, M, is calculated only from m_b.

$$M = 1.59\ m_b - 3.97.$$

Revised magnitude, M and surface-wave magnitude M_s are distinct magnitude scales and should not be confused.

APPENDIX

SURFACE WAVE MAGNITUDES

Gutenberg (1945a) presented an empirical formula for surface wave magnitudes. His formula was derived from a least squares fit to amplitude data from mostly Pacific earthquakes. For shallow earthquakes at distances $15^{o} < \Delta < 130^{o}$, Gutenberg found the formula

$$M_s = \log A_H + 1.656 \log \Delta + 1.818 + C. \qquad (2.11)$$

C is the (empirically determined) station correction and A_H is the horizontal component of the maximum ground movement (in microns) during the surface waves having a period of about 20 seconds. This formula was derived for oceanic paths and for teleseismic distances. (The problems which result from magnitude determination at short distances or along continental paths have been discussed by Alewine (1972) and Marshall and Basham (1972) and will not be covered here.)

The amplitude, A_H, in equation (2.11) is a somewhat ill-defined quantity. Gutenberg intended A_H to be the "total" horizontal amplitude (zero to peak). By this he meant that A_H was the "vector sum"

$$A_H = (A_N^2 + A_E^2)^{1/2} \qquad (2.12)$$

where A_N is the maximum amplitude on the N-S component and A_E the maximum on the E-W component. The "vector sum" probably leads to an amplitude which is larger than the amplitude one would measure from the (rotated) Rayleigh wave or Love wave. The maxima on the N-S and E-W components will rarely occur at the same time; thus the amplitude

derived from equation (2.12) must always be at least as large as the true maximum amplitude, both because A_N and A_E may be measured at different times and because Love and Rayleigh waves may overlap. Gutenberg (1945a) clearly recognized that use of the vector sum leads to increased amplitudes. He recommended that if only one component is available for magnitude determination, its amplitude should be multiplied by 1.4 (i.e. $\sqrt{2}$) for use in equation (2.11).

Many investigators after Gutenberg and Richter proposed their own versions of the surface wave magnitude scale. The results of their research were summarized by Vanek et al. (1962) who proposed the formula

$$M_s = \log (A/T)_{max} + 1.66 \log \Delta + 3.3 \qquad (2.13)$$

which has been adopted officially by the IASPEI (International Association for Seismology and Physics of the Earth's Interior). In equation (2.13) $(A/T)_{max}$ is the maximum of all A/T (amplitude/period) values of the wave groups on a record. For T = 20 sec, equation (2.13) reduces to

$$M_s = \log A_{20} + 1.66 \log \Delta + 2.0 \qquad (2.14)$$

Equation (2.14) is nearly identical to Gutenberg's equation (2.11); the only significant difference is that the additive constant in equation (2.14) is 0.18 larger. The method for measuring A_{20} or $(A/T)_{max}$ is not precisely defined. If the horizontal components are combined "vectorially" then the magnitudes from equation (2.13) or (2.14) will be

systematically higher than Gutenberg's by 0.18. On the other hand, if each horizontal component is used separately, and the two independent horizontal M_s values are averaged, then magnitudes from the IASPEI formula would be virtually identical to Gutenberg's. There does not seem to be a precise definition of how $(A/T)_{max}$ should be measured, although the usual method seems to be vectorial summation. Perhaps an international standard should be developed by the IASPEI.

Since the more widespread use of vertical broadband instruments, and particularly since the advent of the WWSSN, M_s has frequently been determined from the amplitude on the vertical component, using equation (2.13). The relation between the vertical and horizontal amplitudes is not clear. The spectral ratio of horizontal to vertical Rayleigh wave components (ellipticity) probably is a good approximation for the ratio of $(A/T)_{horiz}$ to $(A/T)_{vert}$, even though the amplitudes are measured in the time domain. If the ellipticity is used to approximate the time domain ratio, then one expects the vertical Rayleigh wave amplitude to be about 1.4 times the horizontal. Thus $\log (A/T)_{vert}$ might be 0.15 larger than $\log (A/T)_{horiz}$ for Rayleigh waves. This increase may be offset by the tendency for Love waves, vector summing and higher modes to increase $(A/T)_{horiz}$.

We have discussed only a small fraction of the research on surface wave magnitudes following Gutenberg and Richter. In spite of some later revisions in the procedures for determining magnitudes, the modern definition is essentially equivalent to Gutenberg and Richter's M_s. Their M_s values probably can be compared to modern measurements

without appreciable difficulties.

BODY WAVE MAGNITUDES

Gutenberg (1945b, c) gave formulae for body wave-magnitudes of shallow and deep earthquakes respectively. Later, Gutenberg and Richter (1956) published their final version of the body-wave magnitude formula.

$$m_b = \log (A/T) + Q \qquad (2.15)$$

Q is an empirically determined term which accounts for the source-receiver distance and the source depth. (A/T) is the maximum in the wave group of either P, PP or SH, with separate tables and charts of Q for each phase. (A is either the center to peak or half of the peak to peak ground displacement.)

Although later authors, e.g. Vanek et al. (1962) have proposed revisions of the m_b formula, the Gutenberg-Richter formula continues in wide use. There are two main differences between the original method for implementing equation (2.15) and the current practice of the USGS. These differences, discussed below, result in substantially different m_b values from Gutenberg and Richter's.

One radical change in m_b determination is the different type of instrument used for modern determinations. Most of the P waves used by Gutenberg and Richter, particularly for larger events, were all measured on broad-band instruments at periods of about 6 to 12 seconds, with longer periods for the larger events. The m_b measurements currently made by the USGS use amplitudes and periods from the short

period WWSSN instruments, which are sharply peaked at about 1/2 second. In practice, the period at which the peak amplitude occurs is nearly always about 1 sec. Furthermore, the USGS instructions ask that T be restricted to less than 3 sec. Another change in the way magnitudes are determined is the USGS requirement that (A/T) must be measured in the first 5 seconds of the record. The previous practice had been that the peak (A/T) might be measured longer into the record, to allow for an earthquake with a gradual onset (Bath, 1966). Richter (personal communication) notes that using the first P instead of the maximum leads to representing major earthquakes (about 7 or more) by magnitudes around 5 which are those of minor immediate foreshocks.

The discrepancy between the narrowband m_b values determined by the USGS and the broadband m_b values obtained by seismologists in the eastern hemisphere is well known to observational seismologists (e.g. SIPRI, 1968). Although many factors enter into the problem, the main cause of the discrepancy appears to be the different passbands of the instruments. Because the P-wave spectrum eventually saturates at any given frequency as the seismic moment increases, the time domain amplitude at 1 sec reaches a constant upper limit; thus m_b values measured on short-period narrow-band instruments are saturated for smaller earthquakes than the broadband instruments (Geller, 1976 and Chapter 3 of this thesis).

REFERENCES

Abe, K. (1975). Reliable estimation of the seismic moment of large earthquakes, J. Phys. Earth, 23, 381-390.

Aki, K. (1967). Scaling law of seismic spectrum, J. Geophys. Res., 72, 1217-1231.

Aki, K. (1972). Earthquake mechanism, Tectonophysics, 13, 423-446.

Alewine, R. W., III (1972). Theoretical and observed distance corrections for Rayleigh-wave magnitude, Bull. Seism. Soc. Am., 62, 1611-1619.

Bath, M. (1966). Earthquake energy and magnitude, Phys. and Chem. of the Earth, 7, 115-165.

Brune, J. N. (1968). Seismic moment, seismicity and rate of slip along major fault zones, J. Geophys. Res., 73, 777-784.

Chinnery, M. A. and R. G. North (1975). The frequency of very large earthquakes, Science, 190, 1197-1198.

Davies, G. F. and J. N. Brune (1971). Regional and global fault rates from seismicity, Nature Physical Science, 229, 101-107.

Duda, S. J. (1965). Secular seismic energy release in the Circum-Pacific belt, Tectonophysics, 2, 409-452.

Geller, R. J. (1976). Scaling relations for earthquake source parameters and magnitudes, Bull. Seism. Soc. Am., 66, 1501-1523.

Gutenberg, B. (1945a). Amplitudes of surface waves and magnitudes of shallow earthquakes, Bull. Seism. Soc. Am., 35, 3-12.

Gutenberg, B. (1945b). Amplitudes of P, PP, and S and magnitude of shallow earthquakes, Bull. Seism. Soc. Am., 35, 57-69.

Gutenberg, B. (1945c). Magnitude determination for deep focus earthquakes, Bull. Seism. Soc. Am., 35, 117-130.

Gutenberg, B. (1957). Earthquake energy released at various depths, in Gedenkbook F.A. Vening Meinesz, Verh. Konink. Ned. geol.-Mijnb., Genootschap, The Hague, 165-175.

Gutenberg, B. and C. F. Richter (1936). On seismic waves (third paper), Gerlands Beitr. Geophys., 47, 73-131.

Gutenberg, B. and C. F. Richter (1941). Seismicity of the earth, Geol. Soc. Am. Spec. Pap. 34.

Gutenberg, B. and C. F. Richter (1942). Earthquake magnitude, intensity, energy and acceleration, Bull. Seism. Soc. Am., 32, 163-191.

Gutenberg, B. and C. F. Richter (1954). Seismicity of the earth and Associated Phenomena, 2nd ed., Princeton Univ. Press.

Gutenberg, B. and C. F. Richter (1956). Magnitude and energy of earthquakes, Ann. Geofis., (Rome), 9, 1-15.

Kanamori, H. (1971). Seismological evidence for a lithospheric normal faulting-the Sanriki earthquake of 1933, Phys. Earth Planet. Interiors, 4, 289-300.

Kanamori, H. (1972). Mechanism of tsunami earthquakes, Phys. Earth Planet. Interiors, 6, 346-359.

Kanamori, H. (1977). The energy release in great earthquakes, J. Geophys. Res., in press.

Kanamori, H. and D. L. Anderson (1975). Theoretical basis of some empirical relations in seismology, Bull. Seism. Soc. Am., 65, 1073-1095.

Kanamori, H. and J. J. Cipar (1974). Focal process of the great Chilean earthquake May 22, 1960, Phys. Earth Planet. Interiors, 9, 128-136.

Kanamori, H. and S. Miyamura (1970). Seismometric re-evaluation of the great Kanto earthquake of September 1, 1923, Bull. Earthq. Res. Inst. Tokyo Univ., 48, 115-125.

Marshall, P. D. and P. W. Basham (1972). Discrimination between earthquakes and underground explosions employing an improved M_s scale, Geophys. J., 28, 431-458.

O'Connell, R. J. and A. M. Dziewonski (1976). Excitation of the Chandler Wobble by large earthquakes, Nature, 262, 259-262.

Okal, E. A. (1977). The July 9 and July 23, 1905 Mongolian earthquakes: A surface wave investigation, Earth Plan. Sci. Lett., 34, 326-331.

Richter, C. F. (1935). An instrumental earthquake magnitude scale, Bull. Seism. Soc. Am., 25, 1-32.

Richter, C. F. (1958). Elementary Seismology, W. H. Freeman, San Francisco.

SIPRI (1968). Seismic methods for monitoring underground explosions, International Institute for Peace and Conflict Research, Stockholm.

Sykes, L. R. (1971). Aftershock zones of great earthquakes, seismicity gaps, and earthquake prediction for Alaska and the Aleutians, J. Geophys. Res., 76, 8021-8041.

Vanek, J., A. Zatopek, V. Karnik, N. V. Kondorskaya, Y. V. Riznichenko, E. F. Savarensky, S. L. Solov'ev and N. V. Shebalin (1962). Standardization of magnitude scales, Iz. Akad. Nauk. SSSR, Ser. Geofiz. (AGU Translation), 2, 108-111.

Chapter 3

SCALING RELATIONS FOR EARTHQUAKE SOURCE PARAMETERS AND MAGNITUDES

ABSTRACT

A dataset of forty-one moderate and large earthquakes is used to derive scaling rules for kinematic fault parameters. If effective stress and static stress drop are equal, then fault rise time, τ, and fault area, S, are related by $\tau = 16S^{1/2}/(7\pi^{3/2}\beta)$, where β is shear velocity. Fault length (parallel to strike) and width (parallel to dip) are empirically related by $L = 2W$. Scatter for both scaling rules is about a factor of two. These scaling laws combine to give width and rise time in terms of fault length. Length is then used as the sole free parameter in a Haskell type fault model to derive scaling laws relating seismic moment to M_s (20 sec. surface wave magnitude), M_s to S and m_b (1 sec body wave magnitude) to M_s. Observed data agree well with the predicted scaling relation. The "source spectrum" depends on both azimuth and apparent velocity of the phase or mode, so there is a different "source spectrum" for each mode, rather than a single spectrum for all modes. Furthermore, fault width (i.e. the two dimensionality of faults) must not be neglected. Inclusion of width leads to different average source spectra for surface waves and body waves. These spectra, because of their ω^{-3} high frequency asymptote, in turn imply that m_b and M_s reach maximum values regardless of further increases in L and seismic moment. The m_b:M_s relation from this study differs significantly from the Gutenberg-

Richter relation, because the Gutenberg-Richter equation was derived for body waves with a predominant period of about 5 sec and thus does not apply to modern 1 sec m_b determinations. Previous investigators who assumed that the Gutenberg-Richter relation was derived from 1 sec data were in error. Finally, averaging reported rupture velocities yields the relation $V_R = 0.72\beta$.

BACKGROUND

In the last chapter we studied the definition of various seismic magnitude scales. The magnitude is still the most commonly cited parameter in discussing the "size" of an earthquake. The magnitude is closer to our direct experience than any other fault parameter, because we measure the amplitude and period directly from a seismogram, and need only a distance and depth correction to obtain m_b or M_s. Although it is closest to our experience, the magnitude is not directly related to more physically meaningful fault parameters, such as radiated energy or seismic moment. Other fault parameters, such as fault length and width, rise time, rupture velocity and stress drop cannot be determined without extensive analysis of the observed data. In general, we want to know the physical fault parameters for a given earthquake, but often we know only the magnitudes. In such cases it is natural to try to use the magnitudes to estimate other source parameters.

The earliest such attempt was made by Gutenberg and Richter. Their work culminated with the publication of their final relation between radiated wave energy and magnitude (Gutenberg and Richter, 1956). When they wrote their paper, very little was known about seismic source theory. Indeed, at that time a fierce dispute raged over the question of single couple versus double couple sources.

As a result of the fundamental advances in source theory by Steketee (1958a, b), de Hoop (1958), Maruyama (1963) Burridge and Knopoff (1964) and Haskell (1964), the equivalence of elastic

dislocations with double couples was placed on a firm foundation. Once this equivalence became clear, it could be seen that the seismic source and the effect of the medium could be separated. Burridge and Knopoff (1964) showed that if the Green's function (point force impulse response) for any arbitrarily heterogeneous and anisotropic medium was known, that a distributed shear dislocation could be modeled by convolving the spatial and temporal dislocation density with appropriate derivatives of the Green's function. This is a generalization of Harkrider's (1964) result showing that the source and medium effects could be separated for any plane-layered, isotropic, model.

Once a greater theoretical understanding of the excitation problem was obtained, interest was renewed in studying the details of earthquake source mechanisms. Burridge and Knopoff (1964) had showed that for any finite source the displacement could be obtained by convolving the source density in space and time with the Green's function. However, there are some cases, usually in the far-field, for which very accurate approximate solutions can be obtained by convolving the Green's function in time only with a source time function which includes the effect of fault finiteness in space. Examples of this procedure for a whole space are the line source directivity functions of Ben-Menahem (1961, 1962) and the planar source functions of Hirasawa and Stauder (1965) and Mikumo (1969). Fukao (1971) extended these solutions to a planar, shallow, propagating rupture in a halfspace. It should be noted that each surface

or body-wave phase (e.g. P, pP, S, Love, etc.) has its own time function, or, equivalently, source finiteness spectrum, and that this must be considered, especially when the free surface is important in body-wave problems. The commonly adopted procedure of using a single time function for P, pP and sP may not always be appropriate for shallow finite sources.

The fact that the far-field displacement, at least for P or S waves in a whole space, could be written as the convolution in time of a time function including source finiteness effects, the source time function at a single point and the Green's function was essential to the next major advance in source theory. Aki (1967) introduced the concept of a scaling relation for seismic sources by replacing the temporal convolution by the equivalent product of Fourier transforms. He isolated the source finiteness and rise time effects (which he preferred to treat in a statistical sense, using the concept of spatial and temporal correlation wave numbers) by considering spectral ratios from two earthquakes of different magnitude in the same area. The principal contribution of this paper is the emphasis on relating m_b and M_s to the source spectrum at 1 and 20-sec respectively. As we will see below, there appear to have been specific errors in this work; however, the basic concept of a scaling relation between magnitudes and the source spectrum has stood the test of time and is now almost universally accepted.

INTRODUCTION

The purpose of this chapter is to examine empirical relations between gross fault parameters and the agreement of these relations with theoretical models of seismic sources. The gross parameters to be studied are fault length, width and rise time, rupture velocity, m_b and M_s, and seismic moment. Data from other investigators' studies of individual earthquakes are used to study scaling of source parameters in an approximate way. In general the data are consistent with fault width scaling proportionately to fault length and rise time scaling proportionately to the square root of fault area. This scaling can then be used to find $m_b - M_s$, $\log M_o - M_s$ and $\log S - M_s$ relations. Some of those relations have been studied by Kanamori and Anderson (1975b), who provided a theoretical basis for many of the empirical relationships used in seismology.

Tsuboi (1956) was the first investigator to utilize similarity, the concept of relating earthquakes of different sizes by a one parameter model. By assuming that the horizontal dimensions of the earthquake source volume were three times larger than the vertical dimension, Tsuboi derived from the relation $E = \mu\varepsilon^2 A^{1.5}/6$, where E is released energy, μ is average rigidity, ε is average strain drop and A is aftershock area. Such approximate scaling relations, as first pointed out by Tsuboi, require that the physics of material failure be identical for large and small earthquakes. If that assumption is generally true and if earthquakes tend to be geometrically similar, then it follows that fault length and width, and final

dislocation all will scale together. Differences in material properties will weaken the exactness of the similarity when earthquakes from two different regions are compared, but, in an approximate sense, similarity, as is shown by the data presented below, is a valid concept.

The first paper to systematically relate observed gross seismic source parameters to the source spectrum was the now classic work of Aki (1967). Although the results presented in this chapter modify his results, the methodology and basic outlook are similar to Aki's. Later Brune (1970, 1971) contributed to the understanding of seismic source spectra.

Similarity between earthquakes is a dynamic as well as a static concept. Not only the final static parameters, but also the spectral shape of the equivalent source time function, scales with fault length. Spectral similarity can best be demonstrated by comparing two earthquakes with identical location and focal mechanism, but different magnitude. Such a comparison ensures that seismograms from both events will be affected equally by the medium response, so that all differences between the records will be from the source effects.

Observational studies of similar pairs of earthquakes have been made by Berckhemer (1962) whose results were interpreted by Aki (1967) to support Aki's ω^{-2} model. Tsujiura (1973) studied groups of events from various regions, concluding that most data were in accord with Aki's ω^{-2} model, but that some were better fit by an ω^{-1} or ω^{0} model.

One cannot directly compare spectral characteristics of source mechanisms from different regions without first correcting the seismograms for transmission effects. Removing the effects of medium response will usually require use of synthetic seismogram methods. We assume however that one can compare logarithmic fault parameters, such as m_b, M_s or log L, for events in different regions. These comparisons are made with the intention of looking at order of magnitude relationships rather than details.

In this chapter we will look at scaling relations between five sets of such logarithmic parameters: log L vs. log W (fault length vs. width), log τ vs. log S (fault rise time vs. area), M_s vs. log M_o (surface wave magnitude vs. seismic moment), m_b vs. M_s and log S vs. M_s. What will be shown are not exact correlations, but rather trends which appear to be applicable to most earthquakes. Agreement between the simple model used in this chapter and the data are quite good. (Long narrow transform faults, such as the San Andreas, are a separate class of faults which are not considered in this chapter.)

OBSERVATIONAL DATASET

The earthquake data shown in Table 3.1 are from the same forty-one shallow events used by Kanamori and Anderson (1975b). All values for M_s are from their paper; the sources for all other observational parameters are given in the table of references. Except for minor differences which are primarily due to the use of slightly different references, data for M_o and S are equivalent to Kanamori and Anderson's.

Table 3.1

Earthquake Source Parameters

	Event	Date	M_s	m_b	M_o $\times 10^{27}$ dyne-cm	L km	W km	D m	τ sec	τ^* sec	V_R km/sec	$\Delta\sigma$ bars
1.	Kanto	1 Sept. 1923	8.2	-	7.6	130	70	2.1	7	10	-	21
2.	Tango	27 March 1927	7.75	-	0.46	35	13	3	6	2.5	2.3	115
3.	North Izu	25 Nov. 1930	7.1	-	0.2	20	11	3	-	1.7	-	150
4.	Saitama	21 Sept. 1933	6.75	-	0.068	20	10	1	2	1.6	2.3	59
5.	Sanriku	2 March 1933	8.3	-	43	185	100	3.3	7	12	3.2	42
6.	Long Beach	11 March 1933	6.25	-	0.028	30	15	0.2	2	2.5	2.3	7
7.	Imperial Valley	19 May 1940	7.1	-	0.48	70	11	2	-	3.2	-	55
8.	Tottori	10 Sept. 1943	7.4	-	0.36	33	13	2.5	3	4.0	2.3	99
9.	Tonankai	7 Dec. 1944	8.2	-	15	120	80	3.1	-	9.2	-	39
10.	Mikawa	12 Jan. 1945	7.1	-	0.087	12	11	2.2	-	1.3	-	140
11.	Nankaido	20 Dec. 1946	8.2	-	15	120	80	3.1	-	9.2	-	39
12.	Fukui	28 June 1948	7.3	-	0.33	30	13	2	2	1.9	2.3	100
13.	Tokachi-Oki	4 March 1952	8.3	-	17	180	100	1.9	-	14	-	17
14.	Kern County	21 July 1952	7.7	-	2	60	18	4.6	1	3.6	-	140

Table 3.1 cont.

Earthquake Source Parameters

	Event	Date	M_s	m_b	M_o $\times 10^{27}$ dyne-cm	L km	W km	$\bar{D}$ m	τ sec	τ^* sec	V_R km/sec	$\Delta\sigma$ bars
15.	Fairview	16 Dec. 1954	7.1	-	0.13	36	6	2	-	1.7	-	100
16.	Chile	22 May 1960	8.3	-	2400	800	200	21	-	36	3.5	91
17.	Kitamino	19 Aug. 1961	7.0	-	0.09	12	10	2.5	2	1.3	3.0	170
18.	Wasaka Bay	27 March 1963	6.9	-	0.033	20	8	0.6	2	1.5	2.3	40
19.	North Atlantic I	3 Aug. 1963	6.7	6.1	0.12	32	11	1	-	2.2	-	44
20.	Kurile Islands	13 Oct. 1963	8.2	5.7	75	250	140	3	-	17	3.5	28
21.	North Atlantic II	17 Nov. 1963	6.5	5.9	0.038	27	9	0.48	-	1.8	-	24
22.	Spain	15 March 1964	7.1	6.2	0.13	95	10	0.42	-	3.6	1.4	11
23.	Alaska	28 March 1964	8.5	6.2	520	500	300	7	-	35	3.5	22
24.	Niigata	16 June 1964	7.4	6.1	3.2	80	30	3.3	-	5.3	-	66
25.	Rat Island I	4 Feb. 1965	7.9	6.0	140	500	150	2.5	-	25	4.0	17
26.	Rat Island II	30 March 1965	7.5	5.7	3.4	50	80	1.2	-	5.8	-	33
27.	Parkfield	28 June 1966	6.4	5.3	0.032	26	7	0.6	0.7	1.6	2.7	32
28.	Aleutian	4 July 1966	7.2	6.2	0.226	35	12	1.6	-	2.4	-	64
29.	Truckee	12 Sept. 1966	5.9	5.4	0.0083	10	10	0.3	-	1.2	-	20

Table 3.1 cont.

Earthquake Source Parameters

	Event	Date	M_s	m_b	M_o $\times 10^{27}$ dyne-cm	L km	W km	$\bar{D}$ m	τ sec	τ^* sec	V_R km/sec	$\Delta\sigma$ bars
30.	Peru	17 Oct. 1966	7.5	6.3	20	80	140	2.6	-	9.6	-	41
31.	Borrego	9 Apr. 1968	6.7	6.1	0.063	33	11	0.58	-	2.2	-	22
32.	Tokachi-Oki	16 May 1968	8.0	5.9	28	150	100	4.1	-	12	3.5	37
33.	Saitama	1 July 1968	5.8	5.9	0.019	10	6	0.92	1	0.9	3.4	100
34.	Portuguese	28 Feb. 1969	8.0	7.3	5.5	80	50	2.5	-	6.1	-	53
35.	Kurile Islands	11 Aug. 1969	7.8	7.1	22	180	85	2.9	-	12	3.5	28
36.	Gifu	9 Sept. 1969	6.6	5.5	0.035	18	10	0.6	1	1.7	2.5	35
37.	Peru	31 May 1970	7.8	6.6	10	130	70	1.6	-	8.7	2.5	28
38.	San Fernando	9 Feb. 1971	6.6	6.2	0.12	20	14	1.4	1	2.0	2.4	62
39.	Nemuro-Oki	17 June 1973	7.7	6.5	6.7	60	100	1.6	-	7.5	-	35
40.	Turkey	22 July 1967	7.1	6.0	0.83	80	20	1.7	-	4.7	-	32
41.	Iran	31 Aug. 1968	7.3	5.9	1	80	20	2.1	-	4.7	-	38

REFERENCES TO TABLE 3.1

(1) Kanamori (1971a). Rise time from Kanamori (1974).

(2) Kanamori (1973).

(3) Average of Chinnery (1964), Kasahara (1957) and Kanamori (unpublished data).

(4) Abe (1974b).

(5) Average of Kanamori (1971b) and Kawasaki and Suzuki (1974).

(6) Kanamori (unpublished data) and aftershock zone.

(7) Average of Brune and Allen (1967) and Byerly and DeNoyer (1958).

(8) Kanamori (1972b).

(9) Kanamori (1972a).

(10) Ando (1974).

(11) Kanamori (1972a).

(12) Kanamori (1973).

(13) Area from average of Kanamori (unpublished data) and Utsu and Seki (1954). Moment from Kanamori (unpublished data).

(14) Kanamori (unpublished data).

(15) Savage and Hastie (1966).

(16) Average (for main shock only--precursor not included) of Kanamori and Cipar (1974) and Kanamori and Anderson(1975a).

(17) Kawasaki (1975).

(18) Abe (1974a).

(19) Udias (1971).

(20) Kanamori (1970a).

(21) Udias (1971).

(22) Udias and Arroyo (1970).

(23) Kanamori (1970b).

(24) Abe (1975a).

(25) Wu and Kanamori (1973).

(26) Abe (1972a).

(27) Average of Anderson (1974) and Trifunac and Udwadia (1974).

(28) Udias (1971).

(29) Tsai and Aki (1970).

(30) Abe (1972b).

(31) Hanks and Wyss (1972).

(32) Kanamori (1971c).

(33) Abe (1975b).

(34) Fukao (1973).

(35) Abe (1973).

(36) Mikumo (1973).

(37) Abe (1972b). Average of parameters for each of the two possible fault planes.

(38) Moment and static fault parameters from Kanamori and Anderson (1975b). Rupture velocity and rise time averaged from Boore and Zoback (1974), Mikumo (1973b) and Trifunac (1974).

(39) Shimazaki (1975).

(40) Hanks and Wyss (1972).

(41) Hanks and Wyss (1972).

Each numbered entry in the table of references corresponds to the earthquake with the same number in Table 3.1. All but two of the columns are observational data; τ^*, predicted rise time, and $\Delta\sigma$, calculated stress drop, will be discussed below. Length and width have been taken from the references, or in some cases estimated. Length always refers to length along the strike, regardless of focal mechanism; width refers to width along the dip. Average dislocation comes either from field measurements or from dividing the moment (determined from seismograms) by the area and an assumed value of the shear modulus.

For all events since August 1963 the m_b value is either taken directly from the PDE Monthly Summary, or calculated from the data in Earthquake Data Reports. As reported by L. M. Murphy in Bath (1969), *USCGS (later NOAA and now USGS) asks for the amplitude of the largest* pulse (with period less than three seconds) in the first five cycles of the teleseismic P or P_n arrival. The values of A and T are then used in the Gutenberg-Richter formula

$$m_b = \log_{10}(A/T) + Q\,, \tag{3.1}$$

to derive m_b for each station. Values more than 0.7 magnitude units from the mean are deleted and the final average is then taken.

Estimates of rise times typically were made by fitting the first upswing on long-period local records to synthetic seismograms calculated using the Haskell (1969) whole space model at one or two

stations. Clearly it would be desirable to use synthetics made for more realistic models of earth structure, but they have not yet been calculated for these events. Uncertainties due to the tradeoff between rise time and rupture velocity and due to the model may combine to cause errors which cannot be estimated. In some cases, such as the Tottori earthquake (Kanamori, 1972b), rupture velocity and rise time are independently constrained.

LENGTH VERSUS WIDTH

Fault length (along the strike) is plotted against fault width (down-dip) in Figure 3.1. It can be seen that (with considerable scatter) observational data demonstrate that L = 2W. In Figure 3.1, the numbers refer to earthquakes in Table 3.1. Intraplate events are plotted as open circles and interplate events as solid circles. (This convention is also used in all later figures.) There is not any clear difference between the interplate and intraplate groups. Abe (1975c) has independently found L = 2W for a dataset of Japanese earthquakes.

The Haskell model uses L as the direction in which rupture propagates, while L was measured along the direction of the strike for Figure 3.1. It is implicitly assumed, then, that for these 41 events rupture propagated parallel to the strike. This is almost certainly false for some thrust events such as San Fernando (Boore and Zoback (1974), Trifunac (1974), Mikumo (1973b)), and may well be false for events like Nemuro-Oki with L < W. In spite of these exceptions it seems

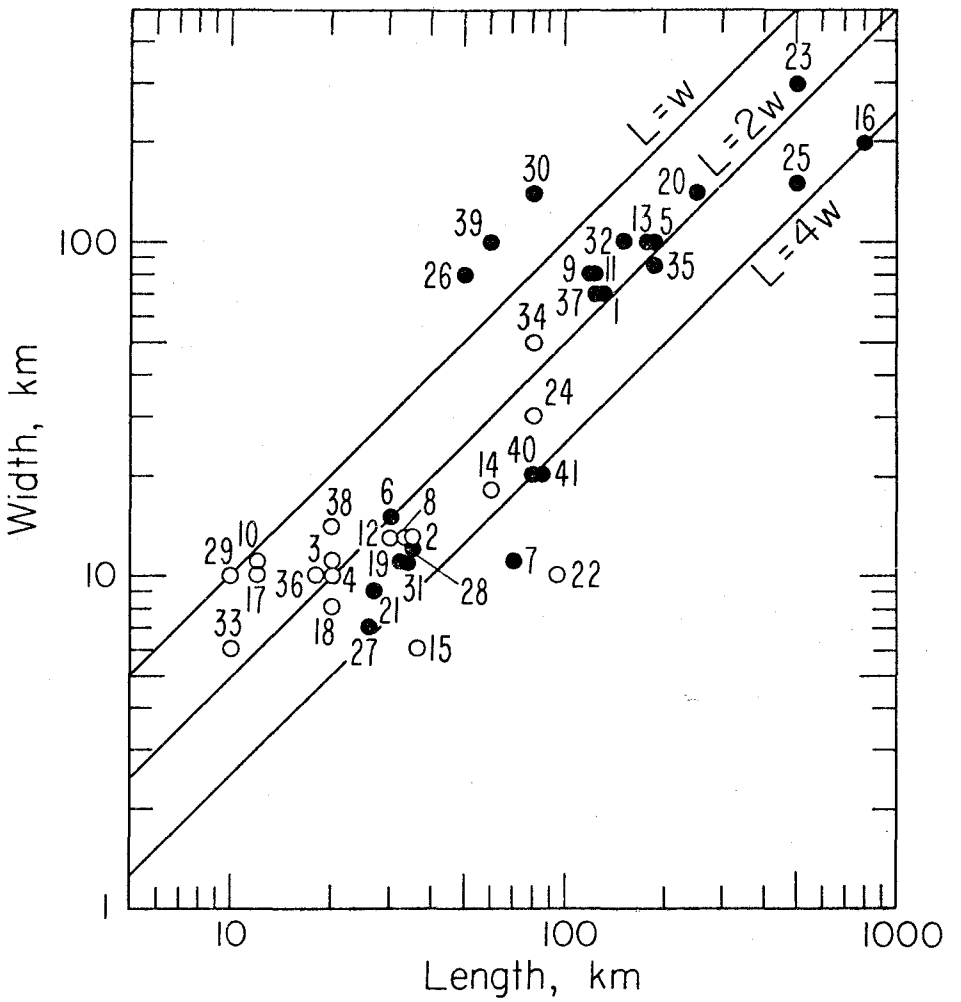

Figure 3.1 - Plot of fault length (along strike) versus fault width (along dip) for earthquakes in Table 3.1. Open circles are intraplate events; closed circles are interplate events. Numbers refer to Table 3.1. These conventions are used for all plots of earthquake data.

that rupture usually propagates parallel to the strike, especially for strike-slip faults.

RISE TIME VERSUS THEORETICAL PREDICTIONS

Kanamori (1972b) showed that

$$\dot{D} = \frac{\bar{D}}{\tau} \simeq \sigma_{e,o} \frac{\beta}{\mu} \tag{3.2}$$

where $\dot{D}$ is dislocation velocity, $\bar{D}$ is average dislocation, τ is rise time, and $\sigma_{e,o}$ is effective stress. If one assumes that effective dynamic stress is equal to static stress drop, $\Delta\sigma$, this assumption can be tested by comparing observed rise times to the theoretically predicted rise time

$$\tau^* = \frac{\mu \bar{D}}{\beta \Delta\sigma} \quad . \tag{3.3}$$

One can obtain stress drop in closed form for only a few simple models. The most straightforward of these is the circular crack with constant stress drop discussed by Keiles-Borok (1959). For that model stress drop is given by

$$\Delta\sigma = 7\pi^{3/2}\mu\bar{D}/(16\sqrt{S}) = 7M_o/(16(LW/\pi)^{3/2}) \tag{3.4}$$

Although this formula does not give the exact stress drop for the rectangular fault model, it follows from the work of Sato (1972) that

this is a good approximation. If we substitute (3.4) in (3.3), where S is the area of the rectangular fault and $\bar{D}$ is average dislocation, we obtain

$$\tau^* = 16S^{1/2}/(7\pi^{3/2}\beta) \tag{3.5}$$

The values of $\Delta\sigma$ and τ^* in Table 3.1 were calculated using (3.4) and (3.5), respectively.

Figure 3.2 is a plot of observed versus predicted (from (3.5)) rise times for a number of earthquakes. It can be seen that, again with considerable scatter, observational and theoretical rise times are in agreement. Abe (1975b) reached a similar conclusion from a dataset of five Japanese earthquakes.

The agreement between theoretical and observed rise times has important implications for engineering seismology. The only observational parameter required in (3.5) is fault area, which frequently can be estimated from geological data. If total dislocation can also be determined from geological field work, then particle velocity near the fault, an important parameter in engineering seismology, can be reliably estimated. This is potentially of great values in areas lacking in historical seismicity or good instrumental data.

RUPTURE VELOCITY

Table 3.1 lists rupture velocities reported by various investigators. These values were determined from matching synthetic

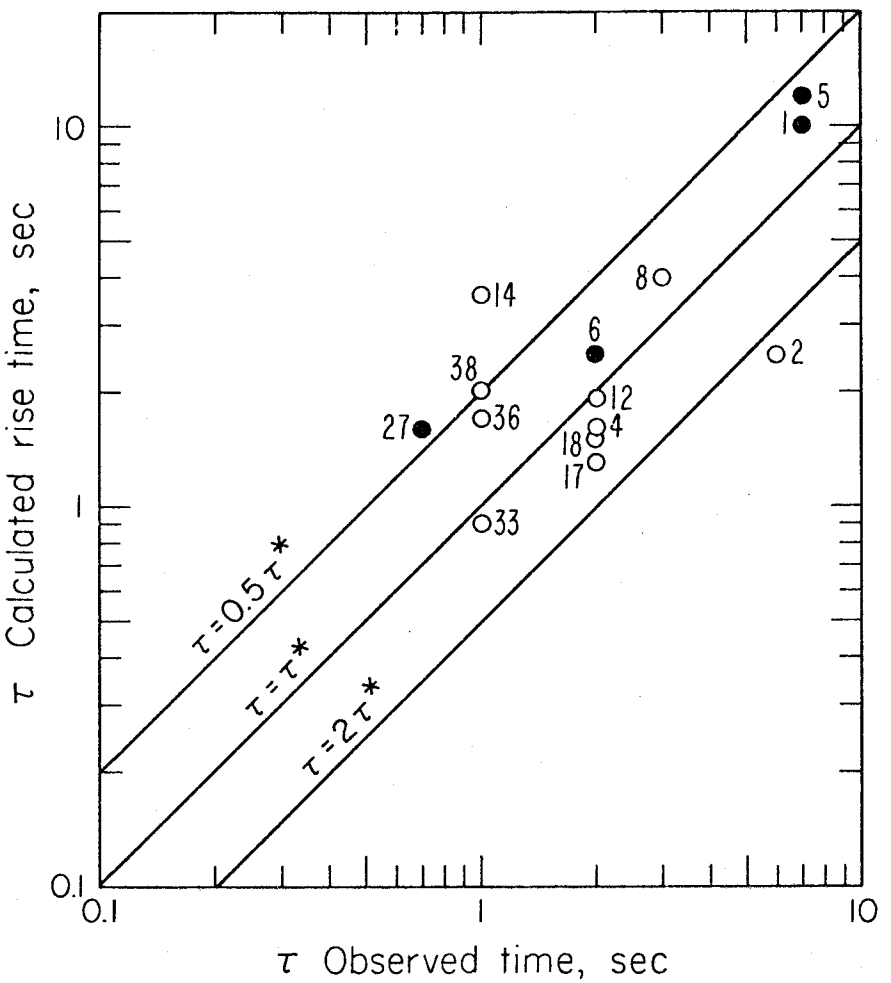

Figure 3.2 - Plot of observed rise time versus theoretical rise times from (3.5).

seismograms to local records or from surface wave analysis. To a certain extent then, these values are model dependent. Some also may be affected by the difficulty in resolution between rise time and rupture velocity. Nevertheless, these measurements probably represent a good average sample of rupture velocity measurements. If one picks values of β ranging from 3.5 km/sec for shallow crustal events to 4.5 km/sec for events breaking the entire lithosphere, one then can calculate that the average value of (V_R/β) is 0.72. (See Table 3.2.)

Archuleta and Brune (1975) found $V_R/\beta = 0.7$ in experiments on fracture of prestressed foam rubber. Their measured value was for the surface of the foam rubber, but if one assumes infinite rupture velocity along the dip, their result agrees very well with the result $V_R/\beta = 0.72$ observed for earthquakes. (Their minimum possible value for V_R/β at depth is 0.63β.) Agreement between the earthquake and foam rubber rupture velocities may be fortuitous or may be caused by a common physical friction mechanism.

CHOICE OF FAULT MODELS

All "deterministic" source models specify some (nearly always kinematic) conditions at the source, which then fix via the representation theorem of de Hoop (1958) and Burridge and Knopoff (1964), the complete time history at every point in the medium. (Aki (1967, 1972) and Haskell (1966) proposed "statistical" models in which only the amplitude spectrum at the source function is specified. Since we will be looking at dislocation rise times, these statistical models

TABLE 3.2

Observed Rupture Velocities

	Event	V_R(Km/sec)	V_R/β
2	Tango 1927	2.3	.65
4	Saitama 1933	2.3	.65
5	Sanriku 1933	3.2	.71
6	Long Beach 1933	2.3	.65
8	Tottori 1943	2.3	.65
12	Fukui 1948	2.3	.65
16	Chile 1960	3.5	.78
17	Kitamino 1961	3.0	.86
18	Wasaka Bay 1963	2.3	.65
20	Kurile Is 1963	3.5	.78
22	Spain 1964	1.4	.40
23	Alaska 1964	3.5	.78
25	Rat Island I 1965	4.0	.89
27	Parkfield 1966	2.7	.77
32	Tokachi-Oki 1968	3.5	.78
33	Saitama 1968	3.4	.97
35	Kurile Is 1969	3.8	.85
36	Gifu 1969	2.5	.71
37	Peru 1970	2.5	.56
38	San Fernando 1971	2.4	.69

Average of V_R/β = .72 (for 20 events)

are not appropriate choices.) Typically the source theory papers calculate seismograms for an isotropic homogeneous whole space. Since our interest is in logarithmic source parameters, we will assume the whole space models are adequate.

In most deterministic source models, either fault dislocation (e.g., Haskell (1969), Mikumo (1973b)) or stress drop (and therefore fault dislocation, e.g., Burridge and Willis (1969), Richards (1973), Sato and Hirasawa (1973)), is specified, which in turn gives displacement at other points in the medium. Other authors, e.g., Hanson et al. (1974) and Andrews (1975), have studied numerical models with friction between the fault surfaces.

All of these models predict far-field pulses which scale linearly with fault dimensions. Also they all yield flat spectra at low frequencies and ω^{-n} high frequency asymptotes ($n \geq 2$). Thus all of the models have at least one "corner frequency" (and some have several). For these models the static or low frequency level, which is proportional to seismic moment, grows as L^3.

We will continue to use the Haskell (1964, 1969) model of a rectangular fault (shown in Fig. 3.3) in this chapter. Most studies have used this model in the determination of rise times from local seismograms. The basic Haskell model is a fault with length L, width W, rise time τ (linear ramp time function), final dislocation $\bar{D}$ and rupture velocity V_R. Rupture is instantaneous in the width direction and propagates (starting at one end) along the length with velocity V_R. Some investigators have made the natural extension to bilateral

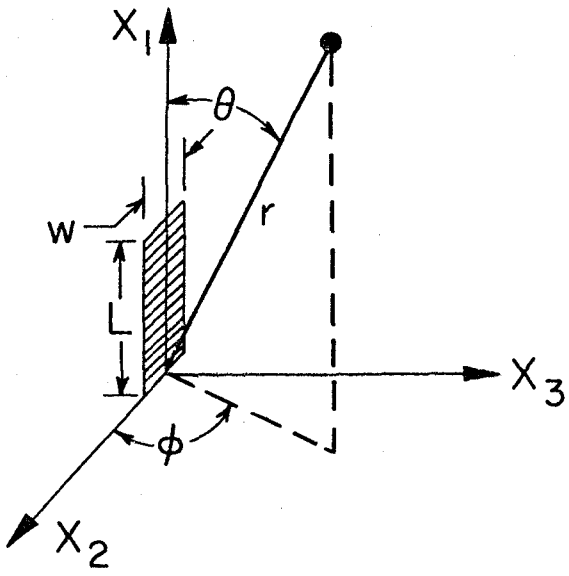

Figure 3.3 - The Haskell (whole space) fault model.

rupture propagation.

Haskell's (1964) expressions are for a "one-dimensional" model in which width is included only as a weighting factor in the moment. Hirasawa and Stauder (1965) and Mikumo (1969) included the complete effect of the width to obtain an expression for spectral source amplitude.

$$\left|U_c(\omega)\right| = \frac{M_o R^c_{\theta\phi}}{4\pi\rho r c^3} \left|\frac{\sin(\omega\chi_\tau)}{\omega\chi_\tau}\right| \left|\frac{\sin(\omega\chi_L)}{\omega\chi_L}\right| \left|\frac{\sin(\omega\chi_W)}{\omega\chi_W}\right| \tag{3.6}$$

In (3.6) M_o is moment, ρ is density, r is distance, c is either P or S velocity and $R^c_{\theta\phi}$ is the radiation pattern (given by Haskell, 1964). χ_L and χ_W are duration times associated with length and width, respectively and determined by fault geometry and position of the observer.

$$\chi_L = \left|L(1/v_R - \cos\theta/c)/2\right| \tag{3.7}$$

$$\chi_W = \left|W(\cos\phi \sin\theta)/(2c)\right| \tag{3.8}$$

$$\chi_\tau = \tau/2 \tag{3.9}$$

SPECTRAL CHARACTERISTICS

For the present, let us adopt (in slightly modified form) the similarity relations given by Kanamori and Anderson (1975b).

$$\frac{W}{L} = C_1 = const \tag{3.10}$$

$$\frac{\bar{D}}{L} = C_2 = \text{const} \tag{3.11}$$

$$\frac{\beta\tau}{L} = C_3 = \text{const} \tag{3.12}$$

(3.10) is the condition of geometrical similarity; (3.11) and (3.12) imply constant stress drop and constant effective stress.

We will select values of the constants which seem to be good averages of observational data. We found that

$$L = 2W \tag{3.13}$$

seemed to be the approximate average of the empirical data. When we substitute (3.13) into (3.5) and set β = 4.0 km/sec we get

$$\tau = (16\sqrt{L^2/2} \;/\; (7\pi^{3/2} \cdot 4)) = .0726L \tag{3.14}$$

where τ is in seconds and L is in kilometers.

We could use (3.11) directly to get a scaling relation between fault displacement and length. In practice though, most estimates of $\bar{D}$ in Table 3.1 come from dividing M_o by μS, so it seems better to relate moment directly to length. Setting L = 2W in (3.4) gives moment in terms of fault length and stress drop.

$$M_o = L^3\Delta\sigma \cdot 16/(7(2\pi)^{3/2}) = (1.45 \times 10^{20})\, L^3\Delta\sigma \tag{3.15}$$

where M_o is in dyne cm, L is in km and $\Delta\sigma$ in bars.

From (3.6) we can isolate a spectral factor, dependent only on fault parameters and frequency.

$$A(\omega) = L^3 \left|\frac{\sin(\omega\chi_\tau)}{\omega\chi_\tau}\right| \left|\frac{\sin(\omega\chi_L)}{\omega\chi_L}\right| \left|\frac{\sin(\omega\chi_W)}{\omega\chi_W}\right| \qquad (3.16)$$

The L^3 term follows from the similarity relation $M_o \sim L^3$. When $A(\omega)$ is multiplied by stress drop and the constant in similarity equation (3.15) we get the source moment rate spectrum.

Equation (3.16) and the factors (3.7)-(3.9) are well known results for the case of a rectangular fault in a whole space. These expressions can also be applied directly to the case of a rectangular fault with horizontal rupture propagation in the earth. (In doing so, Geller's (1976) use of apparent velocity in place of body wave velocity is corrected.)

For body waves the apparent velocity at the receiver, $v_{app} = c/\sin i$, where c is the near-field P or S velocity and i is the takeoff angle of the teleseismic ray from the focal sphere. This can be understood physically by invoking reciprocity. Signals from a source at the position of the teleseismic receiver would be picked up $(L \cos\theta)/(2c)$ sooner at the end of the fault than at the center. Thus for the case of infinite rupture velocity, this is the difference between arrivals at the receiver from the end and center of the fault. This type of geometrical interpretation can be applied to both (3.7) and (3.8), so that these factors are seen to be

the difference in arrival times obtained from geometrical optics. Ben-Menahem (1962) gives a more rigorous derivation of this result.

For surface waves (3.7) is the well known directivity factor first given by Ben-Menahem (1961). If we neglect the variation of the excitation function with depth, (3.8) is the factor for the effect of fault width on the surface wave spectrum. In both (3.7) and (3.8), c is the (frequency dependent) surface wave phase velocity. The geometrical interpretation of (3.7) and (3.8) as phase delay between "arrivals" from the center of the fault and the ends is the same as for body waves.

Typical values of c for teleseismic P waves might be 8 km/sec, while for surface waves 4 km/sec is appropriate. If rupture velocity, v_R = 2.5 km/sec, then for surface waves 1/c will be of the same order of magnitude as $1/v_R$. As θ varies from 0 to 2π, χ_L will range from 0.08L to 0.32L. Thus a horizontally propagating rupture will cause a large directivity effect. On the other hand, for body waves from the same source, $\cos\theta = \sin i$. Because of the relatively steep takeoff angles of teleseismic rays, it is reasonable to assume $|\cos\theta| < 0.5$.

This assumption leads to the conclusion that χ_L will vary only from 0.16L to 0.24L. There will be only a small azimuthal dependence (i.e. directivity effect) of the teleseismic body wave pulse. This implies that one can infer the nature of a horizontal rupture propagation much more easily from surface waves than teleseismic body waves.

Because of the different directivity functions for body and surface waves, it is inadequate to present only a single spectrum

representing the effect of the seismic source, as was done, for example, by Aki (1967, 1972). There is a separate "source spectrum," $A(\omega)$, for each body wave phase or surface wave mode.

The source spectrum depends on azimuth, source dimensions, and the velocity, c. Both the length factor, (3.7) and the width factor, (3.8), are different for each mode. In the next section we will average χ_L and χ_W over all azimuths. In these averages, the value of c will affect only χ_W, even though both factors are affected at nearly every particular azimuth.

Both (3.6) and (3.16) completely neglect the effect of the earth's transfer function on observed seismic waves. If one were to calculate synthetic seismograms for an individual earthquake, it would be necessary to consider the earth's response and the earthquake source parameters, e.g., Fukao (1971) or Langston and Helmberger (1975) for body waves or Harkrider (1964, 1970) for surface waves. Fukao (1971) and Langston and Helmberger (1975) have demonstrated that sP and pP phases play a crucial role in the "P wave" from shallow earthquakes. Similarly one must consider the surface wave excitation functions and the source mechanism to calculate accurate Rayleigh and Love amplitudes.

In this chapter we consider trends among events, rather than accurate determination of parameters of particular events. Therefore, we assume that the effect of the earth structure averages out when we construct scaling relations. Thus we will use (3.16) to get relations between m_b and M_s, log L and M_s, log M_o and M_s.

AVERAGE SPECTRA

We now want to find average asymptotic forms for log $A(\omega)$ from (3.16). In particular we require expressions for teleseismic P phases (from which m_b will be determined) and for 20-second Rayleigh waves (from which we find M_s). For both cases we will find average values of χ_L and χ_W which take the direction of radiation into account. In making our approximation, we will replace $|(\sin X)/X|$ by one for $X < 1$ and by X^{-1} for $X \geq 1$.

Takeoff angles of teleseismic body waves are nearly vertical. We will adopt the approximation that the rays takeoff straight down. Thus, for body waves, we set $\theta = \frac{\pi}{2}$ in (3.7) and (3.8). Also, in that case, $|\cos \phi| = \sin \delta$, where δ is dip angle of the fault plane. Using these values, average spectral factors for body waves are

$$\langle \chi_L \rangle_{body} = L/(2V_R) \tag{3.17}$$

and

$$\langle \chi_W \rangle_{body} = W \sin \delta/(2c) \ . \tag{3.18}$$

For surface waves we will average χ_L and χ_W for $\theta = 0$ to $\theta = 2\pi$. On the earth's surface we get $|\cos \phi| = \cos \delta$. Thus we get

$$\langle \chi_L \rangle_{surf} = L/(2V_R) \tag{3.19}$$

and

$$\langle \chi_W \rangle_{surf} = W \cos \delta / (\pi c). \tag{3.20}$$

Comparison of (3.17) and (3.18) with (3.19) and (3.20) shows that the average corner frequency due to fault length will be the same for body waves and surface waves, but that the corner frequencies due to width will be different. This difference affects the high frequency spectrum only since the average corner frequency for width is higher than that for rise time or length. Note that we have assumed that rupture propagates parallel to the earth's surface to obtain (3.17)-(3.20).

Before calculating numerical values for (3.17)-(3.20) we must fix V_R, δ and c. Also we will use (3.13) to relate L to W. We will set V_R = 2.88 km/sec, $\delta = 45^o$, c = 8 km/sec for P waves and c = 3.9 km/sec for surface waves. (For the earth, c must be the appropriate phase velocity, not the S wave velocity. Neglecting the frequency dependence of surface wave phase velocity is a reasonable approximation.)

From (3.9) and (3.14)

$$\chi_\tau = 0.0363\ L = C_\tau L \tag{3.21}$$

(3.17) and (3.19) both give

$$\langle \chi_L \rangle = 0.174\ L = C_L L \tag{3.22}$$

The width factor for body waves is

$$\langle \chi_W \rangle_{body} = 0.0220\ L = C_{Wb} L \tag{3.23}$$

For surface waves we get

$$\langle X_W \rangle_{surf} = 0.0289\ L = C_{Ws} L \tag{3.24}$$

We now can approximate the logarithm of $A(\omega)$ from (3.16).

$$\begin{aligned}
&\log A(\omega) = 3 \log L && \text{for } \omega < (C_L L)^{-1} \\
&\log A(\omega) = 2 \log L - \log \omega - \log C_L && \text{for } (C_L L)^{-1} < \omega < (C_\tau L)^{-1} \\
&\log A(\omega) = \log L - 2 \log \omega - \log (C_L C_\tau) && \text{for } (C_\tau L)^{-1} < \omega < (C_W L)^{-1} \\
&\log A(\omega) = -3 \log \omega - \log (C_L C_\tau C_W) && \text{for } (C_W L)^{-1} < \omega
\end{aligned} \tag{3.25}$$

The spectra from these relations are plotted in Figure 3.4. Note that the body wave spectra have a much longer interval of ω^{-2} decay than the surface wave spectra. As a result of the error in Geller (1976), the body wave spectrum in Figure 3.4 and the m_b-M_s curve in Figure 3.5 are actually for a fault dipping at $\delta = 24°$.

The asymptotic spectral amplitudes given by (3.25) are very similar to the results obtained by Kanamori and Anderson (1975b). They used the same asymptotic approximation for sin X/X in conjunction with Haskell's (1964) spectral expression. Since Haskell's expression ignores the effect of width on the spectrum, the results of this chapter differ from Kanamori and Anderson's only at frequencies above

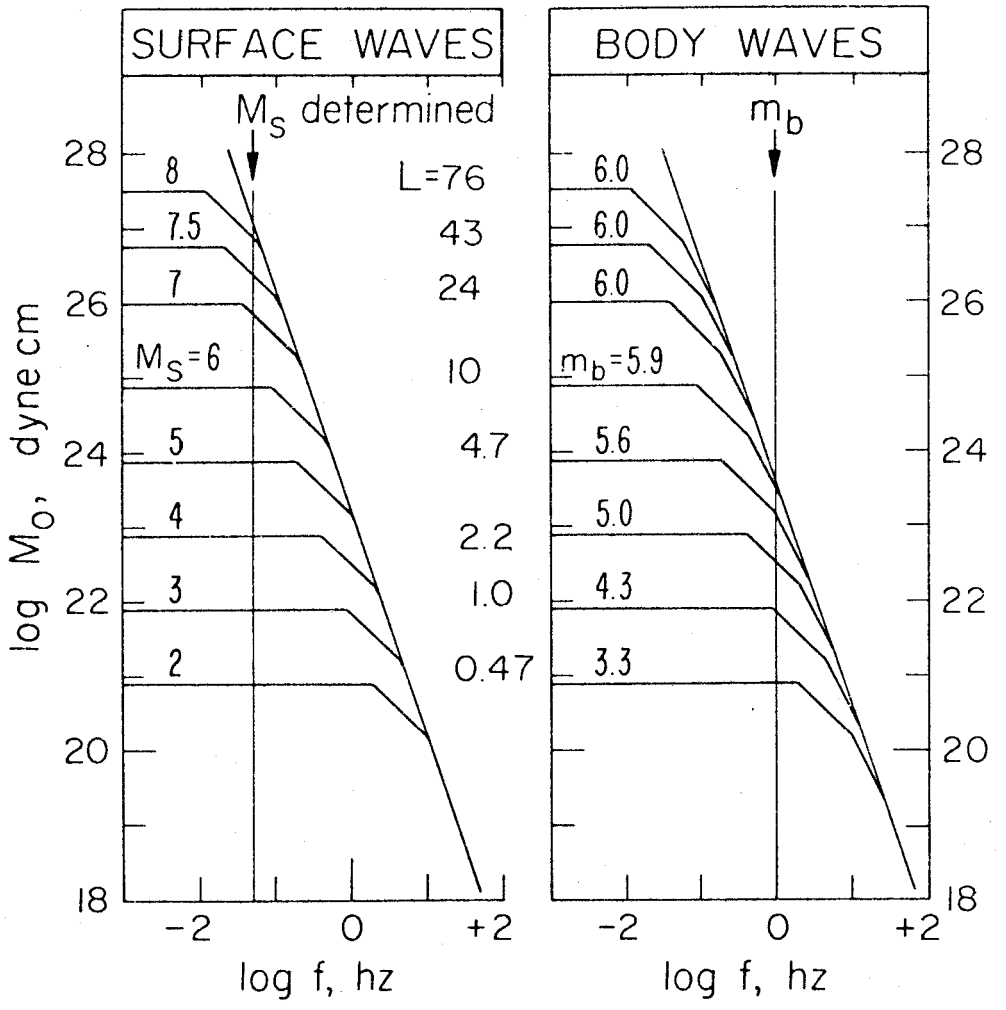

Figure 3.4 - Source spectra for surface waves (on left) and body waves. Both are identical at frequencies below the ω^{-2} corner frequency. The body waves have a higher width corner frequency than surface waves, which follows from (3.18), (3.20), (3.23) and (3.24). This difference occurs because teleseismic P waves, which takeoff essentially straight down, have a much higher apparent velocity (phase velocity) than surface waves. Therefore the separation between rise time and width corner frequencies (the ω^{-2} part of the spectrum) is much greater for body waves than for surface waves.

the corner frequency for width. For example, the model in this chapter predicts constant 20 sec spectral amplitude for faults longer than 110 km while Kanamori and Anderson's predicts amplitudes which increase linearly with L. As a result, their model predicts $M_s \sim \log L$ for large events, while this paper predicts M_s = const.

Even though both spectra in Figure 3.4 have an eventual ω^{-3} asymptote, they are quite different than Aki's (1967) ω-cube model. Aki's models, as a result of his assumption that $vk_L = k_T$, had only a single corner frequency. His ω-cube model makes a fairly abrupt transition from ω^0 to ω^{-3} behavior. The spectra presented here, particularly the body wave spectrum, show a gradual transition from ω^0 to ω^{-3} asymptotes.

m_b - M_s RELATION

Changes in the definition of the body wave magnitude scale have resulted in a large amount of confusion today. Gutenberg and Richter (1942) extended the body wave magnitude scale from local events to fairly distant events which were recorded on Wood-Anderson and strong motion torsion instruments.

Gutenberg (1945) introduced a scheme for m_b differing only in minor details from the summary in Richter (1958). He determined m_b from the instruments available in 1945, which were mostly broadband mechanical types. Gutenberg (1945) stated that "the average period of P waves in teleseisms is about 4-6 seconds." In general, Gutenberg did not publish the period of the P waves he used in determining m_b,

but from the examination of his unpublished data discussed in the last chapter it seems demonstrates that nearly all of his amplitudes were obtained at periods of 4-12 sec.

Gutenberg and Richter (1956) published their final version of the relation between m_b and M_s:

$$m_b = 0.63\ M_s + 2.50 \tag{3.26a}$$

$$M_s = 1.59\ m_b - 3.97 \tag{3.26b}$$

Their primary reason for deriving this relation was to facilitate the construction of a "unified magnitude scale." Investigators at that time apparently viewed the discrepancy between the two magnitude scales as an experimental error, rather than a fundamental effect of the seismic source spectrum. This view was not unreasonable at the time because m_b was measured at periods differing only by a factor of 2 to 5 from M_s and modern source theories had not yet been developed. In any case, as discussed in the last chapter, Gutenberg and Richter found the (body wave) magnitude m_s, corresponding to a given M_s, by using (3.26a). They then took a weighted average of m_b, the actual body wave magnitude, and m_s to obtain m, the unified magnitude. Later Richter (1958) published values of unified (surface wave) magnitude, M, which he obtained by converting m to M using (3.26b). In retrospect, unified magnitude was inappropriate, since it now is clear that for all seismic source theories m_b and M_s represent different parts of the spectrum which are not related by a

factor independent of fault length.

m_b determinations by the USCGS (later NOAA and now the USGS) differ markedly from those used by Gutenberg and Richter. USCGS values for m_b use (3.1), but A and T are measured on the WWSSN short period instrument, which is sharply peaked at 0.5 sec. T nearly always is about 1 sec in WWSSN magnitude determinations. Thus WWSSN magnitudes are based roughly on 1 sec spectral amplitude. On the other hand, Gutenberg and Richter determined m_b for many events at about 5 sec, with even larger T for the largest events. Therefore, it is wrong to take the Gutenberg-Richter m_b as being related to spectral amplitude at any one particular period.

MODELING $m_b - M_s$

Aki (1967) proposed two statistical models of seismic sources, an "ω-square" model (which decayed as ω^{-2} at high frequencies) and an "ω-cube" model, after Haskell (1966) (which decayed as ω^{-3}). Aki compared these two models by calculating spectral ratios for similar events and by calculating the relation of m_b to M_s predicted by each model.

Aki calculated M_s by adding a constant to the logarithm of spectral amplitudes at 20 sec. The constant was chosen to give the best agreement between theoretical and observational spectral ratios of pairs of similar earthquakes studied by Berckhemer (1962). After fixing the additive constant for M_s, Aki then defined a similar relation for m_b. He set m_b = const + (.71 ∿ .83) log A(1 sec) and

found the constant which would make $m_b = M_s$ when $M_s = 6.75$. The coefficient of log A(1 sec) comes from a correction for duration.

Aki (1967) calibrated his curves for the ω-square and ω-cube models in this way. He then compared the m_b-M_s curves predicted by the models to the Gutenberg-Richter m_b-M_s relation (3.26). He suggested that the excellent agreement of the ω-square model with (3.26) strongly supported it, over the ω-cube model. Unfortunately, his theoretical m_b-M_s curve was based on 1-sec spectral amplitudes, while (3.26) was derived from mostly 4 to 10 sec data. Actually it seems that Aki's support for the ω-square model was incorrect. The WWSSN m_b-M_s data (based on 1 sec m_b), discussed below, disagree with the ω-square model.

The approach in this chapter is to match m_b-M_s, log S-M_s, log M_o-M_s and spectral ratio data simultaneously, adjusting the two free parameters to get good overall agreement with the data. A least squares solution is not particularly appropriate because of the large number of parameters and the lack of similarity (e.g., different stress drops) found when earthquakes are examined in detail.

m_b is approximated by a constant plus log A(1 sec) and M_s by another constant plus log A(20 sec). A(ω) was found using (3.25) with the constants in (3.21)-(3.24). After several trials the additive constants for m_b and M_s were determined to be $C_{m_b} = 4.30$ and $C_{M_s} = 2.97$. To obtain seismic moment as a function of L, it was necessary to assign $\Delta\sigma$ for use in (3.15). Kanamori and Anderson (1975b) found that stress drops are 10-30 bars for most interplate earthquakes and 30-100 bars

for most intraplate earthquakes, so $\Delta\sigma$ = 50 bars was used.

Clearly it is not exactly correct to get m_b and M_s directly from spectral amplitudes. A more accurate approach would be computing synthetic seismograms and then measuring m_b and M_s as it is done for data. For this study, using spectral amplitudes seems to be an acceptable approximation.

Archambeau (1975) thoroughly discusses the differences between time domain and frequency domain estimates of m_b and M_s. His study stressed the very small differences which are crucial in the context of seismic discrimination. In general though, his study supports the applicability of using spectral amplitudes to estimate m_b of small and moderate events. Probably any discrepancy between spectral amplitudes and time domain amplitudes is most severe for larger events.

m_b - M_s DATA

Two kinds of m_b - M_s data are plotted in Figure 3.5. Points below the solid line midway up the figure are from a study of almost one thousand events by Evernden (1975). Each point is the average value of M_s for all earthquakes with that m_b value. Because Evernden's m_b values are an average of 0.3 lower than the USGS values, 0.3 is added to the m_b values before plotting them. Points above the line are values for individual events since mid-1963 as listed in Table 3.1.

Data shown in Figure 3.5 are in general agreement with a study of the m_b - M_s relation by Nagamune (1972). Nagamune fitted two straight lines to two years of WWSSN m_b - M_s data. He found

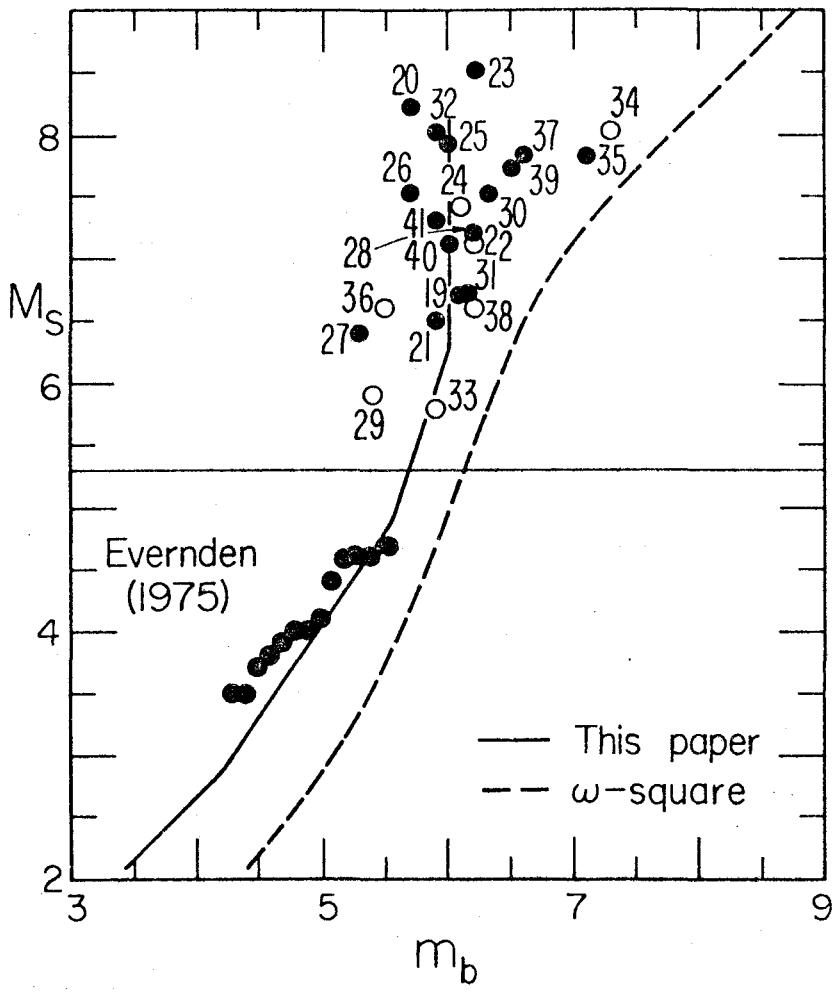

Figure 3.5 - USCGS m_b versus M_s. Lower data points are averages from Evernden (1975), corrected by adding 0.3 to m_b. Upper points (above horizontal line) are individual earthquakes from Table 3.1. Dashed curve is m_b-M_s relation from ω-square model. Solid curve is from (3.21) to (3.25) as described in the text.

$$M_s = 1.89\ m_b - 4.62 \qquad M_s > 5.73$$

and

$$M = 1.05\ m - 0.02 \qquad M < 5.73$$

The latter equation comes from a study of small events mostly in Hokkaido. Magnitudes in the latter equation are very similar to m_b and M_s.

m_b - M_s curves from two models are plotted in Figure 3.5. The curve on the right is the m_b - M_s relation predicted by Aki (1972), which is based just on log A(1), without any correction for duration. It can be seen that all the data lie substantially to the left (smaller m_b) of the ω-square curve. Inclusion of a duration correction for large events would not affect the basic conclusion that the ω-square model does not agree with the data.

The lefthand curve is derived from the Haskell model presented in this chapter. It can be seen that the predicted m_b - M_s curve is generally in good agreement with the data. It would have been better to have averaged the value of m_b for all earthquakes with a particular M_s for all WWSSN events for several years, rather than present just a few data points.

The Evernden data have a slope of one for events with m_b smaller than 5½ while the predicted m_b - M_s curve has a slope of $\frac{3}{2}$ for $m_b > 4.2$, which clearly disagrees with the data. The large events are too scattered to warrant a definite conclusion, but the predicted maximum

m_b of 6.0 is probably 0.3 or 0.4 too small. This discrepancy may be due to use of spectral amplitudes instead of time domain amplitudes. Also, it was assumed above that m_b was always based on 1 sec observations, but this is not strictly true. The Portuguese earthquake of 1969 (number 34 in Table 3.1) has m_b of 7.3, the largest of any of the events in Table 1. The average T for this event was 1.77 sec; the Haskell model predicts that if m_b had been determined at 1 sec, it would be 0.5 smaller. A systematic variation of T as a function of m_b could account for part of the difference between the theoretical curve and observations. Another possible explanation of the difference may be heterogeneity of the source mechanism. This possibility is discussed later in more detail.

HIGH FREQUENCY SPECTRA

The Haskell model, which has ω^{-3} high frequency decay, moment proportional to L^3 and "corner frequency," ω_c, (for fixed source-receiver geometry, source similarity and source mechanism) proportional to L^{-1}, is a particular member of a general class of models having those properties. Following an argument first suggested by Savage (1972), note that for many source models the area radiating energy to a far-field observer will appear to grow as t^2 and dislocation from that area will grow linearly with t. The far-field pulse, which is the time derivative of the moment function will grow as t^2, giving (Bracewell, 1965, p. 144) ω^{-3} high frequency spectral decay (assuming the t^2 onset is the most abrupt discontinuity). Many models will also

have a "corner frequency" proportional to L^{-1}, where L is some characteristic source dimension of that model. Finally, most models give $M_o \sim L^3$, where L is a source dimension. For all models meeting the above three requirements, high frequency spectral amplitudes will behave as

$$A(\omega) \sim M_o(\omega_c/\omega)^3 \sim L^3(L^{-1}/\omega)^3 \sim \omega^{-3} \ .$$

Thus, all events with fixed geometry and source type will share a common high frequency asymptote which is independent of L. Therefore the conclusion that m_b, and for much larger events, M_s, will have a maximum value, applies to a more general class of models. For example, Minster (1973), derived $m_b - M_s$ curves (with a similar shape to the curve from the Haskell model in Figure 3.5) from an Archambeau type (volume) source (also ω^{-3} falloff), although he did not calibrate them against $m_b - M_s$ data. Minster's results also predict maximum values of m_b and M_s.

Many investigators, such as Richards (1973), Dahlen (1974), Sato and Hirasawa (1973) and Madariaga (1976) have outlined crack models for which the initial rupture contributes an ω^{-3} high frequency spectrum while a "stopping phase" caused by simultaneous cessation of fracture everywhere on the fault contributes ω^{-2} and therefore dominates the high frequency spectrum. If such models are applicable, m_b, which is based on the initial rupture, would still have a maximum value, but M_s would not.

M_s VERSUS FAULT AREA

Figure 3.6 is a plot of fault area, S, (taken from Table 3.1) and M_s. The predicted M_s - log S curve derived from (3.21) - (3.25) agrees quite well with the data. Note that the theoretical curve has four different segments. For small earthquakes, up to $M_s = 6.76$, the slope is $\frac{2}{3}$. From $M_s = 6.76$ to $M_s = 8.12$, the region in which most moderately large earthquakes are clustered, the slope is 1. There is a small section for which the slope is 2, from $M_s = 8.12$ to $M_s = 8.22$. After $M_s = 8.22$, the largest value of M_s for this calibration of the Haskell model, the slope is infinite (e.g., S increases with no further increase in magnitude).

There is a systematic difference between the interplate (closed circles) and intraplate (open circles) in Figure 3.6. Half of the intraplate events fall below the predicted M_s - log S curve, while nearly all interplate earthquakes are above the curve. Kanamori and Anderson (1975b) showed that, at least in the region with slope one, this meant intraplate events had a higher apparent stress.

Utsu and Seki (1954) found the empirical relation $\log S = 1.02 \times M - 4.01$. Their M is Japan Meterological Agency (JMA) magnitude, which in practice is roughly equivalent to M_s, and S is in km^2. For the unit slope part of the M_s - log S curve in Figure 3.6 ($M_s > 6.76$) the Utsu-Seki relation predicts about five times the fault area. This may be due to the way Utsu and Seki apparently determined fault area. They used an area encompassing nearly all the aftershocks, rather than the one-day aftershock zone which seems to give much better agreement

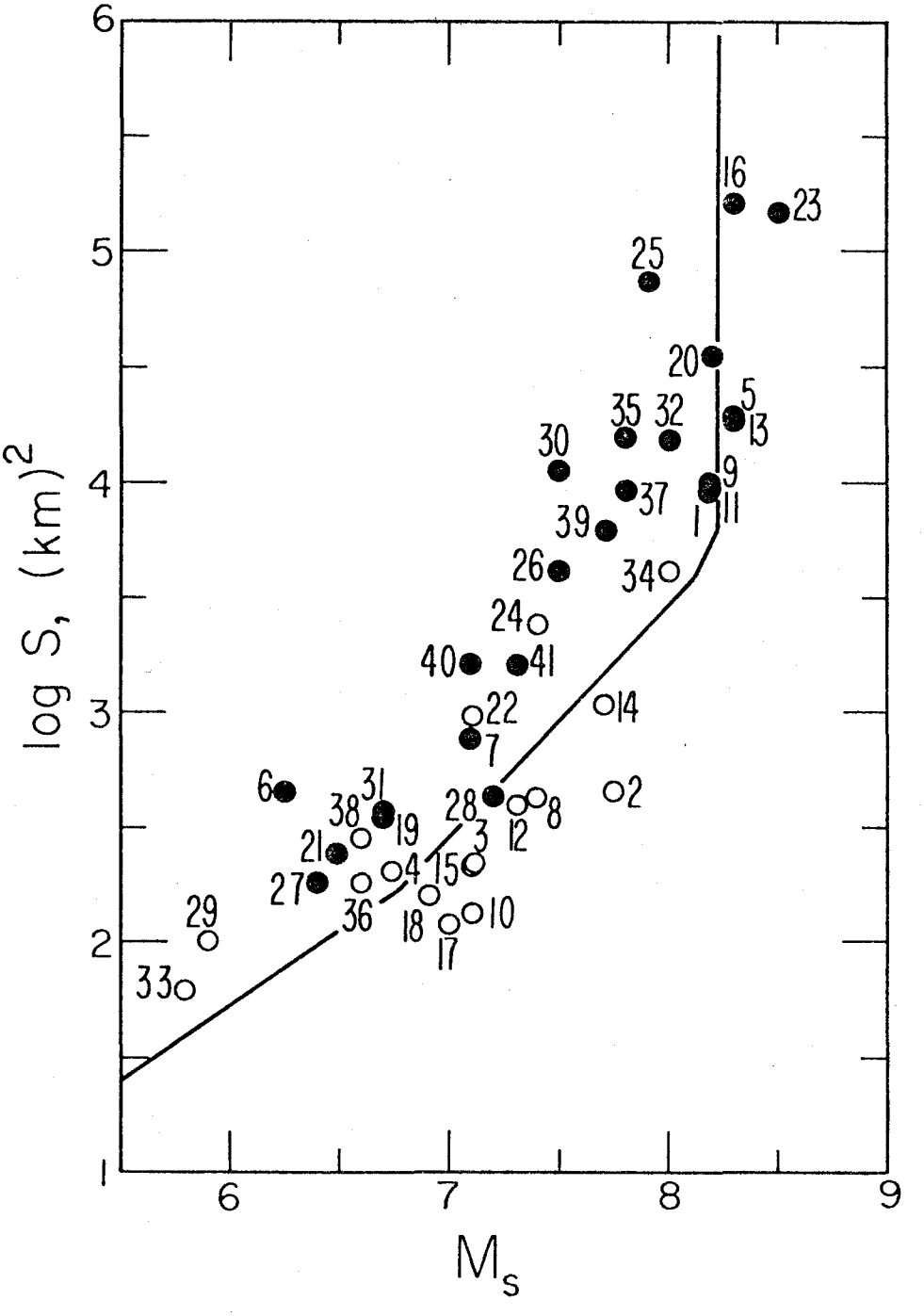

Figure 3.6 - M_s versus log S data with theoretical curve from the model in this chapter.

with observed fault dimensions for earthquakes on continents. Båth and Duda (1964) proposed the relation log S = 1.21 M_s - 5.05, based on a study of six earthquakes from different regions. Båth and Duda used S as aftershock area (in km^2), not fault plane area, so this is basically similar to Utsu and Seki's result. Chinnery (1969) summarizes a number of efforts to find a single linear relation between M_s and the logarithm of other fault parameters.

M_s VERSUS MOMENT

The data of Kanamori and Anderson (1975b) show that $\Delta\sigma$ = 50 bars is a good average, about halfway between values for interplate and intraplate events. Using $\Delta\sigma$ = 50 and (3.15), we find moment (in dyne cm) is related to fault length (in km) by $M_o = (2.05 \times 10^{22}\ L^3$ or log M_o = 22.3 + 3 log L. It was shown above that $M_s \sim n \log L$, where n varies between 0 and 3, as can be seen from the surface wave spectra in Figure 3.4. Therefore, for small earthquakes the M_s:log M_o slope is one; for very large events ($M_s \sim$ constant) the slope is infinite (M_o increases but M_s is already at a maximum.).

The log M_o - M_s data from Table 1 are plotted in Figure 3.7. Most of the moderate sized events (M_s from 6.76 to 8.11) fall on the slope 1.5 portion of the curve ($\log M_o \sim \frac{3}{2} M_s$). This part of the curve corresponds to cases where 20 sec spectral amplitudes are measured on the ω^{-1} part of the spectrum. Because the corner frequency for width is only slightly greater than that for rise time, the slope 3 ($M_o \sim 3 \log M_s$) region is very small, extending only from M_s = 8.12 to

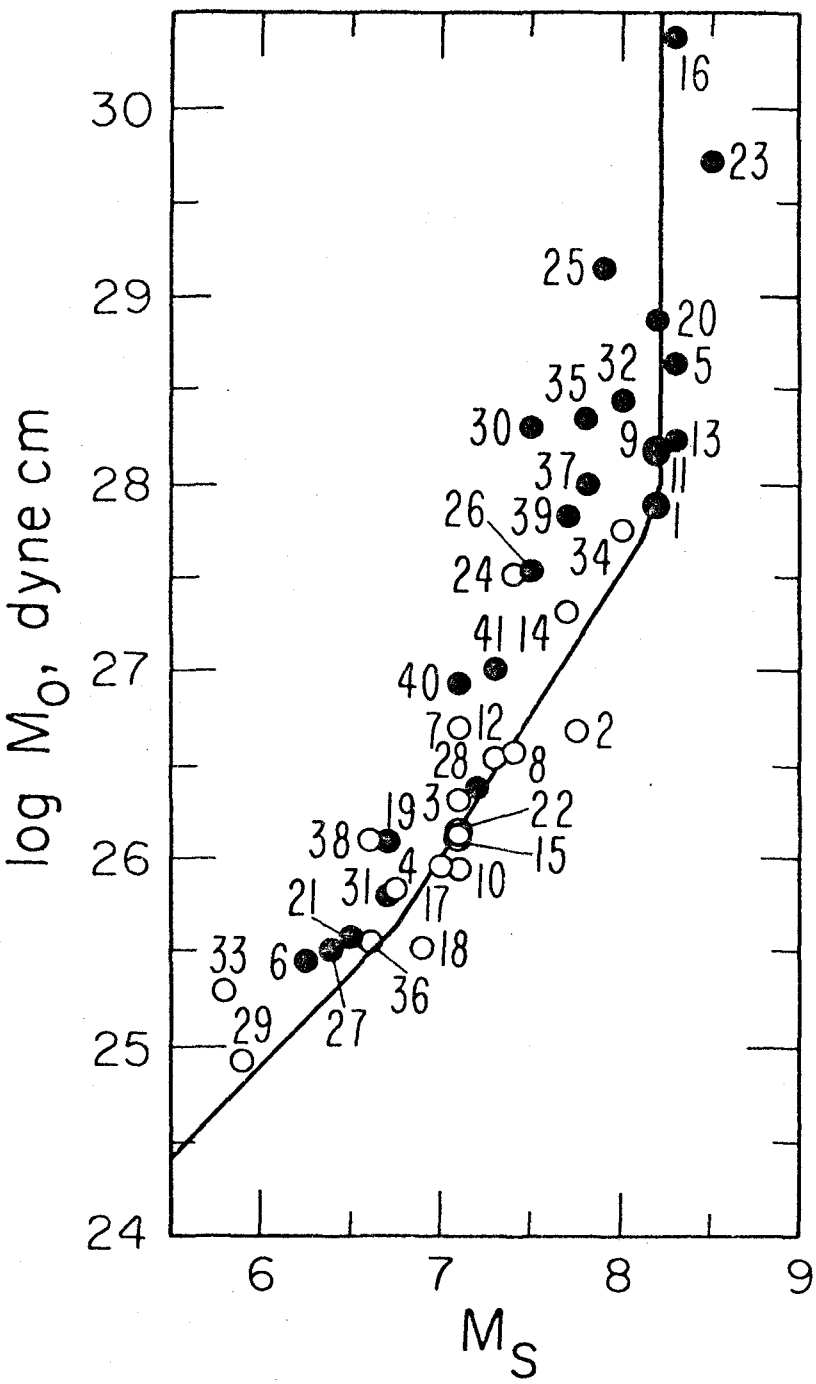

Figure 3.7 - M_s versus log M_o data with theoretical curve from the model in this chapter.

M_s = 8.22. Beyond that, slope is infinite. The data agree quite well with the theoretical curve. As in Figure 3.6, intraplate events tend to have smaller M_o for a given M_s, corresponding to higher apparent stress.

Aki (1972) showed that his ω-square model also agreed well with M_s vs. log M_o data. Brune and co-workers (Brune and King, 1967; Brune, 1968; and Brune and Engen, 1969) presented a magnitude scale based on 100 sec surface wave amplitude. They then assumed log $M_o \sim$ log A(100) and fit two segments, each with slope 1, to the data. Because of their different definition of M_o, their results cannot be directly compared to this chapter.

Data in this section show that when M_o is larger than about 10^{28} dyne cm, M_s reaches its maximum value. It is important to consider this when discussing the "maximum credible earthquake" likely to occur in a particular area. The earthquake size may be specified in terms of M_s for most earthquakes, but when the moment approaches 10^{28}, magnitude no longer is a valid parameter for specifying earthquake "size." Whenever the maximum credible earthquake is in this range, e.g., as is probably the case in discussing the Alaskan pipeline, moment, not M_s, should be the parameter used.

SPECTRAL RATIOS OF SIMILAR EVENTS

Berckhemer (1962) studied spectral ratios of earthquakes with roughly the same location and mechanism. In theory, the spectral ratio method eliminates the effect of earth structure and leaves only effects

due to the difference in source spectra. Aki (1967) used Berckhemer's data to determine the relation between M_s and corner period for the ω-square and ω-cube models.

Berckhemer's original data and Aki's theoretical curves are shown in Figure 3.8 together with the theoretical curve from the model in this paper. Both models seem to agree fairly well with the data. Perhaps Aki's fits slightly better. Berckhemer presented six pairs of spectra, of which only four are presented here. The remaining two pairs used smaller earthquakes, involving mostly short-period data, which probably are less reliable. No attempt at fitting these two pairs was made.

Tsujiura (1973) published spectral ratio data for many pairs of earthquakes. Most of his events could be fit by both Aki's ω-square model or Aki's (1972) version of Brune's "ω-model", although usually one model or the other fit somewhat better. There were, however, two pairs of events from the Aleutians which had spectral ratios that were *unusually flat and could not be fit by either model.* Tsujiura's spectral ratio data have not yet been compared to the model in this chapter.

DISCUSSION

The Haskell model with parameters (3.21)-(3.24) is in general agreement with m_b-M_s data (Fig. 3.5), M_s - log S data (Fig. 3.6), M_s - log M_o data (Fig. 3.7) and spectral ratio data (Fig. 3.8). The most serious discrepancy between the data and the model comes in Figure 3.5.

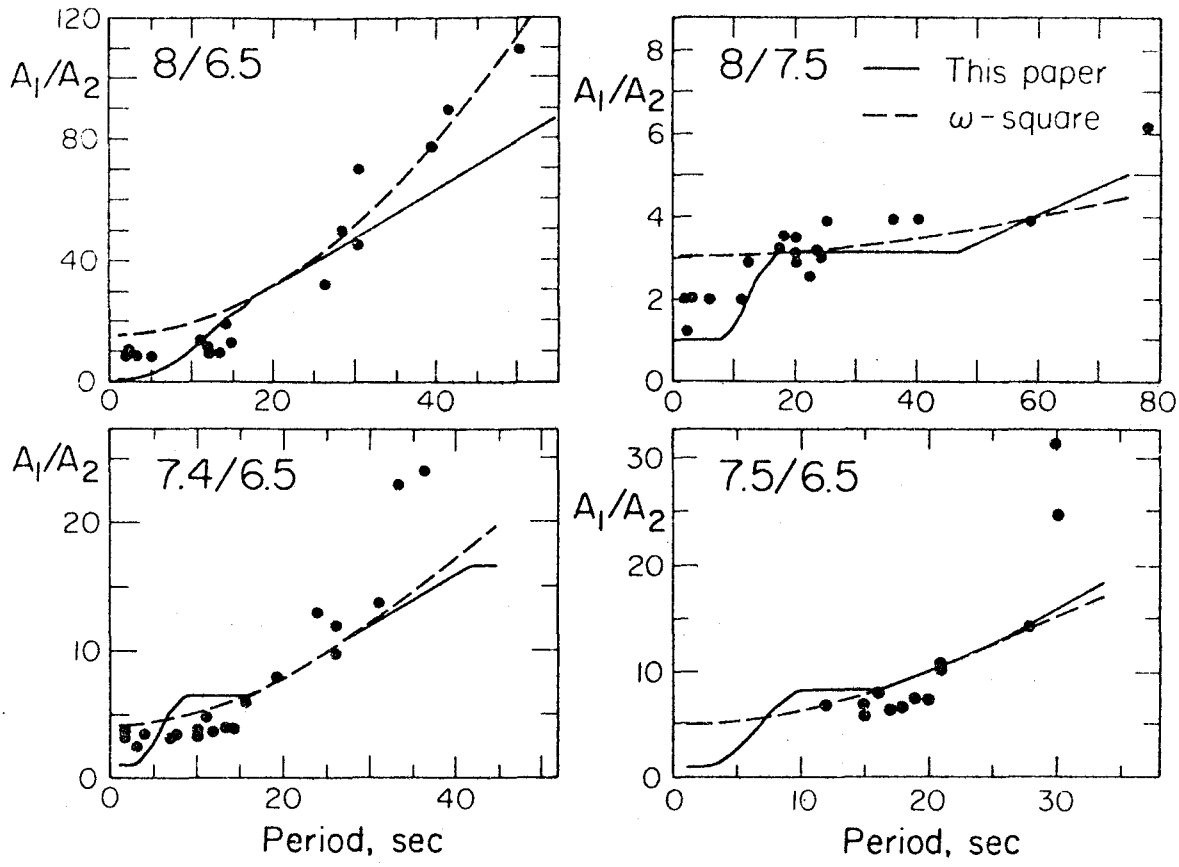

Figure 3.8 - Spectral ratios of similar earthquakes from Berckhemer (1962). Numbers above each figure are magnitudes of the larger and smaller of the events. Dashed line is ω-square model and solid line is model from this chapter.

On one hand, the maximum value of m_b is probably several tenths too small. On the other, the data seem to have a slope of about one up to $m_b = 5\frac{1}{4}$, while the curve from the model has slope one only up to $m_b = 4.19$.

This phenomenon could be explained if most earthquakes are complex sources with the first burst of energy coming from a smaller, substantially higher stress drop, source than the average of the whole earthquake. If this is the case, then m_b would be measured on a flat or flatter part of the spectrum than one would expect for the earthquake as a whole.

Burdick and Mellman (1976) have suggested that for the Borrego earthquake of 1968 most of the body wave energy came from a source region with radius of 8 km, giving about half the area shown in Table 3.1. Since they also found a higher moment, 0.112×10^{27} dyne cm, their stress drop, 96 bars, is about 4 times the value in Table 3.1, taken from Hanks and Wyss (1972). Tucker and Brune (1975) also suggested that sources showed a smaller high stress drop event superimposed on the overall average event. The m_b-M_s data in Figure 3.5 agree with the possibility of the initial fracture having higher stress drop than the bulk event, but certainly do not prove that this happens. Other explanations are equally admissible.

SUMMARY

The following scaling relations relating width and rise time to length and fault area are given:

$$L = 2W$$

$$\tau = 16S^{1/2} / (7\pi^{3/2}\beta) \ .$$

The relation for rise time was derived from the assumption that static stress drop and dynamic effective stress are equal; agreement of theoretical rise times with the data supports that assumption.

Averages of observed rupture velocities show that $V_R = 0.72\beta$.

The Haskell model predicts that magnitude will reach an upper limit regardless of further increases in fault length and seismic moment. Moment, rather than magnitude, should be used to discuss the possible size of great earthquakes.

The "source spectrum" from any source model is a function of apparent (phase) velocity of the mode or phase being considered, as well as of azimuth and source parameters. It is incorrect to speak of single "source spectrum."

Theoretical relations between m_b and M_s from the Haskell model are:

$$M_b = M_s + 1.33 \qquad M_s < 2.86$$

$$m_b = \frac{2}{3} M_s + 2.28 \qquad 2.86 < M_s < 4.90$$

$$m_b = \frac{1}{3} M_s + 3.91 \qquad 4.90 < M_s < 6.27$$

$$m_b = 6.00 \qquad 6.27 < M_s \ .$$

M_s and fault area (in km^2) are related by

$$\log S = \frac{2}{3} M_s - 2.28 \qquad M_s < 6.76$$

$$\log S = M_s - 4.53 \qquad 6.76 < M_s < 8.12$$

$$\log S = 2M_s - 12.65 \qquad 8.12 < M_s < 8.22$$

$$M_s = 8.22 \qquad S < 6080 \text{ km}^2$$

if L = 2W is used.

If we assume a stress drop of 50 bars, then log M_o (in dyne cm) and M_s are related by

$$\log M_o = M_s + 18.89 \qquad M_s < 6.76$$

$$\log M_o = \frac{3}{2} M_s + 15.51 \qquad 6.76 < M_s < 8.12$$

$$\log M_o = 3M_s + 3.33 \qquad 8.12 < M_s < 8.22$$

$$M_s = 8.22 \qquad \log M_o > 28$$

These scaling relations fit observed data quite well. They should not be used to determine the value of a parameter for any individual earthquake, since these "averages," and the assumptions made to derive them,

are not exactly correct for any single event.

A review of work by Gutenberg and Richter reveals that their $m_b - M_s$ relation was derived from m_b data at mostly 5 or 10 second period. Models such as Aki's (1967) ω-square model which fit theoretical 1 sec m_b data to the Gutenberg-Richter relation are probably in error.

REFERENCES

Abe, K. (1972a). Lithospheric normal faulting beneath the Aleutian trench, Phys. Earth. Plan. Interiors, 5, 190-198.

Abe, K. (1972b). Mechanisms and tectonic implications of the 1966 and 1970 Peru earthquakes, Phys. Earth Plan. Interiors, 5, 367-379.

Abe, K. (1973). Tsunami and mechanism of great earthquakes, Phys. Earth Plan. Interiors, 7, 143-153.

Abe, K. (1974a). Fault parameters determined by near and far field data: The Wasaka Bay earthquake of March 26, 1963, Bull. Seism. Soc. Am., 64, 1369-1382.

Abe, K. (1974b). Seismic displacement and ground motion near a fault: The Saitama earthquake of September 21, 1931, J. Geophys. Res., 79, 4393-4399.

Abe, K. (1975a). Re-examination of the fault model for the Niigata earthquake of 1964, J. Phys. Earth, 23, 349-366.

Abe, K. (1975b). Determination of static and dynamic fault parameters: The Saitama earthquake of July 1, 1968, Tectonophysics, 27, 223-238.

Abe, K. (1975c). Reliable estimation of the seismic moment of large earthquakes, J. Phys. Earth, 23, 381-390.

Aki, K. (1967). Scaling law of seismic spectrum, J. Geophys. Res., 72, 1217-1231.

Aki, K. (1972). Scaling law of earthquake source time function, Geophys. J., 31, 3-25.

Anderson, J. (1974). A dislocation model for the Parkfield earthquake, Bull. Seism. Soc. Am., 64, 671-686.

Ando, M. (1974). Faulting in the Mikawa earthquake of 1945, Tectonophysics, 22, 173-186.

Andrews, D. J. (1975). From moment to anti-moment: Plane-strain models of earthquakes that stop, Bull. Seism. Soc. Am., 65, 163-182.

Archambeau, C. B. (1975). Studies of multiple seismic events, ACDA/ST220, Final Report, Seismological Laboratory, California Institute of Technology, Pasadena, Ca. 91125

Archuleta, R. and J. N. Brune (1975). Surface strong motion associated with a stick-slip event in a foam rubber model of earthquakes, Bull. Seism. Soc. Am., 65, 1059-1071.

Båth, M. (1969). Handbook on earthquake magnitude determinations, Seismological Institute, Uppsala, Vesiac Special Report, 7885-36-X (second edition).

Båth, M. and S. J. Duda (1964). Earthquake volume, fault plane area, seismic energy, strain, deformation and related quantities, Ann. Geofis. (Rome), 17, 353-368.

Ben-Menahem, A. (1961). Radiation of seismic surface-waves from finite moving sources, Bull. Seism. Soc. Am., 51, 401-435.

Ben-Menahem, A. (1962). Radiation of seismic body waves from a finite moving source in the earth, J. Geophys. Res., 67, 345-350.

Berckhemer, H. (1962). Die Ausdehnung der Bruchflache im Erdbebenherd und ihr Einfluss auf das seismische Wellenspektrum, Gerlands

Beitr. Geophys., 71, 5-26.

Boore, D. M. and M. D. Zoback (1974). Two-dimensional kinematic fault modeling of the Pacoima Dam strong-motion recordings of the February 9, 1971, San Fernando earthquake, Bull. Seism. Soc. Am., 64, 555-570.

Bracewell, R. (1965). The Fourier transform and its applications, McGraw-Hill.

Brune, J. N. (1968). Seismic moment, seismicity and rate of slip along major fault zones, J. Geophys. Res., 73, 777-784.

Brune, J. N. (1970). Tectonic stress and the spectra of seismic shear waves from earthquakes, J. Geophys. Res., 75, 4997-5009.

Brune, J. N. (1971). Correction, J. Geophys. Res., 76, 5002.

Brune, J. N. and C. R. Allen (1967). A low stress-drop, low-magnitude earthquake with surface faulting: The Imperial, California earthquake of March 4, 1966, Bull. Seism. Soc. Am., 57, 501-514.

Brune, J. N. and G. R. Engen (1969). Excitation of mantle Love waves and definition of mantle wave magnitude, Bull. Seism. Soc. Am., 59, 923-933.

Brune, J. N. and C. Y. King (1967). Excitation of mantle Rayleigh waves of period 100 seconds as a function of magnitude, Bull. Seism. Soc. Am., 57, 1355-1365.

Burdick, L. J. and G. R. Mellman (1976). Inversion of the body waves from the Borrego Mountain earthquake to the source mechanism, Bull. Seism. Soc. Am., 66, 1485-1499.

Burridge, R. and L. Knopoff (1964). Body force equivalents for seismic dislocations, Bull. Seism. Soc. Am., 54, 1875-1888.

Burridge, R. and J. R. Willis (1969). The self-similar problem of the expanding elliptical crack in an anisotropic solid, Proc. Cambridge Phil. Soc., 66, 443-468.

Byerly, P. and J. DeNoyer (1958). Energy in earthquakes as computed for geodetic observations, in Contributions in Geophysics, In Honor of Beno Gutenberg, H. Benioff, M. Ewing, B. F. Howell and F. Press, editors, Pergamon Press, New York, 17-35.

Chinnery, M. A. (1964). The earth's crust under horizontal shear stress, J. Geophys. Res., 69, 2085-2089.

Chinnery, M. A. (1969). Earthquake magnitude and source parameters, Bull. Seism. Soc. Am., 59, 1969-1982.

Dahlen, F. A. (1974). On the ratio of P-wave to S-wave corner frequencies for shallow earthquake sources, Bull. Seism. Soc. Am., 64, 1159-1180.

de Hoop, A. T. (1958). Representation theorems for the displacement in an elastic solid and their application to elastodynamic diffraction theory, Thesis, Technische Hogeschool, Delft.

Evernden, J. F. (1975). Further studies on seismic discrimination, Bull. Seism. Soc. Am., 65, 359-391.

Fukao, Y. (1971). Seismic body waves from surface faults, J. Phys. Earth, 19, 271-281.

Fukao, Y. (1973). Thurst faulting at a lithospheric plate boundary: The Portugal earthquake of 1969, Earth Planet. Sci. Lett., 18, 205-

216.

Geller, R. J. (1976). Scaling relations for earthquake source parameters and magnitudes, Bull. Seism. Soc. Am., 66, 1501-1523.

Gutenberg, B. (1945). Amplitudes of P, PP and S and magnitude of shallow earthquakes, Bull. Seism. Soc. Am., 35, 57-69.

Gutenberg, B. and C. F. Richter (1942). Earthquake magnitude, intensity, energy and acceleration, Bull. Seism. Soc. Am., 32, 163-191.

Gutenberg, B. and C. F. Richter (1956). Magnitude and energy of earthquakes, Ann. Geofis. (Rome), 9, 1-15.

Hanks, T. C. and M. Wyss (1972). The use of body wave spectra in the determination of seismic-source parameters, Bull. Seism. Soc. Am., 62, 561-589.

Hanson, M. E., A. R. Sanford and R. J. Shaffer (1974). A source function for a dynamic brittle unilateral shear fracture, Geophys. J., 38, 365-376.

Harkrider, D. G. (1964). Surface waves in multilayered elastic media, 1. Rayleigh and Love waves from buried sources in a multilayered elastic half-space, Bull. Seism. Soc. Am., 54, 627-679.

Harkrider, D. G. (1970). Surface waves in multilayered elastic media. Part II. Higher mode spectra and spectral ratios from point sources in plane layered earth models, Bull. Seism. Soc. Am., 60, 1937-1987.

Haskell, N. A. (1964). Total energy and energy spectral density of elastic wave radiation from propagating faults, Bull. Seism. Soc.

Am., 54, 1811-1841.

Haskell, N. A. (1966). Total energy and energy spectral density of elastic wave radiation from propagating faults. Part II. A statistical fault model, Bull. Seism. Soc. Am., 56, 125-140.

Haskell, N. A. (1969). Elastic displacements in the near-field of a propagating fault, Bull. Seism. Soc. Am., 59, 865-908.

Hirasawa, T. and W. Stauder (1965). On the seismic body waves from a finite moving source, Bull. Seism. Soc. Am., 55, 237-262.

Kanamori, H. (1970a). Synthesis of long-period surface waves and its application to earthquake source studies - Kurile Islands earthquake of October 13, 1963, J. Geophys. Res., 75, 5011-5027.

Kanamori, H. (1970b). The Alaska earthquake of 1964: Radiation of long period surface waves and source mechanism, J. Geophys. Res., 75, 5029-5040.

Kanamori, H. (1971a). Faulting of the great Kanto earthquake of 1923 as revealed by seismological data, Bull. Earthquake Res. Inst. Tokyo Univ., 49, 13-18.

Kanamori, H. (1971b). Seismological evidence for a lithospheric normal faulting - the Sanriku earthquake of 1933, Phys. Earth Planet. Interiors, 4, 289-300.

Kanamori, H. (1971c). Focal mechanism of the Tokachi-Oki earthquake of May 16, 1968: Contortion of the lithosphere of a junction of two trenches, Tectonophysics, 12, 1-13

Kanamori, H. (1972a). Tectonic implications of the 1944 Tonankai and 1946 Nankaido earthquakes, Phys. Earth Planet. Interiors, 5, 129-

139.

Kanamori, H. (1972b). Determination of effective tectonic stress associated with earthquake faulting, the Tottori earthquake of 1943, Phys. Earth Planet. Interiors, 5, 426-434.

Kanamori, H. (1973). Mode of strain release associated with major earthquakes in Japan, Ann. Rev. of Earth and Planet. Sci., 1, 213-239.

Kanamori, H. (1974). Long period ground motion in the epicentral area of major earthquakes, Tectonophysics, 21, 341-356.

Kanamori, H. and D. L. Anderson (1975a). Amplitude of the earth's free oscillations and long period characteristics of the earthquake source, J. Geophys. Res., 80, 1075-1078.

Kanamori, H. and D. L. Anderson (1975b). Theoretical basis of some empirical relations in seismology, Bull. Seism. Soc. Am., 65, 1073-1095.

Kanamori, H. and J. J. Cipar (1974). Focal processes of the great Chilean earthquake May 22, 1960, Phys. Earth Planet. Interiors, 9, 128-136.

Kasahara, K. (1957). The nature of seismic origins as inferred from seismological and geodetic observations, 1, Bull. Earthquake Res. Inst. Tokyo Univ., 35, 473-532.

Kawasaki, I. and Y. Suzuki (1974). Rise time and effective stress estimation from comparison of near field data with theoretical seismograms in a semi-infinite medium: The Sanriku earthquake of March 3, 1933, J. Phys. Earth, 22, 223-236.

Kawasaki, I. (1975). The focal processes of the Kita-Mino earthquake of August 19, 1961 and its relationship to a Quaternary fault, the Hatogayu-Koike fault, J. Phys. Earth, 23, 227-250.

Keiles-Borok, V. (1959). An estimation of the displacement in an earthquake source and of source dimensions, Ann. Geofis. (Rome), 12, 205-214.

Langston, C. A. and D. V. Helmberger (1975). A procedure for modelling shallow dislocation sources, Geophys. J., 42, 117-130.

Madariaga, R. (1976). Dynamics of an expanding circular fault, Bull. Seism. Soc. Am., 66, 639-666.

Maruyama, T. (1963). On the force equivalents of dynamical elastic dislocations with reference to the earthquake mechanism, Bull. Earthq. Res. Inst. Tokyo Univ., 41, 467-486.

Mikumo, T. (1969). Long-period P waveforms and the source mechanism of intermediate earthquakes, J. Phys. Earth, 17, 169-192.

Mikumo, T. (1973a). Faulting mechanism of the Gifu earthquake of September 9, 1969, and some related problems, J. Phys. Earth, 21, 191-212.

Mikumo, T. (1973b). Faulting processes of the San Fernando earthquake of February 9, 1971 inferred from static and dynamic near-field displacements, Bull. Seism. Soc. Am., 63, 249-269.

Minster, J. B. (1973). Elastodynamics of failure in a continuum, Ph. D. Thesis, California Institute of Technology.

Nagamune, T. (1972). Magnitudes estimated from body waves for great earthquakes (in Japanese), Quarterly Journal of Seismology, 47, 1-8.

Richards, P. G. (1973). The dynamic field at a growing plane elliptical shear crack, Int. J. Solids Structures, 9, 843-861.

Richter, C. F. (1958). Elementary Seismology, W. H. Freeman, San Francisco.

Sato, R. (1972). Stress drop for a finite fault, J. Phys. Earth, 20, 397-407.

Sato, T. and T. Hirasawa (1973). Body wave spectra from propagating shear cracks, J. Phys. Earth, 21, 415-431.

Savage, J. C. (1972). Relation of corner frequency to fault dimensions, J. Geophys. Res., 77, 3788-3795.

Savage, J. C. and L. M. Hastie (1966). Surface deformation associated with dip-slip faulting, J. Geophys. Res., 71, 4897-4904.

Shimazaki, K. (1975). Nemuro-Oki earthquake of June 17, 1973: A lithospheric rebound at the upper half of the interface, Phys. Earth Planet. Interiors, 9, 314-327.

Steketee, J. A. (1958a). On Volterra's dislocations in a semi-infinite medium, Can. J. Phys., 36, 192-205.

Steketee, J. A. (1958b). Some geophysical applications of the elasticity theory of dislocations, Can. J. Phys., 36, 1168-1198.

Trifunac, M. D. (1974). A three-dimensional dislocation model for the San Fernando, California, earthquake of February 9, 1971, Bull. Seism. Soc. Am., 64, 149-172.

Trifunac, M. D. and F. E. Udwadia (1974). Parkfield, California, earthquake of June 27, 1966: A three-dimensional moving dislocation, Bull. Seism. Soc. Am., 64, 511-533.

Tsai, Y. and K. Aki (1970). Source mechanism of the Truckee, California earthquake of September 12, 1966, Bull. Seism. Soc. Am., 60, 1199-1208.

Tsuboi, C. (1956). Earthquake energy, earthquake volume, aftershock area, and strength of the earth's crust, J. Phys. Earth, 4, 63-66.

Tsujiura, M. (1973). Spectrum of seismic waves and its dependence on magnitude, J. Phys. Earth, 21, 373-391.

Tucker, B. E. and J. N. Brune (1975). Source mechanism and surface wave excitation for aftershocks of the San Fernando earthquake, preprint.

Udias, A. (1971). Source parameters of earthquakes from spectra of Rayleigh waves, Geophys. J. , 22, 353-376.

Udias, A. and A. L. Arroyo (1970). Body and surface wave study of source parameters of the March 15, 1964 Spanish earthquake, Tectonophysics, 9, 323-346.

Utsu, T. and A. Seki (1954). A relation between the area of aftershock region and the energy of main-shock (in Japanese), J. Seism. Soc. Japan (Zisin), 7, 233-240.

Wu, F. T. and H. Kanamori (1973). Source mechanism of February 4, 1965, Rat Island earthquake, J. Geophys. Res., 78, 6082-6092.

PART II.

AMPLITUDES OF ROTATIONALLY SPLIT NORMAL MODES FOR THE 1960 CHILEAN AND 1964 ALASKAN EARTHQUAKES

Chapter 1

INTRODUCTION

The study of the free oscillations of the earth began as theoretical research. Love (1944) gives the spheroidal and torsional modes of a homogeneous elastic sphere. Love's analytic solution could be extended to a vertically heterogeneous body only by numerical integration.

The first instrument capable of observing free oscillations was Benioff's (1935) strainmeter. Benioff et al. (1954) and Benioff (1958) reported seeing a wave with a period of 57 minutes which they speculated might be a free mode of the earth. Although Benioff's claim was greeted with skepticism, it served as a motivation for additional work on the theoretical problem of finding the normal modes of more realistic earth models.

Pekeris and Jarosch (1958) and Alterman et al. (1959) calculated the eigenfrequencies for realistic earth models. The basic formalism developed by Alterman et al. was later extended by Saito (1967) and still is the generally accepted framework for current studies of normal modes (e.g. Okal, 1977).

Serendipitously, soon after the theoretical methods for calculating eigenfrequencies had been developed, the 1960 Chilean earthquake provided the first conclusive observations of free oscillations. Benioff et al. (1961), using the Caltech Isabella strainmeter, and Ness et al. (1961), using the UCLA tidal gravimeter, found nearly identical values for the eigenperiods. Both groups, also independently,

found that the gravest modes were split into several very closed spaced peaks in the spectrum.

Pekeris et al. (1961) and Backus and Gilbert (1961) showed that the splitting could be explained by the perturbation caused by the earth's rotation. The formalism for studying the perturbation is identical to that used in atomic physics or in Lamb's (1945) study of waves in a rotating basin of water. The frequency separation predicted by Pekeris et al. and Backus and Gilbert agrees very well with the observed splitting.

Since the Chilean earthquake, extensive theoretical work (summarized in the next chapter) has been done on splitting caused by the earth's ellipticity and lateral heterogeneity. However, nearly all of this work was concerned with calculating the amount of frequency separation caused by different effects. Very little work has been done on the amplitudes of split normal modes.

Also, very little work has been done on studying the observed amplitudes of split modes. Pekeris et al. and Backus and Gilbert used simple source models to study ${}_0S_2$ and ${}_0S_3$ for the Chilean earthquake. However, no one has ever compared the observed amplitudes to those predicted by a double couple source model. It is also remarkable that, although the Chilean earthquake records are the best dataset for studying splitting, no further analyses of these data have been performed since the work of Benioff et al., Smith (1961) and Ness et al.

In this thesis, methods are developed for calculating the

amplitudes of split normal modes excited by double couple sources. These methods are then used to calculate relative spectral amplitudes for comparisons with published observed spectra. The Isabella strain record is reexamined and split modes are studied in the time domain by narrow band filtering the data. Synthetics are computed using the theoretical methods developed in this thesis. Comparison of the observations with the synthetics demonstrates the existence of splitting for modes for which splitting had not been established, and allows the use of time domain synthetics for Q determination. The methods developed in this thesis should prove extremely useful in the study of split normal modes.

REFERENCES

Alterman, Z., H. Jarosch and C. L. Pekeris (1959). Oscillations of the earth, Proc. R. Soc. London, A252, 80-95.

Backus, G. and F. Gilbert (1961). The rotational splitting of the free oscillations of the Earth, Proc. Nat. Acad. Sci. U.S., 47, 362-371.

Benioff, H. (1935). A linear strain seismograph, Bull. Seism. Soc. Am., 25, 283-309.

Benioff, H. (1958). Long waves observed in the Kamchatka earthquake of November 4, 1952, J. Geophys. Res., 63, 589-593.

Benioff, H., B. Gutenberg and C. F. Richter (1954). Progress report, Seismological Laboratory, California Institute of Technology, Trans. Am. Geophys. Un., 35, 979-987.

Benioff, H., F. Press and S. Smith (1961). Excitation of the free oscillations of the earth by earthquakes, J. Geophys. Res., 66, 605-619.

Lamb, H. (1945). Hydrodynamics, Dover, New York.

Love, A. E. H. (1944). A treatise on the mathematical theory of elasticity, Dover, New York.

Ness, N., J. Harrison and L. Slichter (1961). Observations of the free oscillations of the earth, J. Geophys. Res., 66, 621-629.

Okal, E. A. (1977). A physical classification of the earth's spheroidal modes, J. Phys. Earth, submitted.

Pekeris, C. L., Z. Alterman, and H. Jarosch (1961). Rotational multiplets in the spectrum of the Earth, Phys. Rev., 122, 1692-

1700.

Pekeris, C. L. and H. Jarosch (1958). The free oscillations of the earth, in Contributions in geophysics in honor of Beno Gutenberg, H. Benioff, M. Ewing, B. F. Howell and F. Press editors, Pergamon Press, New York.

Smith, S. W. (1961). An investigation of the earth's free oscillations, Ph. D. Thesis, California Institute of Technology.

Chapter 2

AMPLITUDES OF THE SPLIT NORMAL MODES OF A ROTATING, ELLIPTICAL EARTH EXCITED BY A DOUBLE COUPLE

ABSTRACT

This chapter develops the theory necessary to explain the amplitudes of the earth's split normal modes. Expressions are derived for the amplitudes of the free oscillations of a laterally homogeneous rotating and elliptical earth excited by a point double couple. The eigenfunctions for this problem are the complex vector spherical harmonics about the north pole. The amplitudes of the normal modes are obtained by transforming Saito's (1967) results, expressed in vector spherical harmonics about the earthquake source, into geographic coordinates. The dependence of the excitation of each singlet within a multiplet is explicitly separated into factors for geometric fault parameters, seismic moment, source depth, earth structure and the geographic coordinates of the source and receiver. Synthetic torsional and spheroidal displacement and strain spectra are presented for low order fundamental modes ($_0S_2$-$_0S_5$, $_0T_2$-$_0T_5$) excited by four basic fault geometries.

These results are suitable for the synthesis of observed spectra and time domain records in which splitting is an important effect. These results are applied to the Chilean and Alaskan earthquakes in the following chapters. Very good agreement with observations is obtained.

INTRODUCTION

Following the observation of split peaks with varying amplitudes in the free oscillation spectra of the 1960 Chilean earthquake (by Ness, Harrison and Slichter, 1961 and Benioff, Press and Smith, 1961), Pekeris, Alterman and Jarosch (1961) and Backus and Gilbert (1961) showed that the splitting could be explained by the earth's rotation. Pekeris *et al.* and Backus and Gilbert calculated the relative amplitudes of the low order spheroidal modes excited by several simple sources. In this chapter we calculate the amplitudes of the split modes of a rotating and elliptical earth due to a realistic model of an earthquake source, a double couple of arbitrary orientation.

These results for the excitation of the split modes allow one to use the relative amplitudes of singlets to study earthquake source mechanisms. In the next chapter we calculate for the first time the theoretical singlet amplitude ratios from published source parameters for the 1960 Chilean earthquake and the 1964 Alaskan earthquake. For both events the synthetic relative spectral amplitudes are in remarkable agreement with observations of very low order modes. It is also possible to analyze several hundred hours of records from the Chilean earthquake for these low order modes. These records are dominated by a complicated signal generated by rotational splitting which is matched quite closely in the time domain (Chapter 4) using the results derived in this chapter.

The calculation of the excitation of the normal modes of a non-rotating, laterally homogeneous earth is greatly simplified by its

spherical symmetry. As a result of the degeneracy arising from this symmetry, vector spherical harmonics in coordinates with the source on the polar axis may be chosen as eigenfunctions. This choice greatly simplifies the excitation calculations, because the eigenfrequency depends only on the angular order number, ℓ, and only modes with azimuthal order numbers $m = 0, \pm 1, \pm 2$ are excited by a point double couple.

The earth's rotation and ellipticity remove the degeneracy of the problem. For the nondegenerate problem, splitting is caused by the perturbing effects of the Coriolis force, centripetal force and ellipticity, all of which are symmetric about the earth's rotation axis. In contrast to the degenerate case, there is a distinct eigenfrequency, $\omega_{\ell m}$, for each singlet. Dahlen (1968, 1969) showed that the *zeroeth order eigenfunctions are complex vector spherical harmonics* about the North Pole, and calculated the eigenfrequencies of the split modes for several earth models. Although the frequency splitting within a multiplet depends on the earth's rotation rate, ellipticity and structure, the zeroeth order amplitudes of the split normal modes do not depend on the rotation rate and the ellipticity, and may thus be calculated without taking into account the precise frequency separation.

A substantial portion of the method for calculating the excitation of the degenerate modes may be adapted to the nondegenerate case, although much additional complexity results because the source is not on the axis of symmetry. The most important consequence of the removal

of the degeneracy is that in general, for a double couple point source, modes of every azimuthal order number from $m = -\ell$ to $m = +\ell$ are excited. We show that the spectral amplitudes of the pair of singlets of orders m are equal. Furthermore, the geographic coordinates of the source and receiver appear individually in the expressions for the amplitudes, while for the degenerate case only their relative position affects the final result.

If the additional perturbation induced by lateral heterogeneity is introduced, then in general the eigenfunctions are linear combinations of the spherical harmonics (Saito, 1971; Usami, 1971; Madariaga, 1972; Madariaga and Aki, 1972; Luh, 1974; Dahlen, 1976). In this study we consider only the effects of rotation and ellipticity which are the primary causes of the splitting of the low order modes. In the remainder of the thesis nondegenerate is used to denote the case of a laterally homogeneous, rotating and elliptical earth, which has complete symmetry about the rotation axis.

Many authors have considered the excitation of the earth's normal modes. Saito (1967) presented expressions for the excitation of free oscillations by a point source in a spherically symmetric earth. Kanamori (1970 a, b, 1971, 1976), Abe (1970), Fukao and Abe (1971), Shimazaki (1975), Okal (1976), and other authors applied Saito's normal mode results to the synthesis of long period surface waves. Kanamori and Cipar (1974) presented compact expressions for the excitation problem. Gilbert (1970, 1973) introduced the moment tensor representation of a seismic source, which was used by Dziewonski and Gilbert

(1974) and Gilbert and Dziewonski (1975) to calculate the excitation of the degenerate modes. (The moment tensor (Gilbert, 1970) is formally equivalent to the double couples and couples without moment used by Saito (1967) and Takeuchi and Saito (1972). The equivalence has been discussed by several authors, e.g. Geller (1976). Luh and Dziewonski (1976) modified the moment tensor solution to include the effects of rotation and ellipticity.

In this chapter we extend Saito's results to obtain the excitation of the nondegenerate normal modes. This approach allows us to apply solutions for the excitation of degenerate normal modes (Saito, Kanamori and Cipar) to the nondenerate modes. We derive expressions for torsional and spheroidal displacement and strain fields in the time domain. These expressions may then be used to calculate spectral amplitudes.

We calculate synthetic displacement and strain spectra for low order fundamental mode torsional and spheroidal multiplets (angular orders two through five) excited by four basic fault geometries (vertical and 45^{o} dip; pure dip slip and strike slip). For particular source and receiver locations we present figures showing the relative spectral amplitudes of the individual singlets within each multiplet for each displacement and strain component. In general, the relative amplitudes within a multiplet will vary substantially with angular order number or even between different displacement or strain components for the same order number. Usually there is no consistency in the preferential excitation of singlet pairs with azimuthal order numbers

±m between multiplets.

Our method may be summarized as follows. We use Dahlen's (1968) results for the case of complete symmetry about the rotation axis. Since the zeroeth order eigenfunctions are the complex vector spherical harmonics about the north pole, we obtain the excitation in terms of these eigenfunctions. To do so we use the rotation matrix elements to transform the excitation expanded in vector spherical harmonics about the source into the geographic coordinates.

This first order perturbation theory using zeroeth order eigenfunctions and first order eigenfrequencies is, of course, an approximation. Such an approximation, in which the eigenvalue is found to a higher order than the eigenfunction, is a common practice in applications of perturbation theory. We regard the resulting zeroeth order amplitudes as being adequate for our purposes, as our intent is to derive results suitable for comparison to observations. For this purpose we require far greater precision in the eigenfrequency than in the eigenfunction.

By examining spectra, eigenfrequencies can be determined quite precisely. On the other hand, spectral amplitudes cannot be measured very precisely; the uncertainty is probably at least 10%. Since the error made in omitting the first order correction to the eigenfunctions is of the same order as the first order correction of the eigenfrequencies, and is almost certainly smaller than the experimental uncertainty in the amplitudes, it seems sufficient to use the zeroeth order amplitudes. Similarly, the first order eigenfrequencies seem

acceptable in view of present experimental errors.

The true test of such an approximation is in its application to the data. Because we are successful in synthesizing spectra (chapter 3) and time domain records (chapter 4) it appears that the first order perturbation theory is all that is required. As better data become available, perhaps from the new long period network (Agnew et al., 1976), it may be necessary to employ higher order perturbation theory.

Our method, using the rotation matrix elements, could also be generalized to the case of a laterally heterogeneous earth. Since the eigenfunctions are now linear combinations of the spherical harmonics about the north pole (Luh, 1974), we would again transform the excitation into the geographic coordinates. The final result would then be obtained by taking the appropriate linear combinations. Due to the complexity of this procedure and our ability to fit data for very low order modes with a model including only rotation and ellipticity, we do not include the effect of lateral heterogeneity in this thesis.

NORMAL MODES OF A ROTATING ELLIPTICAL EARTH

We adapt Saito's (1967) results for the normal modes of a spherically symmetric earth to the case of a laterally homogeneous, rotating and elliptical earth. The displacements and stresses are expanded in complex vector spherical harmonics about the north pole.

The torsional and spheroidal displacements are respectively

$$\vec{U}^T(\vec{r},t) = \sum_{n=0}^{\infty} \sum_{\ell=0}^{\infty} \sum_{m=-\ell}^{\ell} {}_nA_{\ell m} \vec{T}_{\ell m}(\theta,\phi) \; {}_n\left[y_1^T(r)\right]_{\ell m} \left(e^{i\,{}_n\omega^+_{\ell m} t} + e^{i\,{}_n\omega^-_{\ell m} t} \right) \quad (2.1)$$

and

$$\vec{U}^S(\vec{r},t) = \sum_{n=0}^{\infty} \sum_{\ell=0}^{\infty} \sum_{m=-\ell}^{\ell} {}_nD_{\ell m} \left\{ {}_n\left[y_1^S(r)\right]_{\ell m} \vec{S}^1_{\ell m}(\theta,\phi) + {}_n\left[y_3^S(r)\right]_{\ell m} \vec{S}^2_{\ell m}(\theta,\phi) \right\}$$

$$\times \left(e^{i\,{}_n\omega^+_{\ell m} t} + e^{i\,{}_n\omega^-_{\ell m} t} \right). \quad (2.2)$$

The torsional and spheroidal vertical stresses, $\vec{P} = (P_{rr}, P_{r\theta}, P_{r\phi})$ are respectively

$$\vec{P}^T(\vec{r},t) = \sum_{n=0}^{\infty} \sum_{\ell=0}^{\infty} \sum_{m=-\ell}^{\ell} {}_nA_{\ell m} \vec{T}_{\ell m}(\theta,\phi) \cdot {}_n\left[y_2^T(r)\right]_{\ell m} \left(e^{i\,{}_n\omega^+_{\ell m} t} + e^{i\,{}_n\omega^-_{\ell m} t} \right) \quad (2.3)$$

and

$$\vec{P}^S(\vec{r},t) = \sum_{n=0}^{\infty} \sum_{\ell=0}^{\infty} \sum_{m=-\ell}^{\ell} {}_nD_{\ell m} \left\{ {}_n\left[y_2^S(r)\right]_{\ell m} \vec{S}^1_{\ell m}(\theta,\phi) + {}_n\left[y_4^S(r)\right]_{\ell m} \vec{S}^2_{\ell m}(\theta,\phi) \right\}$$

$$\times \left(e^{i\,{}_n\omega^+_{\ell m} t} + e^{i\,{}_n\omega^-_{\ell m} t} \right). \quad (2.4)$$

We follow established usage, and denote eigenfrequencies for both torsional and spheroidal modes by ${}_n\omega_{\ell m}$, although the torsional eigenfrequencies (in 2.1 and 2.3) differ from the spheroidal ones (in 2.2 and 2.4). The frequency in question should be clear from the context.

For the degenerate problem, each mode has two eigenfrequencies

with equal absolute value, but opposite sign. However, when a perturbation is applied, the eigenfrequencies associated with a particular mode no longer have the same absolute value. The positive eigenfrequencies ($_n\omega^+_{\ell m}$) may be considered as the "physical" frequencies of the split modes. The negative eigenfrequencies ($_n\omega^-_{\ell m}$) arise from any application of perturbation theory to the splitting problem (e.g. Backus and Gilbert, 1961). In later sections the negative eigenfrequencies will be eliminated from the final expressions.

The sum over n sums all the overtones. From this point we consider only a single overtone and suppress the sum over n and all overtone indices. The complete displacement and stress fields can always be derived by adding all the overtones.

$A_{\ell m}$ and $D_{\ell m}$ are the amplitudes of the individual spheroidal and torsional modes and are found by solving the excitation problem. $(y_i^S)_{\ell m}$ and $(y_i^T)_{\ell m}$ are the spheroidal and torsional radial eigenfunctions. Though derived for the degenerate case, they remain valid, to zeroeth order, for the nondegenerate case. Following Alterman et al. (1959) and Saito (1967) we will suppress all subscripts on the $(y_i)_{\ell m}$ in the remainder of the thesis.

The surficial basis vectors are the complex vector spherical harmonics

$$\vec{T}_{\ell m}(\theta,\phi) = \left(0 \quad , \quad \frac{1}{\sin\theta} \frac{\partial Y_{\ell m}(\theta,\phi)}{\partial \phi} \quad , \quad -\frac{\partial Y_{\ell m}(\theta,\phi)}{\partial \theta} \right) \qquad (2.5)$$

$$\vec{S}^1_{\ell m}(\theta,\phi) = \left(Y_{\ell m}(\theta,\phi) \quad , \quad 0 \quad , \quad 0 \right)$$

$$\vec{S}^2_{\ell m}(\theta,\phi) = \left(0 \quad , \quad \frac{\partial Y_{\ell m}(\theta,\phi)}{\partial \theta} \quad , \frac{1}{\sin\theta} \frac{\partial Y_{\ell m}(\theta,\phi)}{\partial \phi} \right)$$

where

$$Y_{\ell m}(\theta,\phi) = (-1)^m \left[\frac{(\ell-m)!}{(\ell+m)!} \right]^{\frac{1}{2}} P^m_\ell(\cos\theta)\, e^{im\phi} \quad (m \geq 0) \tag{2.6}$$

and

$$Y_{\ell m}(\theta,\phi) = (-1)^m\, Y^*_{\ell -m}(\theta,\phi). \qquad (m < 0)$$

θ is the colatitude and ϕ is the longitude. The associated Legendre polynomials are defined as

$$P^m_\ell(x) = (1-x^2)^{m/2} \frac{d^m}{dx^m} P_\ell(x) \tag{2.7}$$

The vector spherical harmonics then have the orthogonality and normalization properties

$$\int_0^{2\pi} \int_0^{\pi} \left(\vec{T}^*_{\ell',m'}(\theta,\phi) \right) \cdot \left(\vec{T}_{\ell m}(\theta,\phi) \right) \sin\theta \, d\theta \, d\phi$$

$$= L^2 \int_0^{2} \int_0^{\pi} \left(\vec{S}^{1*}_{\ell',m'}(\theta,\phi) \right) \cdot \left(\vec{S}^1_{\ell m}(\theta,\phi) \right) \sin\theta \, d\theta \, d\phi$$

$$= \int_0^{2\pi} \int_0^{\pi} \left(\vec{S}^{2*}_{\ell',m'}(\theta,\phi) \right) \cdot \left(\vec{S}^2_{\ell m}(\theta,\phi) \right) \sin\theta \, d\theta \, d\theta$$

$$= \frac{4\pi\ L^2}{2\ell+1}\ \delta_{\ell\ell'}\ \delta_{mm'} \tag{2.8}$$

where

$$L^2 = \ell(\ell+1).$$

Equation (2.6) gives us the symmetry relations

$$\vec{T}_{\ell m}(\theta,\phi) = (-1)^m\ \vec{T}^*_{\ell -m}(\theta,\phi) \tag{2.9}$$

$$\vec{S}^1_{\ell m}(\theta,\phi) = (-1)^m\ \vec{S}^{1*}_{\ell -m}(\theta,\phi)$$

$$\vec{S}^2_{\ell m}(\theta,\phi) = (-1)^m\ \vec{S}^{2*}_{\ell -m}(\theta,\phi)$$

for the vector spherical harmonics.

Dahlen (1968) applied perturbation theory to the degenerate case, and calculated the splitting for several earth models. The perturbed eigenfrequencies may be found from the unperturbed eigenfrequency, using

$$\omega_{\ell m} = \omega_\ell + (\delta\omega)_{\ell m}. \tag{2.10}$$

Here the perturbed eigenfrequency, $\omega_{\ell m}$, and the unperturbed eigenfrequency, ω_ℓ, may be either positive or negative but must have the same sign. The frequency shift $(\delta\omega)$ is given by

$$(\delta\omega)_{\ell m} = \omega_\ell(\alpha_\ell + m\beta_\ell + m^2\gamma_\ell) \tag{2.11}$$

in Dahlen's notation, where the splitting parameters α_ℓ and γ_ℓ are due to the ellipticity, and β_ℓ is due to the earth's rotation. Because of the m^2 dependence of $(\delta\omega)_{\ell m}$, the perturbed eigenfrequencies are not symmetrically spaced about the unperturbed eigenfrequency or the central perturbed frequency.

The splitting parameters for positive and negative frequencies are related by

$$\alpha_\ell(\omega_\ell^+) = \alpha_\ell(\omega_\ell^-) \tag{2.12}$$

$$\beta_\ell(\omega_\ell^+) = -\beta_\ell(\omega_\ell^-)$$

$$\gamma_\ell(\omega_\ell^+) = \gamma_\ell(\omega_\ell^-).$$

Since $\omega_\ell^+ = -\omega_\ell^-$, (2.11) and (2.12) show that

$$(\delta\omega)_{\ell m}^+ = -(\delta\omega)_{\ell -m}^- \tag{2.13}$$

and thus

$$\omega_{\ell m}^+ = -\omega_{\ell -m}^- \tag{2.14}$$

but in general $\left|\omega_{\ell m}^+\right| \neq \left|\omega_{\ell m}^-\right|$.

We will use (2.14), together with the symmetry relations between spherical harmonics (2.9), to eliminate the negative eigenfrequencies

from the final expressions for the displacements.

TRANSFORMATION OF THE SOURCE DISCONTINUITIES INTO GEOGRAPHIC COORDINATES

We now generalize Saito's (1967) results to the case of a rotating, elliptical earth. A point source causes discontinuities in stress and displacement across an infinitesimal shell, which are expanded in vector spherical harmonics. The expansion coefficients are required to find the amplitudes of the free oscillations. For the nondegenerate case, the expansion must be carried out in the geographic coordinate frame. Luh and Dziewonski (1976) calculate these expansion coefficients from scratch for each individual source location and mechanism.

Our approach is to use Saito's expansion coefficients for the discontinuities resulting from a double couple, in a coordinate system with the source on the polar axis. We then use elements of the rotation matrices to transform this spherical harmonic expansion into the geographic coordinate frame. Thus for any source location we perform a simple transformation rather than completely recalculate the expansion coefficients.

It is first necessary to introduce the coordinate system of the earthquake source, and to show how the rotation matrix elements allow us to transform the expansion coefficients from this coordinate system to the geographic system.

We adopt the fault geometry of Kanamori and Cipar, shown in figure 2.1. We use a coordinate system in which the source is at

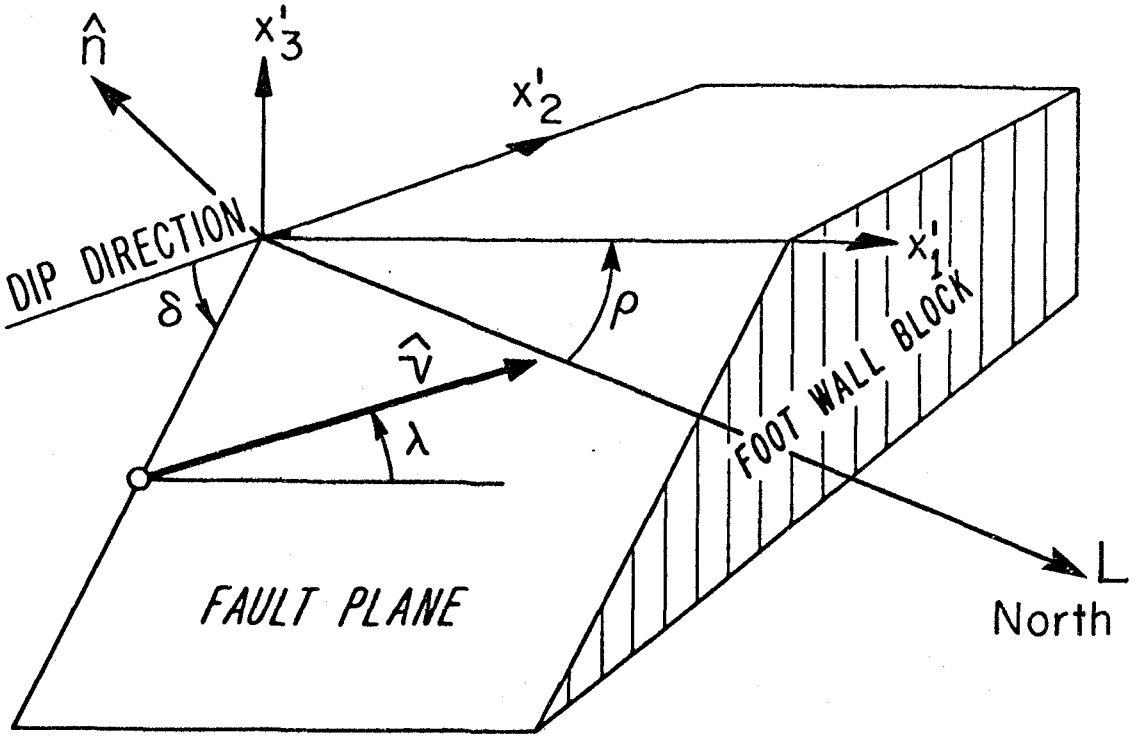

Figure 2.1 - Fault representation of Kanamori and Cipar (slightly modified). $\hat{\nu}$ is the slip vector, and gives the displacement of the hanging wall block. $\hat{n}$ is the normal to the fault plane, and L points north. The strike ρ is measured counterclockwise from L. The dip angle δ is measured from the negative X_2' axis, and the slip angle λ is measured in the fault plane counterclockwise from X_1'.

$(r = r_s, \theta' = 0, \phi' = 0)$ and describe points in this system by (r, θ', ϕ'). In this frame the fault strike, at an angle ρ measured counterclockwise from north, is the X_1' axis. The X_3' axis is vertical. The fault plane dips at an angle δ measured from the negative X_2' axis, and the slip angle λ, which gives the direction in which the hanging wall block moves with respect to the foot wall block, is measured counterclockwise from X_1' in the fault plane. The cartesian unit vector in the direction of slip is given by

$$\hat{\nu} = (\cos \lambda, \sin \lambda \cos \delta, \sin \lambda \sin \delta) \tag{2.15}$$

and the unit normal to the fault plane is

$$\hat{n} = (0, -\sin \delta, \cos \delta). \tag{2.16}$$

The geographic coordinates of the source are (r_s, θ_s, ϕ_s), and points in the geographic system have coordinates (r, θ, ϕ). The X_3 axis is the polar axis and the X_1-X_3 plane is the plane of the prime meridian. Thus the unit vector $\hat{\theta}$ points south at any point and $\hat{\phi}$ points east.

Hereafter, we will use primes $(X_i', f_i', y_i', A_{\ell m}')$ to denote quantities associated with the source coordinate frame. The corresponding unprimed quantities are associated with the geographic coordinates.

The source and geographic systems can be related to each other through the three Euler angles which allow us to rotate the geographic (X_1, X_2, X_3) axes into the source (X_1', X_2', X_3') axes. To perform this

transformation we start with the X_1, X_2, X_3 axes and make three counter-clockwise rotations. We first rotate by α about the X_3 axis, then by β about the resulting X_2 (or X_2^*) axis, and finally by γ about the X_3' axis. This process is shown in figure 2.2. The line L, drawn to clarify the choice of Euler angles, points north in the X_1'-X_2' plane. We see that for a source at θ_s, ϕ_s, with fault strike ρ,

$$\begin{aligned} \alpha &= \phi_s \\ \beta &= \theta_s \\ \gamma &= \pi + \rho . \end{aligned} \tag{2.17}$$

(This is only true for the Euler angle conventions of Brink and Satchler (1968) - at least three other conventions are used by other authors.)

Brink and Satchler show that spherical harmonics in the two coordinate systems are related by the rotation matrices $D^{\ell}_{mk}(\alpha,\beta,\gamma)$ which are irreducible representations of the rotation group. For brevity, we will denote this set of three Euler angles by $R = (\alpha,\beta,\gamma)$. The rotation matrix elements are then given by

$$D^{\ell}_{mk}(R) = e^{-i(\alpha m + \gamma k)} d^{\ell}_{mk}(\beta) \tag{2.18}$$

where

$$d^{\ell}_{mk}(\beta) = \sum_t (-1)^t \frac{\left[(\ell+m)!\ (\ell-m)!\ (\ell+k)!\ (\ell-k)!\right]^{1/2}}{t!(\ell+m-t)!\ (\ell-k-t)!\ (t+k-m)!} \times \tag{2.19}$$

$$\left[\sin\ (\beta/2)\right]^{2t+k-m} \left[\cos\ (\beta/2)\right]^{2\ell+m-k-2t}$$

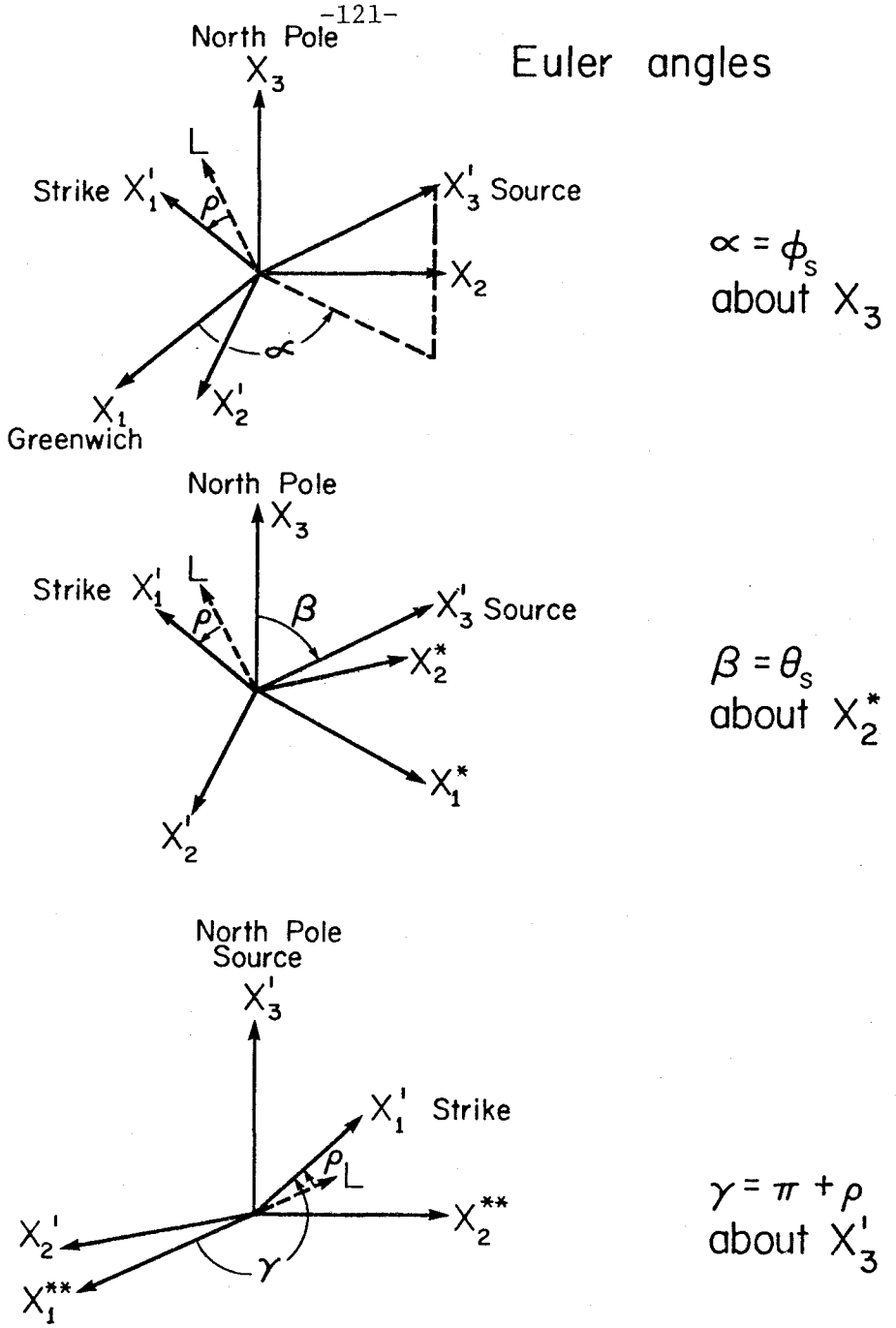

Figure 2.2 - Euler angles which rotate geographic (X_1, X_2, X_3) axes into source (X_1', X_2', X_3') axes. All rotations are right handed. The line L points north in the X_1' - X_2' plane.

and the summation ranges over all values of t which give non-negative factorials. (An alternative derivation of the rotation matrix elements is given by Backus (1964).)

The relation between spherical harmonics in the source and geographic frames is then

$$Y_{\ell k}(\theta', \phi') = \sum_{m=-\ell}^{\ell} D^{\ell}_{mk}(R)\ Y_{\ell m}(\theta,\phi). \tag{2.20}$$

Since the vector spherical harmonics are themselves vectors, we may write equalities between vectors (rather than their components)

$$\begin{aligned}
\vec{T}_{\ell k}(\theta',\phi') &= \sum_{m=-\ell}^{\ell} D^{\ell}_{mk}(R)\ \vec{T}_{\ell m}(\theta,\phi) \\
\vec{S}^{1}_{\ell k}(\theta',\phi') &= \sum_{m=-\ell}^{\ell} D^{\ell}_{mk}(R)\ \vec{S}^{1}_{\ell m}(\theta,\phi) \\
\vec{S}^{2}_{\ell k}(\theta',\phi') &= \sum_{m=-\ell}^{\ell} D^{\ell}_{mk}(R)\ \vec{S}^{2}_{\ell m}(\theta,\phi).
\end{aligned} \tag{2.21}$$

(To compare individual components in (2.21) directly, the (θ,ϕ) components must be rotated into the (θ',ϕ') frame, or vice versa.)

We now use the rotation matrix elements to obtain the expansion in geographic coordinates of the discontinuities in displacement and stress caused by a point source. We begin with this expansion in the source coordinates, and derive the relations between the two expansions. These relations will allow us to convert Saito's source frame results to the geographic results we require.

In the source frame, Saito's expressions for the discontinuities in displacement and stress can be rewritten as

$$\delta\vec{U}(\vec{r}_s;t) = \vec{U}(r_s + \varepsilon,t) - \vec{U}(r_s - \varepsilon, t) =$$

$$\frac{1}{2\pi}\int_{-\infty}^{\infty}\sum_{\ell=0}^{\infty}\sum_{m=-\ell}^{\ell}\left[g_1'^{T}(\omega)\ \vec{T}_{\ell m}(\theta',\phi') + g_1'^{S}(\omega)\ \vec{S}^{1}_{\ell m}(\theta',\phi') + g_3'^{S}(\omega)\ \vec{S}^{2}_{\ell m}(\theta',\phi')\right] \times e^{i\omega t}\ d\omega \qquad (2.22)$$

and

$$\delta\vec{P}(\vec{r}_s;t) = \vec{P}(r_s + \varepsilon,t) - \vec{P}(r_s - \varepsilon, t) =$$

$$\frac{1}{2\pi}\int_{-\infty}^{\infty}\sum_{\ell=0}^{\infty}\sum_{m=-\ell}^{\ell}\left[g_2'^{T}(\omega)\ \vec{T}_{\ell m}(\theta',\phi') + g_2'^{S}(\omega)\ \vec{S}^{1}_{\ell m}(\theta',\phi') + g_4'^{S}(\omega)\ S^{2}_{\ell m}(\theta',\phi')\right] \times e^{i\omega t}\ d\omega \qquad (2.23)$$

where $\delta\vec{U}(\vec{r}_s;t)$ and $\delta\vec{P}(\vec{r}_s;t)$ are the jumps in displacement and stress respectively across a spherical shell at the source depth $r = r_s$.

For the special case of a step function source time dependence, the frequency dependent discontinuity coefficients $g_i'(\omega)$ may be written

$$g_i'(\omega) = \frac{(f_i)'}{i\omega} \qquad (2.24)$$

where the f_i' are the expansion coefficients for the spatial dependence

of the discontinuity. Each $(f_i^T)'$ or $(f_i^S)'$ has an implicit dependence on ℓ and m.

To transform (2.22) and (2.23) to the geographic coordinates, we use the results derived in (2.21) for the vector spherical harmonics, and derive a general relation between the discontinuity expansion coefficients in geographic coordinates and those in source coordinates in terms of the rotation matrix elements

$$(f_i)_{\ell m} = \sum_{k=-\ell}^{\ell} D^{\ell}_{mk}(R)\ (f_i)'_{\ell k} \tag{2.25}$$

In this equation we have written the ℓ, m dependence of the f_i explicitly. We will omit these subscripts in the remainder of our discussions. Note that, as the f_i are coefficients of the basis vectors, they transform (2.25) in the opposite sense as the vector spherical harmonics (2.21).

Using this relation between the discontinuity expansion coefficients, we could rewrite (2.22) and (2.23) to obtain expressions for the discontinuities in displacement and stress in the geographic coordinates. We will not do so, because in calculating the excitation, we require the discontinuity expansion coefficients, f_i (2.25) rather than the discontinuities themselves.

TORSIONAL MODES EXCITED BY A POINT DOUBLE COUPLE

We now use the expansion coefficients in geographic coordinates to apply Saito's excitation results to the nondegenerate case. We derive the excitation of the torsional modes in some detail in this section; we present results for spheroidal modes in the next section. It is shown that although (in source coordinates) only singlets of orders m=-2 through m=+2 are excited in the degenerate case, all $2\ell+1$ singlets within a multiplet are excited in the nondegenerate case.

We now modify Saito's results for the displacements resulting from a point source with step function time dependence and unit seismic moment. To zeroeth order, in the geographic frame, Saito's expression may be written as

$$\vec{U}^T(\vec{r},t) = \sum_{\ell=0}^{\infty} \sum_{m=-\ell}^{\ell} A_{\ell m}\, y_1^T(r)\, \vec{T}_{\ell m}(\theta,\phi) \left[e^{i\omega^+_{\ell m} t} + e^{i\omega^-_{\ell m} t} \right], \tag{2.26}$$

where $\vec{r}$ is the position of the receiver, $y_1^T(r)$ and $y_2^T(r)$ are the eigenfunctions for the torsional modes, and I_1^T is an energy integral defined by Saito.

$A_{\ell m}$ is the modal amplitude

$$A_{\ell m} = \frac{\left[r^2 \left(f_2^T\, y_1^T(r) - f_1^T\, y_2^T(r) \right) \right]_{r=r_s}}{2\omega_\ell^2\, I_1^T} \quad . \tag{2.27}$$

As we have shown, we can express this as

$$A_{\ell m} = \sum_{k=-\ell}^{\ell} D^{\ell}_{mk}(R)\, A'_{\ell k} \tag{2.28}$$

where the source frame modal amplitude is

$$A'_{\ell k} = \frac{\left(r^2\left[(f_2^T)'\, y_1^T(r) - (f_1^T)'\, y_2^T(r)\right]\right)_{r=r_s}}{2\omega^2\, I_1^T} \tag{2.29}$$

These equations are valid for an arbitrary point source. Saito gives expressions for $(f_1^T)'$ and $(f_2^T)'$ for a double couple, in terms of the real spherical harmonics ($P_\ell^m(\cos\theta)\cos m\phi$ and $P_\ell^m(\sin\theta)\sin m\phi$) and in terms of the cartesian components of the unit slip vector, $\hat{\nu}$, and the unit normal to the fault plane, $\hat{n}$. These can be transformed into the coefficients of positive and negative complex spherical harmonics for the fault representation of Kanamori and Cipar. For the complex (but still completely unnormalized) spherical harmonics, $P_\ell^m(\cos\theta)\, e^{im\phi}$, the coefficients become

$$r_s^2(f_1^T)' = \frac{2\ell+1}{4\pi L^2}\,\frac{1}{\mu_s}\,\frac{1}{2}\,(-\sin\lambda\cos 2\delta \mp i\cos\lambda\cos\delta) \tag{2.30}$$

for $m = \pm 1$, and

$$r_s^2(f_2^T)' = \frac{2\ell+1}{4\pi L^2}\,\frac{1}{r_s}\,\frac{1}{2}\,(-\cos\lambda\sin\delta \pm i\sin\lambda\sin\delta\cos\delta) \tag{2.31}$$

for $m = \pm 2$. Both of these quantities are zero for $m = 0$, and $|m| > 2$. (μ_s is the rigidity at the source depth r_s.)

To convert these coefficients into the coefficients of our normalized complex spherical harmonics, we multiply by the conversion

factors,

$$C_{\ell m} = \left[\frac{(\ell+m)!}{(\ell-m)!}\right]^{\frac{1}{2}} (-1)^m \qquad \text{for } m \geq 0 \tag{2.32}$$

and

$$C_{\ell m} = C_{\ell -m} (-1)^m \qquad \text{for } m < 0.$$

For convenience, we introduce the source amplitude factors defined by Kanamori and Cipar for the degenerate excitation problem

$$L_1 = \left(\frac{2\ell+1}{4\pi\omega_\ell^2 L^2 I_1^T}\right)\left(\frac{1}{\mu_s}\right) y_2^T(r_s) \tag{2.33}$$

and

$$L_2 = \left(\frac{2\ell+1}{4\pi\omega_\ell^2 L^2 I_1^T}\right)\left(\frac{1}{r_s}\right) y_1^T(r_s).$$

We now calculate the source frame modal amplitude (2.29), $A'_{\ell m}$, which is zero for $|m| > 2$. If the radiation pattern terms are expressed as

$$P_1 = \frac{1}{4} \left(-\sin\lambda \cos 2\delta - i \cos\lambda \cos\delta\right)$$

and

$$P_2 = \frac{1}{4} \left(-\cos\lambda \sin\delta + i \sin\lambda \sin\delta \cos\delta\right) \tag{2.34}$$

we can write

$$
\begin{aligned}
A'_{\ell 2} &= L_2 p_2 C_{\ell 2} \\
A'_{\ell 1} &= L_1 p_1 C_{\ell 1} \\
A'_{\ell 0} &= 0 \\
A'_{\ell -1} &= L_1 p_1^* C_{\ell -1} \\
A'_{\ell -2} &= L_2 p_2^* C_{\ell -2} \ .
\end{aligned}
\tag{2.35}
$$

Thus we have the symmetry relation

$$
A'_{\ell m} = (-1)^m A'^*_{\ell -m} \ . \tag{2.36}
$$

Brink and Satchler give a symmetry relation for the D^{ℓ}_{mk} functions,

$$
D^{\ell}_{mk}(R) = \left[D^{\ell}_{-m-k}(R) \right]^* (-1)^{m-k} \tag{2.37}
$$

Substituting (2.35) and (2.36) into (2.28), we find the same symmetry for the geographic modal amplitudes as for the source frame amplitudes

$$
A_{\ell m} = (-1)^m A^*_{\ell -m} . \tag{2.38}
$$

We use (2.38) and the symmetry properties of the vector spherical harmonics (2.9) to eliminate the negative eigenfrequencies, $\omega_{\ell \bar{m}}$, from (2.26). Defining

$$
\vec{B}_{\ell m}(\vec{r}) = y_1^T(r) \ A_{\ell m} \ \vec{T}_{\ell m}(\theta, \phi) \ , \tag{2.39}
$$

we obtain the torsional mode displacements resulting from a double couple point source with step function source time history;

$$\vec{U}^T(\vec{r},t) = \sum_{\ell=0}^{\infty} \sum_{m=-\ell}^{\ell} \left\{ \vec{B}_{\ell m}(\vec{r})\ e^{i\omega_{\ell m} t} + \vec{B}^*_{\ell m}(\vec{r})\ e^{-i\omega_{\ell m} t} \right\} , \tag{2.40}$$

where $\omega_{\ell m}$ is the positive eigenfrequency. We can also combine terms to write the displacements in terms of real quantities

$$\vec{U}^T(\vec{r},t) = \sum_{\ell=0}^{\infty} \sum_{m=-\ell}^{\ell} \left\{ 2\mathrm{Re}(\vec{B}_{\ell m}(\vec{r}))\ \cos \omega_{\ell m} t \cdot \right.$$

$$\left. -2\mathrm{Im}(\vec{B}_{\ell m}(\vec{r}))\ \sin \omega_{\ell m} t \right\} . \tag{2.41}$$

The displacements from spatially finite sources, or those with more complicated time functions, may be derived from (2.40) or (2.41) by convolution.

SPHEROIDAL MODES EXCITED BY A POINT DOUBLE COUPLE

To find the spheroidal mode solutions, we modify Saito's results for the displacements resulting from an arbitrary point source with step function time dependence and unit seismic moment. To zeroeth order, in the geographic frame, Saito's expression is

$$\vec{U}^S(\vec{r},t) = \sum_{\ell=0}^{\infty} \sum_{m=-\ell}^{\ell} D_{\ell m} \left\{ y_1^S(r)\ \vec{S}^1_{\ell m}(\theta,\phi) + y_3^S(r)\ \vec{S}^2_{\ell m}(\theta,\phi) \right\} \tag{2.42}$$

$$\times \left[e^{i\omega^+_{\ell m} t} + e^{i\omega^-_{\ell m} t} \right]$$

where

$$D_{\ell m} = \frac{\left[r^2 \left(f_2^S y_1^S(r) - f_1^S y_2^S(r) \right) + L^2 r^2 \left((f_4^S y_3^S(r) - f_3^S y_4^S(r) \right) \right]_{r=r_s}}{2\omega_\ell^2 \left(I_1^S + L^2 I_2^S \right)} \qquad (2.43)$$

We relate the geographic and source frame modal amplitudes by

$$D_{\ell m} = \sum_{k=-2}^{2} D_{mk}^{\ell}(R)\ D'_{\ell k} \ . \qquad (2.44)$$

Thus in the source frame,

$$D'_{\ell k} = \frac{\left[r^2 \left((f_2^S)' y_1^S(r) - (f_1^S)' y_2^S(r) \right) + L^2 r^2 \left((f_4^S)' y_3^S(r) - (f_3^S)' y_4^S(r) \right) \right]_{r=r_s}}{2\omega_\ell^2 \left(I_1^S + L^2 I_2^S \right)} \qquad (2.45)$$

I_1^S and I_2^S are energy integrals for the spheroidal modes, also defined by Saito.

As we did for the torsional modes, we convert Saito's expansion coefficients for a double couple to those of the normalized complex vector spherical harmonics. These expressions are simplified by introducing the amplitude factors K_o, K_1, K_2 of Kanamori and Cipar:

$$K_o = \left(\frac{2\ell + 1}{4\pi\, \omega_\ell^2 (I_1^S + L^2 I_2^S) r_s} \quad \frac{2(3\lambda_s + 2\mu_s)}{\lambda_s + 2\mu_s} \right)$$

$$\times \left(y_1^S(r_s) - \frac{r_s}{3\lambda_s + 2\mu_s}\, y_2^S(r_s) - \frac{L^2}{2}\, y_3^S(r_s) \right)$$

$$K_1 = \frac{2\ell + 1}{4\pi\ \omega_\ell^2 (I_1^S + L^2 I_2^S)}\ \frac{y_4^S(r_s)}{\mu_s} \qquad (2.46)$$

$$K_2 = \frac{2\ell + 1}{4\pi\ \omega_\ell^2 (I_1^S + L^2 I_2^S)}\ \frac{y_3^S(r_s)}{r_s} \quad ,$$

where λ_s *and* μ_s *are the elastic constants at the source depth. Using* these, and the radiation pattern terms

$$q_o = \frac{1}{2} \sin\lambda \sin\delta \cos\delta$$

$$q_1 = \frac{1}{4} (-\cos\lambda \cos\delta + i \sin\lambda \cos 2\delta) \qquad (2.47)$$

$$q_2 = \frac{1}{4} (-\sin\lambda \cos\delta \sin\delta - i \cos\lambda \sin\delta)$$

we can derive our final relations for the $D'_{\ell m}$ (which are zero for $|m| > 2$)

$$\begin{aligned} D'_{\ell 2} &= K_2 q_2\ C_{\ell 2} \\ D'_{\ell 1} &= K_1 q_1\ C_{\ell 1} \\ D'_{\ell o} &= K_o q_o\ C_{\ell o} \\ D'_{\ell -1} &= K_1 q_1^*\ C_{\ell -1} \\ D'_{\ell -2} &= K_2 q_2^*\ C_{\ell -2} \end{aligned} \qquad (2.48)$$

Again, note that $D'_{\ell m} = (-1)^m\ D'^*_{\ell -m}$. Thus for the geographic expansion *coefficients*

$$D_{\ell m} = (-1)^m D^*_{\ell -m} \ . \tag{2.49}$$

To obtain our final results for the displacements, we define

$$\vec{E}_{\ell m}(\vec{r}) = D_{\ell m}\left\{ y_1^S(r)\ \vec{S}^1_{\ell m}(\theta,\phi) + y_3^S(r)\ \vec{S}^2_{\ell m}(\theta,\phi)\right\} \tag{2.50}$$

We can then write (after disposing of the negative frequencies) that

$$\vec{U}^S(\vec{r},t) = \sum_{\ell=0}^{\infty} \sum_{m=-\ell}^{\ell} \left\{ \vec{E}_{\ell m}(\vec{r})\ e^{i\omega_{\ell m} t} + \vec{E}^*_{\ell m}(\vec{r})\ e^{-i\omega_{\ell m} t} \right\} \tag{2.51}$$

or

$$\vec{U}^S(\vec{r},t) = \sum_{\ell=0}^{\infty} \sum_{m=-\ell}^{\ell} \left\{ 2\mathrm{Re}(\vec{E}_{\ell m}(r))\ \cos \omega_{\ell m} t \right. \tag{2.52}$$

$$\left. -2\mathrm{Im}(\vec{E}_{\ell m}(\vec{r}))\ \sin \omega_{\ell m} t \right\} \ .$$

Note that (2.52) shows that the displacements are real. As with the torsional modes, $\omega_{\ell m}$ is the positive eigenfrequency.

For an isotropic source of unit moment (2.42) through (2.45), (2.51) and (2.52) are used, but the only nonzero excitation coefficient in the source frame is

$$D'_{\ell o} = K'_o\ C_{\ell o} \tag{2.53}$$

where the source amplitude factor K'_o is adapted from Takeuchi and Saito (1972)

$$K_o' = \frac{2\ell + 1}{4\pi\, \omega_\ell^2 (I_1^S + L^2 I_2^S)} \left[- \frac{4\mu_s}{(\lambda_s + 2\mu_s)} \frac{y_1^S(r_s)}{r_s} \right. \tag{2.54}$$

$$\left. - \frac{y_2^S(r_s)}{(\lambda_s + 2\mu_s)} + \frac{2L^2 \mu_s\, y_3^S(r_s)}{(\lambda_s + 2\mu_s) r_s} \right] .$$

NUMERICAL RESULTS

The final expressions for the displacements of spheroidal (2.52) and torsional (2.41) modes are suitable for numerical computation. We require only the source amplitude factors K_o, K_1, K_2, L_1 and L_2, the radial eigenfunctions $y_i(r)$, the three geometric fault parameters (strike, dip and slip), the locations of the source and receiver and the seismic moment. We investigate the dependence of the displacement and strain spectra of the fundamental torsional and spheroidal modes on the geometric fault parameters and the positions of the source and receiver. This also provides us with a method of checking our results. We ensure that the total of the displacements and strains within each multiplet at time t = 0 are equal to those calculated from the expressions of Kanamori and Cipar (1974) for the degenerate modes. Note that the velocities at t = 0 would be identically zero if there was no splitting, but that they differ slightly from zero because of the approximation inherent in the perturbation expansion. A second test is to verify that for an isotropic source we derive the same results

from the addition theorem for Legendre polynomials (Pekeris et al., 1961).

The values of the source amplitude factors K_o, K_1, K_2 and L_1, L_2, which were used by Kanamori and Cipar are listed in Table 2.1. These amplitude factors are for a hypocentral depth of 55 km and a moment of 10^{27} dyne-cm. We also list the radial displacement eigenfunctions at the earth's surface (r = a) for each mode. $y_1^T(a)$ and $y_1^S(a)$ are normalized to one; only $y_3^S(a)$ varies from mode to mode.

We also require the radiation pattern coefficients, which are given in Table 2.2 for each of the four basic faults. For the degenerate case, q_o is the coefficient for radially symmetric Rayleigh waves; q_1 and p_1, for two-lobed Rayleigh and Love waves respectively and q_2 and p_2, for a four-lobed radiation pattern. Seismologists have developed considerable intuition in using surface wave radiation patterns to find fault geometries. It is much more difficult to interpret the singlet amplitudes in our figures intuitively, because each singlet amplitude involves a sum, (2.28) or (2.44), of source frame amplitudes weighted by the rotation matrix elements. Thus, except for some special cases, it is difficult to find simple explanations of the relative amplitudes of singlets within a multiplet.

Strain and displacement spectra are calculated for eight fundamental low order number modes: ${}_0S_2 - {}_0S_5$ and ${}_0T_2 - {}_0T_5$. These modes were chosen because it appears almost certain that they are not seriously affected by perturbations resulting from lateral inhomogeneities. Furthermore, it is only for the lowest order modes that individual

Table 2.1

Source Amplitude Factors and Surface Eigenfunctions

Mode	K_o	K_1	K_2	$y_1^S(a)$(cm)	$y_3^S(a)$(cm)
${}_0S_2$	$.616 \times 10^{-3}$	$.209 \times 10^{-5}$	$.678 \times 10^{-5}$	1.	$.252 \times 10^{-1}$
${}_0S_3$	$.773 \times 10^{-3}$	$.245 \times 10^{-5}$	$-.160 \times 10^{-4}$	1.	-.124
${}_0S_4$	$.768 \times 10^{-3}$	$.243 \times 10^{-5}$	$-.137 \times 10^{-4}$	1.	-.150
${}_0S_5$	$.760 \times 10^{-3}$	$.204 \times 10^{-5}$	$-.105 \times 10^{-4}$	1.	-.146

Mode	L_1	L_2	$y_1^T(a)$(cm)
${}_0T_2$	$.493 \times 10^{-5}$	$.987 \times 10^{-4}$	1.
${}_0T_3$	$.391 \times 10^{-5}$	$.337 \times 10^{-4}$	1.
${}_0T_4$	$.341 \times 10^{-5}$	$.178 \times 10^{-4}$	1.
${}_0T_5$	$.308 \times 10^{-5}$	$.114 \times 10^{-4}$	1.

Table 2.2

Source Frame Radiation Pattern Terms

Fault Type	λ	δ	q_o	q_1	q_2	p_1	p_2
Vertical dip slip (Fig. 3 & 8)	90°	90°	0	$-\frac{i}{4}$	0	$\frac{1}{4}$	0
Vertical strike slip (Fig. 4 & 9)	0°	90°	0	0	$-\frac{i}{4}$	0	$-\frac{1}{4}$
45° dipping dip slip (Fig. 5 & 10)	90°	45°	$\frac{1}{4}$	0	$-\frac{1}{8}$	0	$\frac{i}{8}$
45° dipping strike slip (Fig. 6 & 11)	0°	45°	0	$-\frac{1}{4\sqrt{2}}$	$-\frac{i}{4\sqrt{2}}$	$-\frac{i}{4\sqrt{2}}$	$\frac{-1}{4\sqrt{2}}$

singlet peaks have definitely been resolved observationally.

In figures 2.3 - 2.6 we show synthetic line spectra for four fundamental spheroidal modes. For graphical purposes the lines are drawn symmetrically and evenly spaced about the central frequency, although the eigenfrequency spacing is in fact uneven and asymmetric. The effect of attenuation in broadening these lines has not been included. Amplitudes are normalized within each displacement and strain component.

We plot the spectral amplitude of each displacement and horizontal strain derived from $\vec{E}_{\ell m}$. Note that the spectral amplitudes are equal for the positive and negative (± m) members of each singlet pair. It is also interesting that the amplitudes depend separately on the colatitude of the source and receiver, rather than only on the separation. In fact, the longitudes have no effect on the amplitude spectra and affect only the phase. (For a spatially finite source, the longitudes will affect the spectral amplitudes through interference, and the ±m amplitudes will no longer be equal.)

Figures 2.3 - 2.6 show spectra for four basic fault geometries: vertical dip slip, vertical strike slip, 45^{o} dipping dip slip and 45^{o} dipping strike slip. Two cases are shown in each figure. The top halves of the figures show spectra for the case of fault strike, $\rho = 0^{o}$ and the bottom halves are for $\rho = 45^{o}$. Each half is organized as follows. The columns, from left to right, display the multiplets ${}_{0}S_{2}$, ${}_{0}S_{3}$, ${}_{0}S_{4}$ and ${}_{0}S_{5}$. The rows, from top to bottom, show the displacement components U_r, U_θ, U_ϕ and strain components $e_{\theta\theta}$, $e_{\phi\phi}$ and

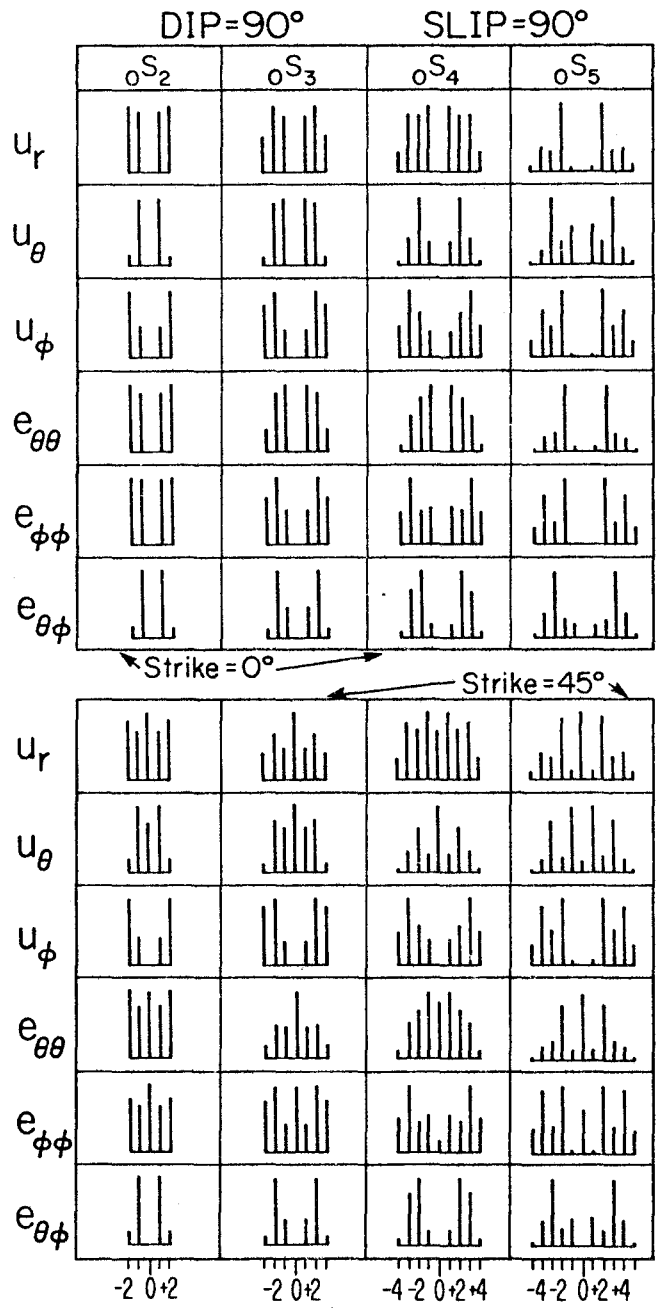

Figure 2.3 - Spheroidal mode amplitude spectra for a vertical strike slip fault at $\theta_s = 30^o$, $\phi_s = 0^o$ observed at $\theta = 105^o$, $\phi = 120^o$ for $\rho = 0^o$ and $\rho = {}_s45^o$.

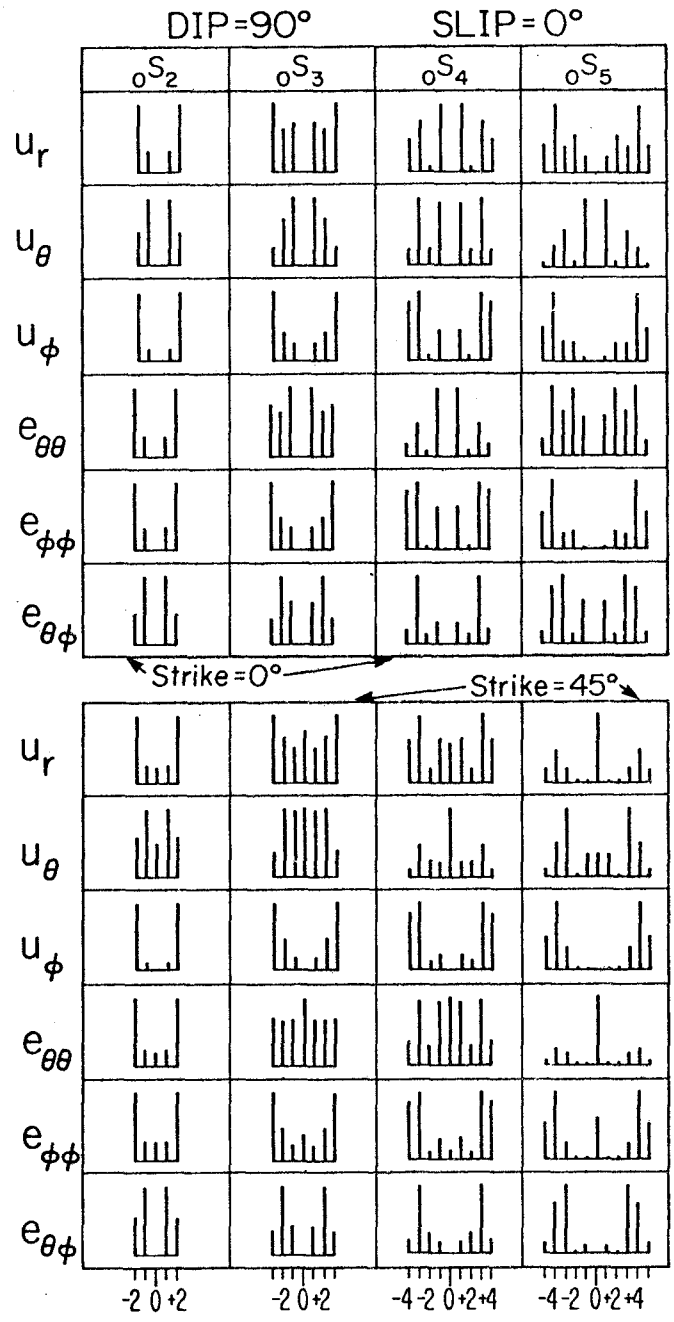

Figure 2.4 - Spheroidal mode amplitude spectra for a vertical strike slip fault at $\theta_s = 30^o$, $\phi_s = 0^o$ observed at $\theta = 105^o$, $\phi = 120^o$ for $\rho = 0^o$ and $\rho = 45^o$.

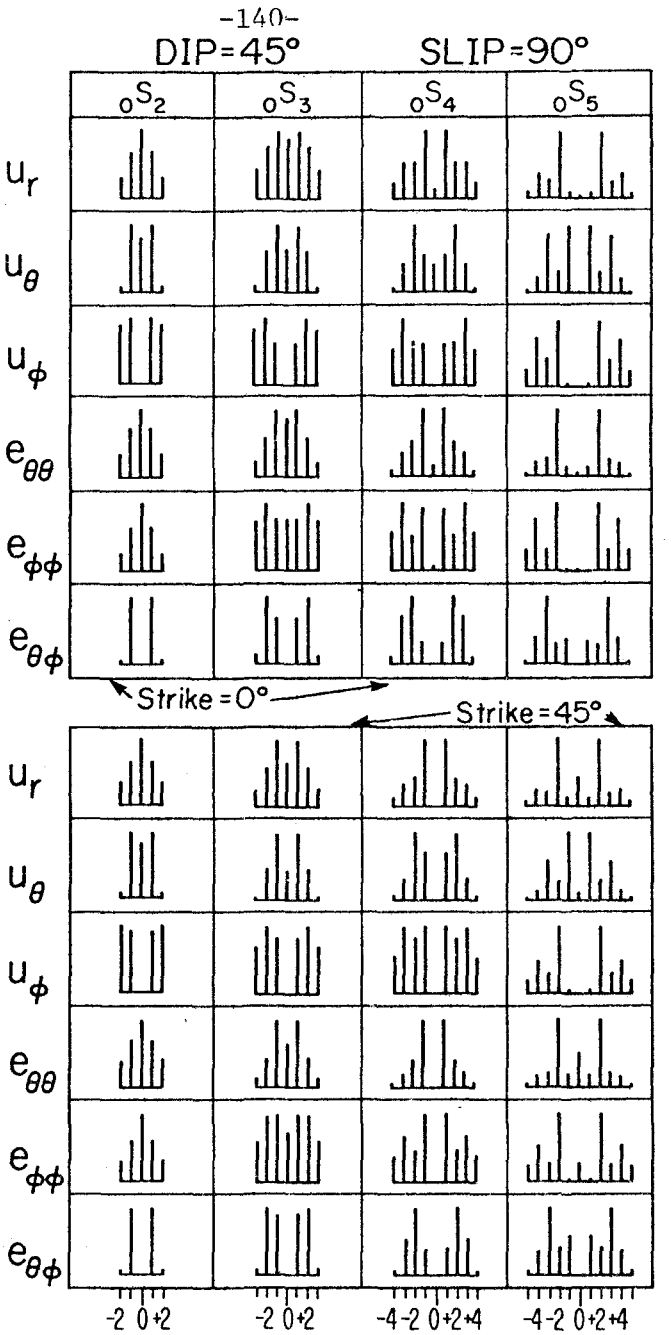

Figure 2.5 - Spheroidal mode amplitude spectra for a 45^o dipping dip slip fault at $\theta_s = 30^o$, $\phi_s = 0^o$ observed at $\theta = 105^o$, $\phi = 120^o$ for $\rho = 0^o$ and $\rho = 45^o$.

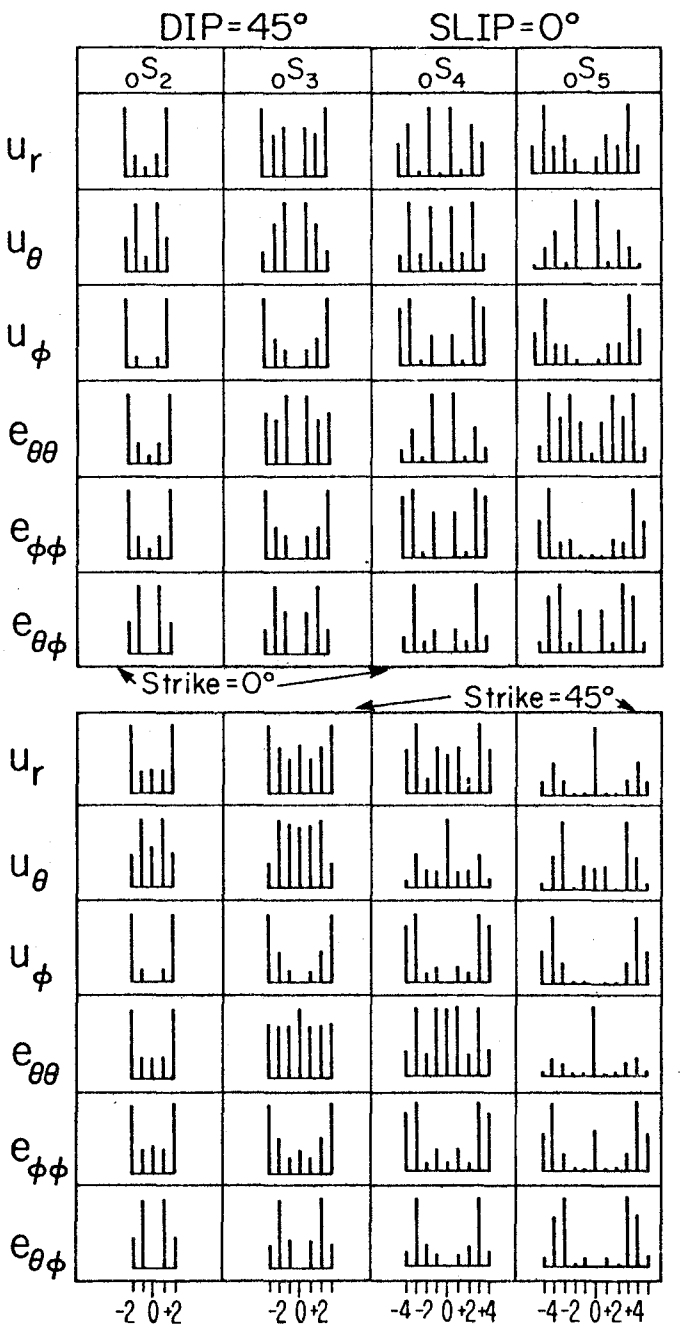

Figure 2.6 - Spheroidal mode amplitude spectra for a 45^o dipping strike slip fault at $\theta_s = 30^o$, $\phi_s = 0^o$ observed at $\theta = 105^o$, $\phi = 120^o$ for $\rho = 0^o$ and $\rho = 45^o$.

$e_{\theta\phi}$. All of the plots were made with the epicenter at $\theta_s = 30^o$, $\phi_s = 0^o$ and a receiver at $\theta = 105^o$, $\phi = 120^o$. Thus, regardless of the source geometry, several singlets always have low amplitudes in these figures because of the small values of $P_\ell^m(\cos 105^o)$ or its derivatives. Even so, the changes in relative spectral amplitudes at a given receiver site (for which the arguments of the associated Legendre polynomials and their derivatives are fixed) caused by variations in fault parameters are substantial.

In general the effect of varying the fault strike appears to be less significant than that of varying the dip or slip angles. In certain cases though, a change in the strike can cause substantial changes in the spectra. For example, for the 45^o dipping strike slip fault with $\rho = 0^o$ in figure 2.6, the m = 0 (zonal) singlet is small for all four multiplets. On the other hand, the 45^o striking fault has large zonal amplitudes for several components. In fact, the zonal term dominates the U_r component of ${}_0S_5$, U_θ of ${}_0S_4$ and $e_{\theta\theta}$ of ${}_0S_5$, which contrast sharply to the same components for the north striking fault. The change in strike has an even more remarkable effect for figure 2.4, the vertical strike slip fault. The zonal term is identically zero for the north striking fault, but dominates some of the components of the 45^o striking fault (e.g. U_r and $e_{\theta\theta}$ of ${}_0S_5$ and U_θ of ${}_0S_4$). (It can be seen either intuitively, from the asymmetry of the displacement about the fault with longitude, or formally, from (2.44), that the zonal terms are zero for the north striking strike slip fault.) In figures 2.3 through 2.6 the 45^o striking fault

usually has a larger amplitude for the zonal singlet than the north striking fault; of course the amplitude of the zonal singlet is always zero for U_ϕ and $e_{\theta\phi}$. Changes in the strike alter the relative excitation within all of the multiplets in these figures; the 45^o dipping dip slip fault (figures 2.5) is affected least.

The effects of varying the dip and slip directions are even more noticeable. For our four figures this effect stems from the different radiation pattern factors, q_i, listed in Table 2.2 The q_i in turn affect the polar frame excitation coefficients given by (2.44). Note that for a particular strike (either $\rho = 0^o$ or 45^o), the ${}_0S_4$ and ${}_0S_5$ multiplets look similar for the two strike slip faults (figures 2.4 and 2.6), and that these multiplets are less similar for the dip slip faults (figures 2.3 and 2.5). The strike-slip pair is quite dissimilar to the dip slip pair. Such generalizations cannot be made for ${}_0S_2$ and ${}_0S_3$. For example, for ${}_0S_2$ the U_r components of the strike slip faults appear similar while the dip slip faults are very different. These effects can be understood in terms of the coefficients in Tables 2.1 and 2.2, the rotation matrices and the vector spherical harmonics, but each individual case must be analyzed in detail. For example, ${}_0S_2$ changes substantially with a change in strike for the vertical dip slip fault (figure 2.3), but hardly at all for the 45^o dipping dip slip fault (figure 2.5). The reason for this is discussed in detail below.

In figure 2.7 we show the spectra for an "isotropic" point source (e.g. an explosion). The relative spectral amplitudes within a

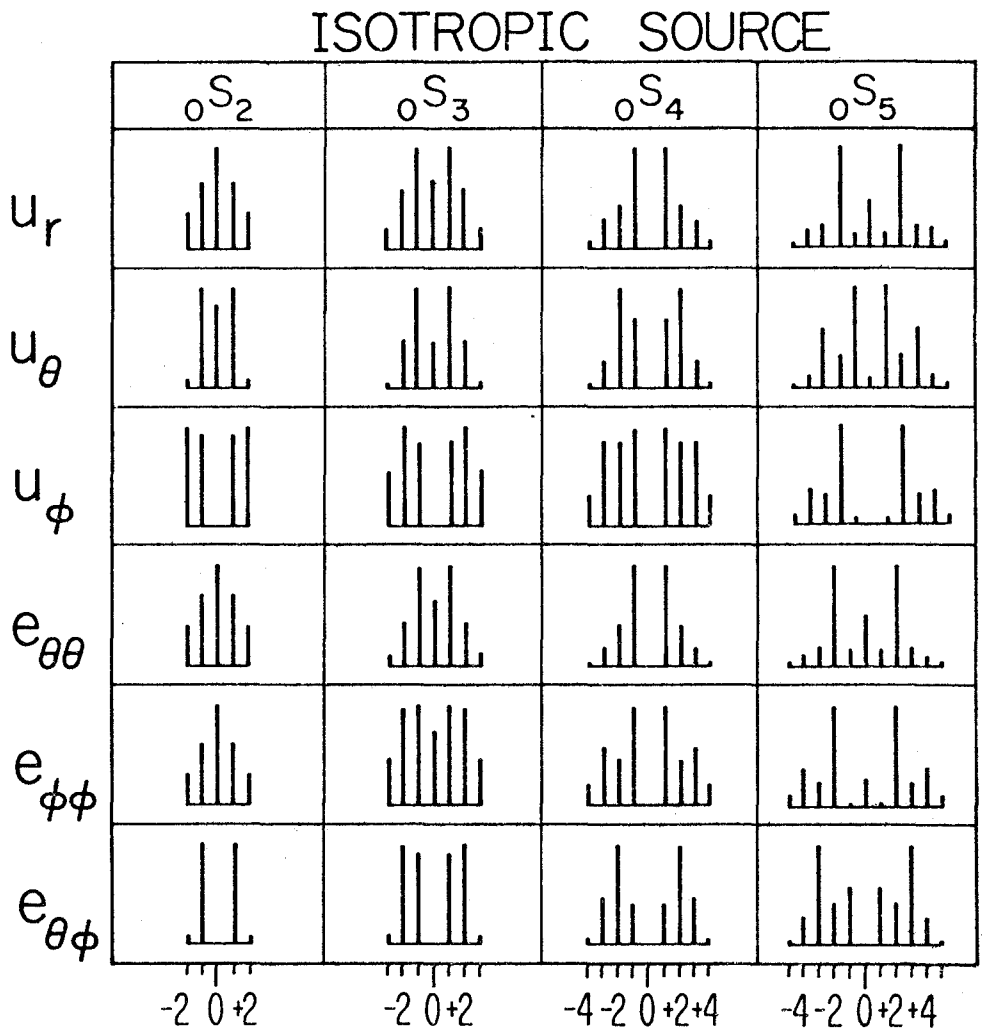

Figure 2.7 - Spheroidal mode amplitude spectra for an isotropic source at $\theta_s = 30^o$, $\phi_s = 0^o$ observed at $\theta = 105^o$, $\phi = 120^o$

multiplet are obtained from (2.50), (2.53) and (2.54). (It can be seen from (2.17), (2.19) and (2.44) that "fault strike," ρ, has no effect on these spectra.) Note that for ${}_0S_2$ and ${}_0S_3$ the spectra in figure 2.7 are nearly identical to the spectra in figures 2.5a and 2.5b. Even if the fault dip is reduced to 10^o (not shown here) the similarity remains. The explanation of this similarity is as follows. From Table 2.1 we see that, for ${}_0S_2$ and ${}_0S_3$, K_o is about one hundred times larger than K_1 or K_2. Whenever q_o, the coefficient of K_o in (2.48), is comparable in magnitude to $\dot{q}_1$ and q_2, then the "isotropic" term will dominate the spectra. From Table 2.2 we see that for the four basic fault geometries only the 45^o dipping dip slip fault has $q_o \neq 0$. Thus the spectra from this fault resemble the isotropic spectra, while the spectra in figures 2.3, 2.4 and 2.6 do not.

Thus the spectra from a shallow angle thrust fault closely resemble the spectra from an isotropic source for low order spheroidal modes. In chapter 3 we discuss the observational consequences of this similarity. Kanamori and Cipar (1974) determined the mechanism of the 1960 Chilean earthquake to be a low angle thrust fault. Due to this particular geometry, Pekeris et al. (1961) were able to match the observed relative spectral amplitudes with an isotropic source model. Spectra from the isotropic source would not have matched the spectra of a pure strike-slip earthquake or an earthquake on a fault with $\delta = 0^o$ or $\delta = 90^o$.

Figures 2.8 - 2.11 show the displacement and strain spectra for torsional modes ${}_0T_2$ - ${}_0T_5$, for the same set of four fault geometries

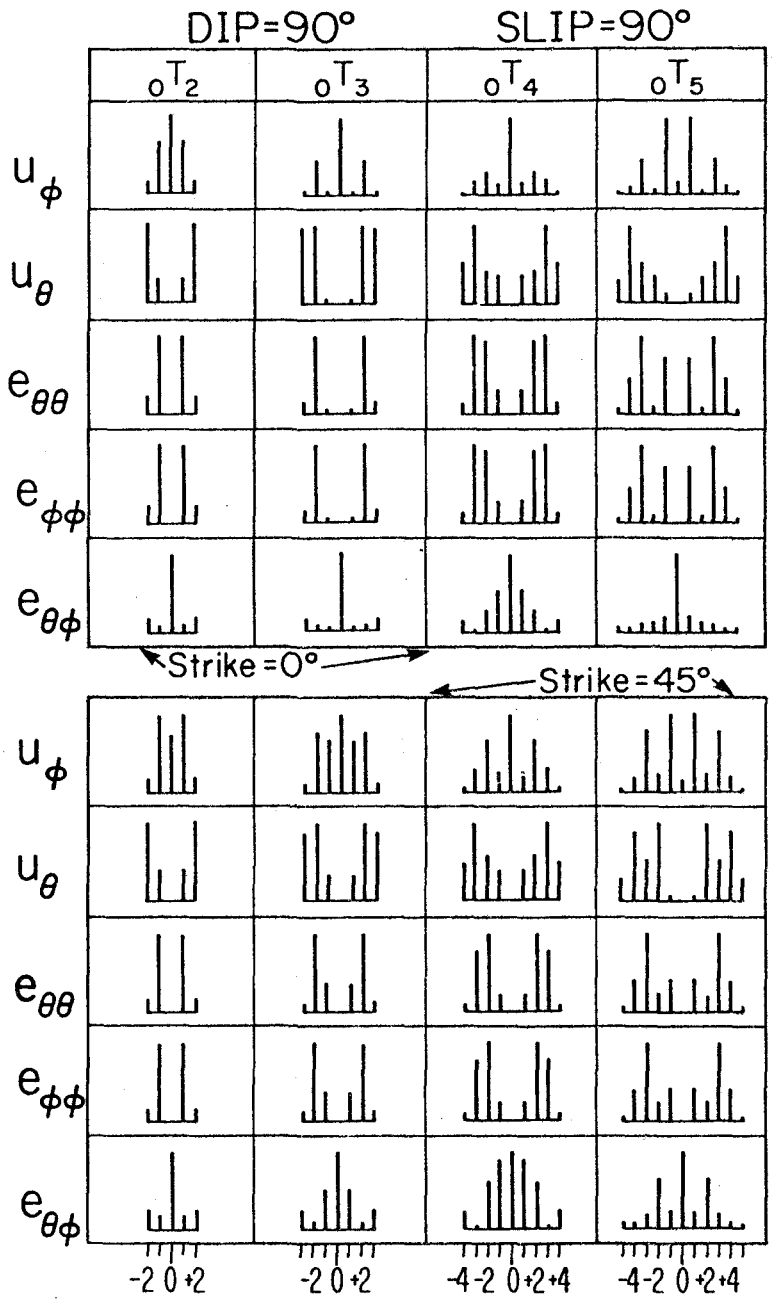

Figure 2.8-Torsional mode amplitude spectra for a vertical dip slip fault at $\theta_s = 30^\circ, \phi_s = 0^\circ$ observed at $\theta = 105^\circ$, $\phi = 120^\circ$ for $\rho = 0^\circ$ and $\rho = 45^\circ$.

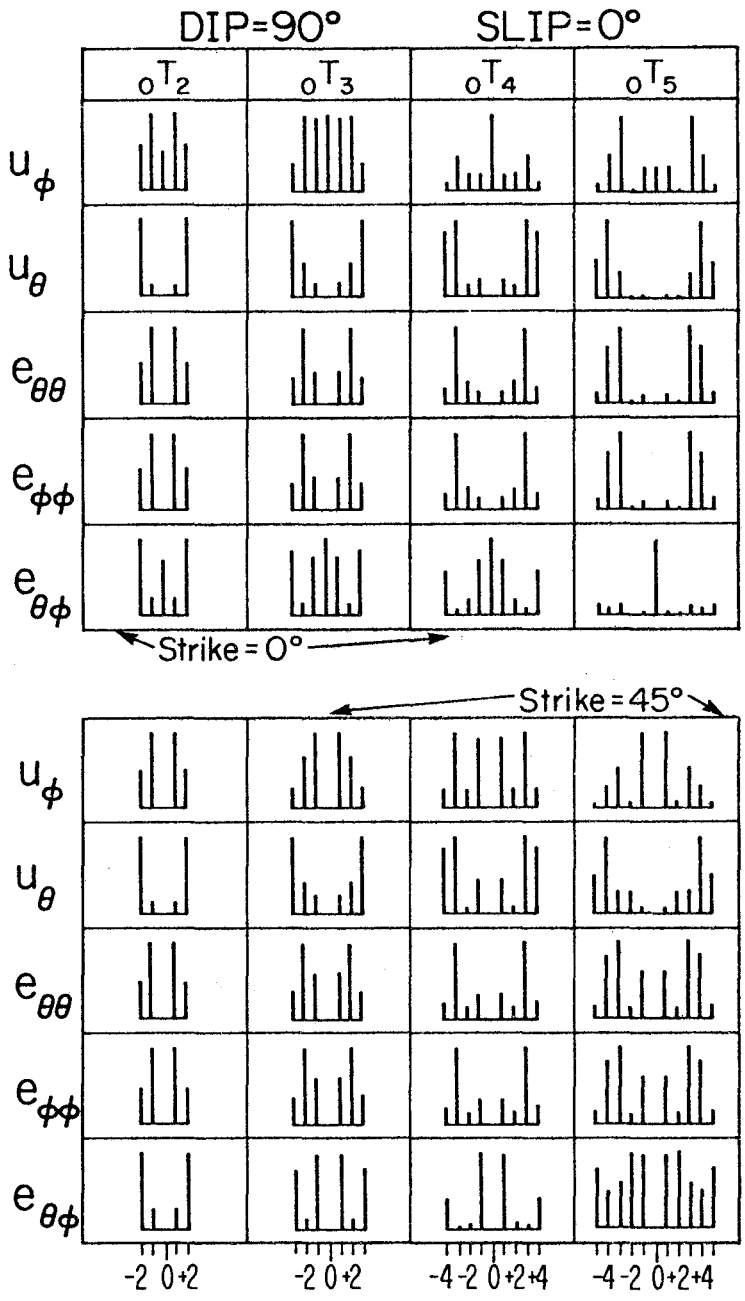

Figure 2.9 - Torsional mode amplitude spectra for a vertical strike slip fault at $\theta_s = 30^o$, $\phi_s = 0^o$ observed at $\theta = 105^o$, $\phi = 120^o$ for $\rho = 0^o$ and $\rho = 45^o$.

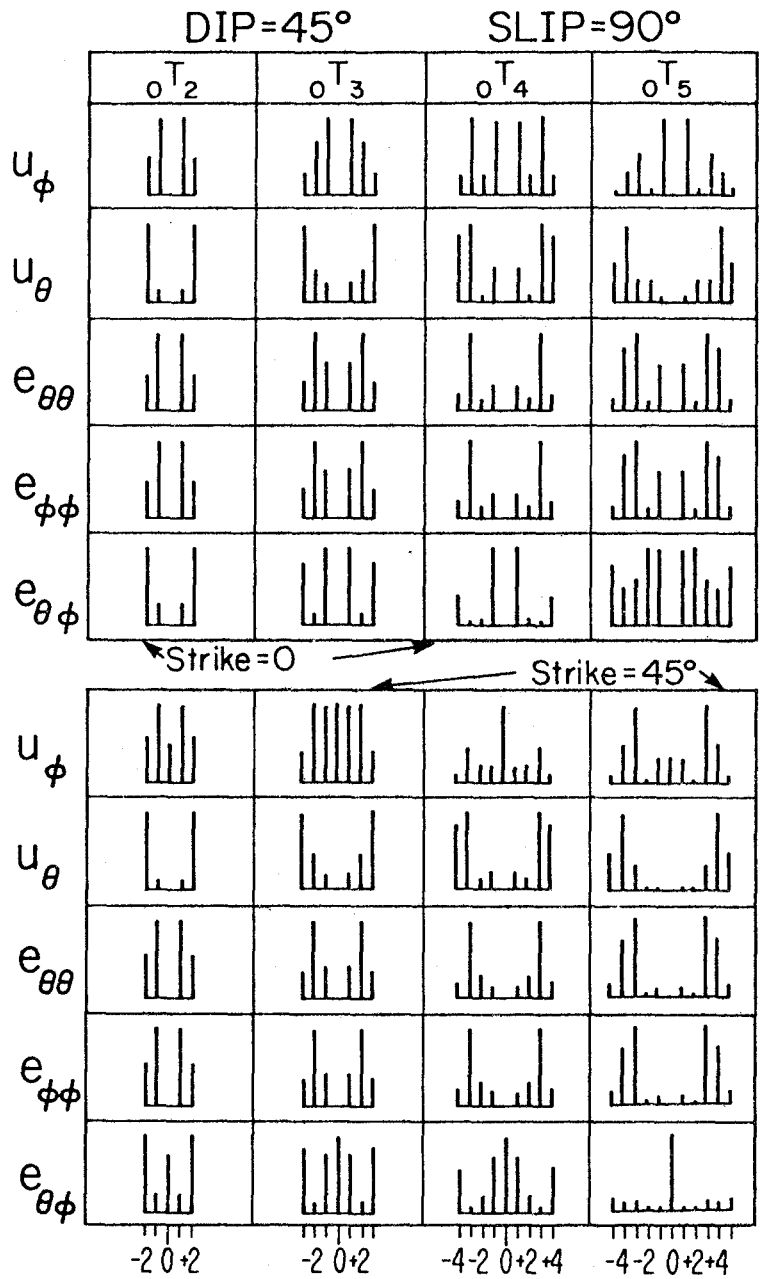

Figure 2.10 - Torsional mode amplitude spectra for a 45^{o} dipping dip slip fault at $\theta_s = 30^{o}$, $\phi_s = 0^{o}$ observed at $\theta = 105^{o}$, $\phi = 120^{o}$ for $\rho = 0^{o}$ and $\rho = 45^{o}$.

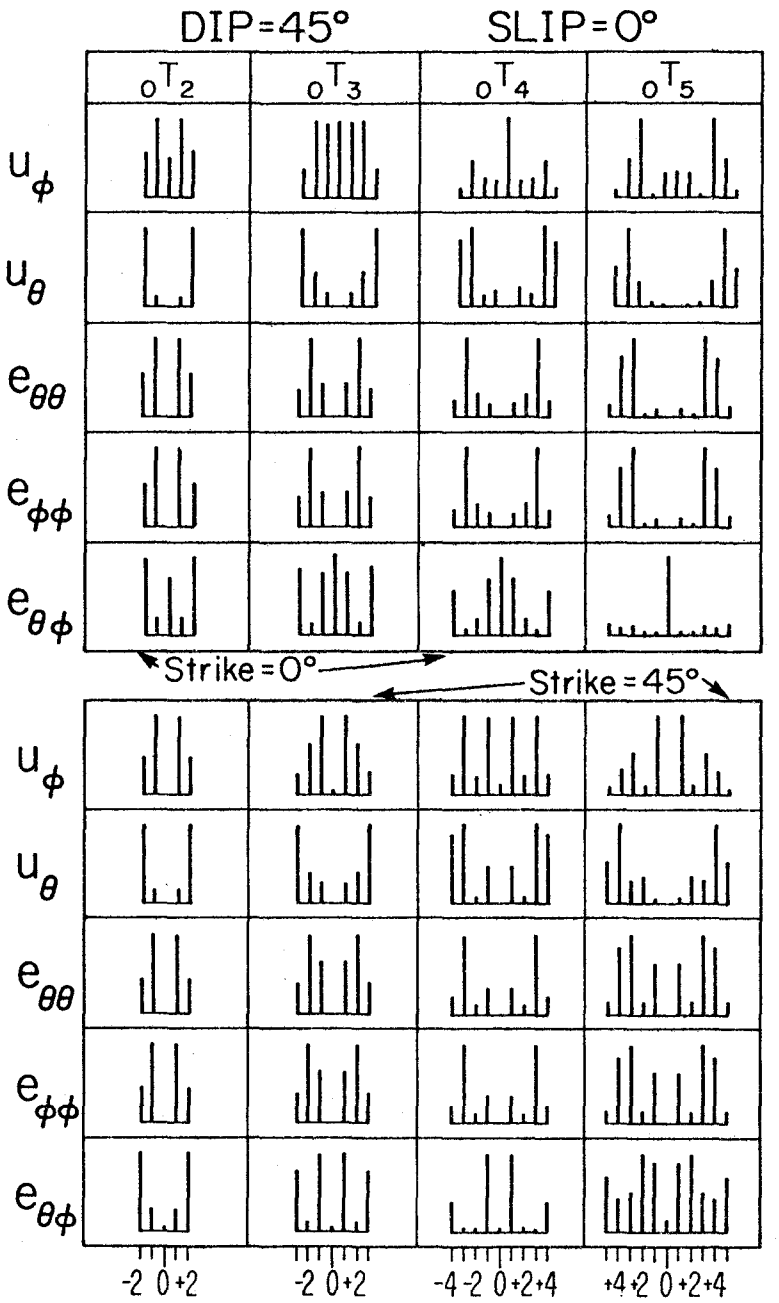

Figure 2.11 - Torsional mode amplitude spectra for a 45^{o} dipping strike slip fault at $\theta_s = 30^{o}$, $\phi_s = 0^{o}$ observed at $\theta = 105^{o}$, $\phi = 120^{o}$ for $\rho = 0^{o}$ and $\rho = 45^{o}$.

as for the spheroidal modes. The torsional modes have no zonal terms in the source frame, but the zonal singlet in the geographic frame is often excited. A spectacular example is the excitation of the U_ϕ component of ${}_0T_4$, and the $e_{\theta\phi}$ components of ${}_0T_5$, by the vertical strike slip fault (figure 2.9). The torsional modes, of course, have no radial displacement component. They also have the property that $e_{\theta\theta} = - e_{\phi\phi}$ since there is no net dilatation. The amplitude spectra of these two strain components are thus identical.

The spectra of the components of ${}_0T_4$ and ${}_0T_5$ are generally similar for the two strike slip faults. This resemblance is much weaker for the dip slip faults. For example, ${}_0T_5$ is similar in figures 2.8 and 2.10, but ${}_0T_4$ is quite different. For the two lower angular order modes the spectra of the strike slip faults are generally very similar, while those of the dip slip faults are sometimes similar, but often show substantial differences. An excellent example of this variability can be seen by examining the two displacement components of ${}_0T_2$ in figures 2.8 and 2.10 - the U_θ components are similar while the U_ϕ components are very different. These same two components show interesting results from a change in strike, which can be seen by contrasting the U_ϕ components of ${}_0T_2$ between the two halves of figure 2.10. As we observed for the spheroidal modes, the 45^o striking fault excites the zonal singlet more strongly.

In conclusion, the amplitude spectra for both displacements and strains show a complicated dependence on the fault parameters for a variety of faults. It is not possible to predict the spectra using

only the locations of the source and receiver to compute the values of the vector spherical harmonics. The geometric fault parameters (strike, dip and slip) must also be used for a complete synthesis of the relative spectral amplitudes.

DISCUSSION

Although our derivations are lengthy and somewhat complicated, the results may be easily used to compute the strains and displacements excited by arbitrary faults. The computations are simplified by the separation of the expressions into factors for five different effects. When any single parameter is charged only part of the results need be recalculated.

The radiation pattern terms q_i and p_i are controlled by the fault dip and slip angles. The Euler angles, and thus the arguments of $D^{\ell}_{mk}(R)$, depend on the fault strike and the geographic coordinates of the epicenter. The receiver position provides the arguments of the vector spherical harmonics. The earth's structure controls the radial eigenfunctions and the energy integrals. Finally, the source depth controls the values of $y_i(r_s)$, $\lambda(r_s)$ and $\mu(r_s)$. For computational purposes the earth structure and source depth effects are combined in the source amplitude factors K_o, K_1, K_2 and L_1, L_2.

It is important to note that for a given source-receiver geometry and fault mechanism, the relative amplitudes of the singlet pairs within a multiplet often differ between multiplets, and even between strain and displacement components of the same multiplet. Our figures

show that in general, similar patterns are not observed for different multiplets.

Luh and Dziewonski (1976) suggested that certain patterns might persist between multiplets in the excitation of singlets. (Their excitation coefficients roughly correspond to our $A_{\ell m}$ and $D_{\ell m}$.) Their suggestion, which seems to be correct, refers to excitation coefficients which are independent of receiver location. On the other hand, the singlet spectral amplitudes are obtained by multiplying the excitation coefficients by the appropriate components of the vector spherical harmonics. Therefore, since each singlet involves a different spherical harmonic the observed spectral amplitudes are strongly dependent on receiver position. For example, Luh and Dziewonski commented that the prominent $m = \pm 1$ peaks in the strain record of the Chilean earthquake at Isabella (Benioff et al., 1961) might support their suggestion. Since the strain spectrum includes the effect of the receiver location, this similarity is fortuitous. However, in this case the $m = \pm 1$ excitation was so dominant that these lines would be largest at most receivers.

Our synthetic spectra have some implications for the determination of the eigenfrequencies of an "equivalent degenerate earth model" from the actual data. It is not uncommon for a multiplet to be excited such that one pair of singlets (e.g. the U_r or U_ϕ components of ${}_0S_2^{\pm 2}$ for both 45° dipping strike slip faults in figure 2.6) has much larger amplitudes than the remainder of the multiplet. If the equivalent degenerate central frequency for the multiplet were determined

by finding the frequency midway between ${}_0S_2^2$ and ${}_0S_2^{-2}$, this estimate would be inaccurate because of the asymmetry of the nongenerate eigenfrequencies about the unperturbed singlet frequency.

Gilbert (1971) suggests that if sources and receivers are distributed randomly on the earth's surface, then stacking a large number of spectral observations would yield an accurate estimate of the degenerate eigenfrequencies if the averaged amplitudes of the individual singlets are approximately equal. However, the spectral amplitudes are influenced by geometric fault parameters as well as source and receiver locations. Thus, it may also be necessary to stack the spectra for a random sample of fault mechanisms. Failure to do so may lead to systematic errors in estimates of the unperturbed eigenfrequencies of the lowest order modes. Since the present dataset used for eigenfrequency estimation probably does not include a random sample of fault parameters and since it has not been demonstrated that stacking will yield approximately equal singlet amplitudes, further study of this question would be useful.

CONCLUSIONS

Expressions are derived for the displacement and strain components of the free oscillations of a laterally homogeneous, rotating and elliptical earth excited by a point double couple. The rotation matrix elements, $D^{\ell}_{mk}(R)$, are used to derive the excitation of the nondegenerate modes from results developed for the degenerate modes of a nonrotating spherically symmetric earth. These results are

presented in a condensed form suitable for computational use. Calculations of the excitation of low order modes are shown for a variety of source and receiver locations and for a number of different fault parameters. These methods allow the synthesis of spectra and time domain records of low order modes for which individual singlets have been observationally resolved. This represents a powerful new tool which is applied to the study of normal mode amplitude data in the following chapters.

REFERENCES

Abe, K. (1970). Determination of seismic moment and energy from the earth's free oscillation, Phys. Earth Planet. Interiors, 4, 49-61.

Agnew, D., J. Berger, R. Buland, W. Farrell and F. Gilbert (1976). International deployment of accelerometers: a network for very long period seismology, EOS, Trans. Am. Geophys. Un., 57, 180-188.

Alterman, Z., H. Jarosch, and C. L. Pekeris (1959). Oscillations of the earth, Proc. R. Soc. London, A252, 80-95.

Backus, G. E. (1964). Geographical interpretation of measurements of average phase velocities over great circular and great semi-circular paths, Bull. Seism. Soc. Am., 54, 571-610.

Backus, G. and F. Gilbert (1961). The rotational splitting of the free oscillations of the Earth, Proc. Nat. Acad. Sci. U.S., 47, 362-371.

Benioff, H., F. Press, and S. Smith (1961). Excitation of the free oscillations of the earth by earthquakes, J. Geophys. Res., 66, 605-619.

Brink, D. M. and G. R. Satchler (1968). Angular Momentum, Clarendon Press, Oxford.

Dahlen, F. A. (1968). The normal modes of a rotating, elliptical Earth, Geophys. J., 16, 329-367.

Dahlen, F. A. (1969). The normal modes of a rotating, elliptical earth - II, near-resonance multiplet coupling, Geophys. J., 18, 397-436.

Dahlen, F. A. (1976). Models of the lateral heterogeneity of the earth consistent with eigenfrequency splitting data, Geophys. J., 44, 77-106.

Dziewonski, A. M. and F. Gilbert (1974). Temporal variation of the seismic moment tensor and the evidence of precursive compression for two deep earthquakes, Nature, 247, 185-188.

Fukao, Y. and K. Abe (1971). Multimode Love waves excited by shallow and deep earthquakes, Bull. Earthq. Res. Inst. Tokyo Univ., 49, 1-12.

Geller, R. J. (1976). Body force equivalents for stress drop seismic sources, Bull. Seism. Soc. Am., 66, 1801-1804.

Gilbert, F. (1970). Excitation of the normal modes of the Earth by earthquake sources, Geophys. J., 22, 223-226.

Gilbert, F. (1971). The diagonal sum rule and averaged eigenfrequencies, Geophys. J., 23, 119-123.

Gilbert, F. (1973). Derivation of source parameters from low frequency spectra, Phil. Trans. R. Soc., A274, 369-371.

Gilbert, F. and A. M. Dziewonski (1975). An application of normal mode theory to the retrieval of structural parameters and source mechanisms from seismic spectra, Phil. Trans. R. Soc., A278, 187-269.

Kanamori, H. (1970a). Synthesis of long-period surface waves and its application to earthquake source studies - Kurile Islands earthquake of October 13, 1963, J. Geophys. Res., 75, 5011-5025.

Kanamori, H. (1970b). The Alaska earthquake of 1964: Radiation of long period surface waves and source mechanism, J. Geophys. Res., 75, 5029-5040.

Kanamori, H. (1971). Focal mechanism of the Tokachi-Oki earthquake of May 16, 1968: Contortion of the lithosphere at a junction of two trenches, Tectonophysics, 12, 1-13.

Kanamori, H. (1976). Re-examination of the earth's free oscillations excited by the Kamchatka earthquake of November 4, 1952, Phys. Earth Planet. Interiors, 11, 216-226.

Kanamori, H. and J. J. Cipar (1974). Focal process of the great Chilean earthquake, May 22, 1960, Phys. Earth. Planet. Interiors, 9, 128-136.

Luh, P. C. (1974). Normal modes of a rotating, self-gravitating inhomogenous earth, Geophys. J., 38, 187-224.

Luh, P. C. and A. M. Dziewonski (1976). Theoretical normal-mode spectra of a rotating elliptical earth, Geophys. J., 45, 617-645.

Madariaga, R. (1972). Toroidal free oscillations of the laterally heterogeneous earth, Geophys. J., 27, 81-100.

Madariaga, R. and K. Aki (1972). Spectral splitting of toroidal-free oscillations due to lateral heterogeneity of the earth's structure, J. Geophys. Res., 77, 4421-4431.

Ness, N., J. Harrison, and L. Slichter (1961). Observations of the free oscillations of the earth, J. Geophys. Res., 66, 621-629.

Okal, E. A. (1976). A surface wave investigation of the Gobi-Altai (December 4, 1957) earthquake, Phys. Earth Planet. Interiors, 12, 319-328.

Pekeris, C. L., Z. Alterman, and H. Jarosch (1961). Rotational multiplets in the spectrum of the earth, Phys. Rev., 122, 1692-1700.

Saito, M. (1967). Excitation of free oscillations and surface waves by a point source in a vertically heterogeneous earth, J. Geophys. Res., 72, 3689-3699.

Saito, M. (1971). Theory for the elastic-gravitational oscillation of a laterally heterogeneous earth, J. Phys. Earth, 19, 259-270.

Shimazaki, K. (1975). Nemuro-Oki earthquake of June 17, 1973: A lithospheric rebound at the upper half of the interface, Phys. Earth Planet. Interiors, 9, 314-327.

Takeuchi, H. and M. Saito (1972). Seismic surface waves, Methods in Computational Physics, 11, 217-295.

Usami, T. (1971). Effect of horizontal heterogeneity on the torsional oscillation of an elastic sphere, J. Phys. Earth, 19, 175-180.

Chapter 3

SPLIT FREE OSCILLATION AMPLITUDES FOR THE 1960 CHILEAN AND 1964 ALASKAN EARTHQUAKES

ABSTRACT

Splitting of the earth's normal modes was observed for both the 1960 Chilean and 1964 Alaskan earthquakes. The strong peaks in the observed spectrum of each split multiplet correspond to singlets with much higher amplitudes than the others. The theoretical results derived in the last chapter predict this pattern. The source mechanisms inferred for these earthquakes from surface waves are consistent with the observed pattern of relative spectral amplitudes of the split modes. However other mechanisms, such as a slow isotropic volume change, are also consistent with the split mode amplitudes and are excluded only by additional data.

INTRODUCTION

Splitting of the earth's normal modes was first observed by Benioff, Press and Smith (1961), and Ness, Harrison and Slichter (1961) for the Chilean earthquake. Pekeris, Alterman and Jarosch (1961) and Backus and Gilbert (1961) calculated the frequency separation due to the earth's rotation and obtained good agreement with the observed data. Pekeris et al. and Backus and Gilbert both calculated the relative amplitudes of each peak for some simple sources. However, the spectral amplitudes resulting from realistic models of the Alaskan and Chilean earthquakes as double couple sources have not previously been calculated. In this chapter we use the results developed in the last chapter to calculate the split mode amplitudes for the Chilean and Alaskan earthquakes. The predicted spectra agree quite well with published observation of the split spectra.

At the time of the Chilean earthquake, the major interest in free oscillation studies was the accurate determination of the eigenfrequencies of the normal modes of the earth. Accordingly, when the split peaks were discovered in the spectra of ${}_0S_2$ and ${}_0S_3$ by the Caltech (Benioff et al.) and UCLA (Ness et al.) groups, the principal question of interest was the amount of frequency separation between peaks. Both Pekeris et al. and Backus and Gilbert did calculate the amplitudes for simple source models, obtaining reasonably good agreement with observations, but the amplitude data were not studied in detail.

A more detailed study of the amplitudes of the split free oscillations could not be carried out until two related results had been

achieved. The first was the realization (by Burridge and Knopoff, 1964) that an earthquake source could be modeled as a shear dislocation, which in turn is completely equivalent to a double couple. (The research leading up to this conclusion is reviewed in chapter 3 of part I.) The second item was the first complete solution for the excitation of the earth's normal modes by a point force, couple or double couple, which was derived by Saito (1967). After these two studies had been completed, it then was possible to study the amplitudes of the split normal modes excited by a realistic model of an earthquake source.

When these basic theoretical results had been derived, interest in studying the amplitude data had waned. As discussed in the last chapter, extensive theoretical work was later done on the splitting caused by the earth's ellipticity, lateral heterogeneity and attenuation. However no further work was done on studies of the data for the rotationally split normal modes, which are the only examples of splitting ever to have been observed. The work in this chapter thus represents the first comparison of the theoretical split spectra calculated for the realistic source models to the previously published observations for the Chilean and Alaskan earthquakes.

THEORETICAL SPLIT MODE AMPLITUDES

The earth's rotation (Pekeris et al., 1961 and Backus and Gilbert, 1961) and ellipticity (Dahlen, 1968) split the $2\ell + 1$ singlets belonging to the multiplet of angular order ℓ such that each one has a distinct

eigenfrequency. The splitting is observable only for low angular order modes, for which the frequency separation of the singlets caused by rotation and ellipticity is greater than the broadening of spectral lines due to attenuation. For modes for which the splitting is observable, some singlets have much larger amplitudes than others in their multiplet. Thus the relative amplitudes of the split modes serve as an additional constraint in determining the character of earthquake source mechanisms at very long periods.

The theoretical results of the last chapter allow us to synthesize the split normal mode amplitudes excited by a realistic model of an earthquake source: a double couple of arbitrary orientation resulting from slip on a fault plane. (An extensive discussion of other previous work is given in the last chapter.) The solution is obtained by transforming the spherical harmonic expansion of the excitation from the frame of reference of the source into geographic coordinates. We write the singlet amplitudes so that there are separate factors for source location (latitude and longitude), source depth, fault geometry (strike, dip and slip direction), receiver location and the normalized energy of each mode.

For the spheroidal modes and for a step function dislocation with unit moment, the displacement spectrum of the normal mode with angular order ℓ and azimuthal order m is given to zeroeth order by equation 2.50 of the last chapter.

Since the Chilean earthquake spectrum was observed on a strain meter, we compute the horizontal strain components

$$e_{\theta\theta} = \frac{1}{r}\frac{\partial U_\theta}{\partial \theta} + \frac{U_r}{r}$$

$$e_{\phi\phi} = \frac{1}{r \sin\theta}\frac{\partial U_\phi}{\partial \phi} + \frac{U_\theta}{r}\cot\theta + \frac{U_r}{r}$$

$$e_{\theta\phi} = \frac{1}{2}\left[\frac{1}{r}\frac{\partial U_\phi}{\partial \theta} - \frac{U_\phi \cot\theta}{r} + \frac{1}{r \sin\theta}\frac{\partial U_\theta}{\partial \phi}\right] . \qquad (3.1)$$

The strains are given in geographic coordinates, so the strain in a strain rod of arbitrary orientation is

$$e_{rod} = e_{\theta\theta}\cos^2\gamma + 2e_{\theta\phi}\cos\gamma\sin\gamma + e_{\phi\phi}\sin^2\gamma \qquad (3.2)$$

where γ is the strain rod orientation measured counterclockwise from north.

OBSERVED SPECTRA

There are very few reliable observations of split spectra. Not only are great lengths of record needed to resolve splitting, but, because attenuation broadens the peaks, even a very long record length does not allow resolution of splitting for any but the lowest angular order modes. This problem is discussed in Benioff et al. (1961).

Here we use the three best observations of split spectra, two for the Chilean earthquake ($_0S_2$ and $_0S_3$) and one for the Alaskan earthquake ($_0S_2$). Using the theory summarized in the previous chapter, and fault geometries determined from the study of long period surface waves, we

compute synthetic spectra. We also compute synthetic spectra for an isotropic source, and compare the two sets of theoretical spectra to observations. Our synthetic relative spectral amplitudes are in excellent agreement with the data.

Figure 3.1 (from Benioff et al., 1961) shows the spectra of the spheroidal multiplets ${}_0S_2$ and ${}_0S_3$ excited by the Chilean earthquake, as observed on a strainmeter (striking 38.4°W of N) at Isabella, California. Dahlen's (1968) splitting parameters are used to identify the azimuthal order numbers of the peaks in figure 3.1 and the center frequency is adjusted to give the best fit. The singlet pair with $m = \pm 1$ has much larger amplitudes than the rest of the ${}_0S_2$ multiplet and, similarly, ${}_0S_3^{\pm 2}$ stands out from its multiplet. (The results of a later analysis by Smith (1961) of the spectrum differed somewhat but did not later the basic conclusion that ${}_0S_2^{\pm 1}$ and ${}_0S_3^{\pm 2}$ had much larger amplitudes than the other singlets of their multiplets.)

As well as the observed spectra, we show our synthetic relative spectral amplitudes computed for the finite fault geometry determined by Kanamori and Cipar (1974) from long period surface wave studies ($\rho = 350^\circ$, $\lambda = 90^\circ$, $\delta = 10^\circ$, $\theta_s = 128^\circ$, $\phi_s = 286.5^\circ$, $L = 800$ km, $V_R = 3.5$ km/sec) and including a precursory slip ($t_p = 900$ sec and $\tau_0 = 300$ sec) inferred from a time domain observation (Kanamori and Cipar, 1974) and from spectral holes (Kanamori and Anderson, 1975). We also show the relative spectra for an isotropic point source, a model which was used by Pekeris et al. (1961) for the Chilean earthquake. For both sources the spectral amplitudes do not depend on the precise frequency

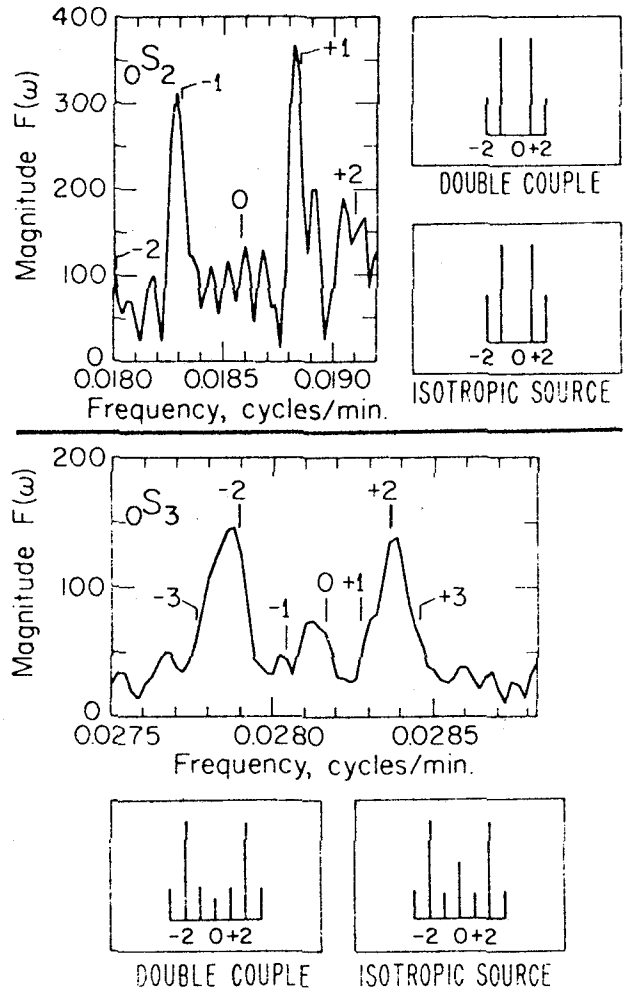

Figure 3.1 - Split spheroidal mode spectra for ${}_0S_2$ (top) and ${}_0S_3$ (bottom) excited by the 1960 Chilean earthquake, as observed on a strainmeter at Isabella, California (after Benioff et al., 1961). The vertical scale of the observed eigenfrequency separation is taken from Dahlen (1968), but the central frequency is chosen to yield a best fit with the observed peaks. Synthetic relative spectra for an isotropic source and for the finite fault geometry of Kanamori and Cipar (1974) are given for each mode. The amplitudes are normalized and plotted with regular spacing.

separation, so for convenience we plot our theoretical amplitudes with regular spacing, although the actual spacing is somewhat asymmetric. The amplitudes of the split modes are symmetric for a point source; interference effects may cause a slight asymmetry for a finite source. However, in this case the finiteness and directivity have only a negligible effect on the relative spectral amplitudes.

Figure 3.2 shows the spectrum from a gravity meter record (Slichter, 1967) of the Alaskan earthquake, after processing and filtering by Wiggins and Miller (1972). In this spectrum the singlet pair ${}_0S_2^{\pm 1}$ has much greater amplitude than the rest of the multiplet. Below this figure we show synthetic spectra (which have the same relative amplitudes as the vertical displacements) for the finite fault geometry ($\rho = 114^o$, $\lambda = 90^o$, $\delta = 20^o$, $\theta_s = 29.9$, $\phi_s = 212.4^o$, $L = 500$ km, $V_R = 3.5$ km/sec) determined by Kanamori (1970) and for an isotropic source.

For both earthquakes, the double couple mechanism derived from long period surface waves yields relative spectra which fit the observations. The exact amplitudes of the lower amplitude peaks are somewhat uncertain, and so the primary consideration is the overall agreement of our theoretical spectra with the observed peaks. These calculations demonstrate that the fault geometry determined from surface waves at periods of several hundred seconds is consistent with free oscillation data at a period of almost one hour. However, the relative spectra for the isotropic source are also consistent with the observations and in fact closely resemble the double couple spectra.

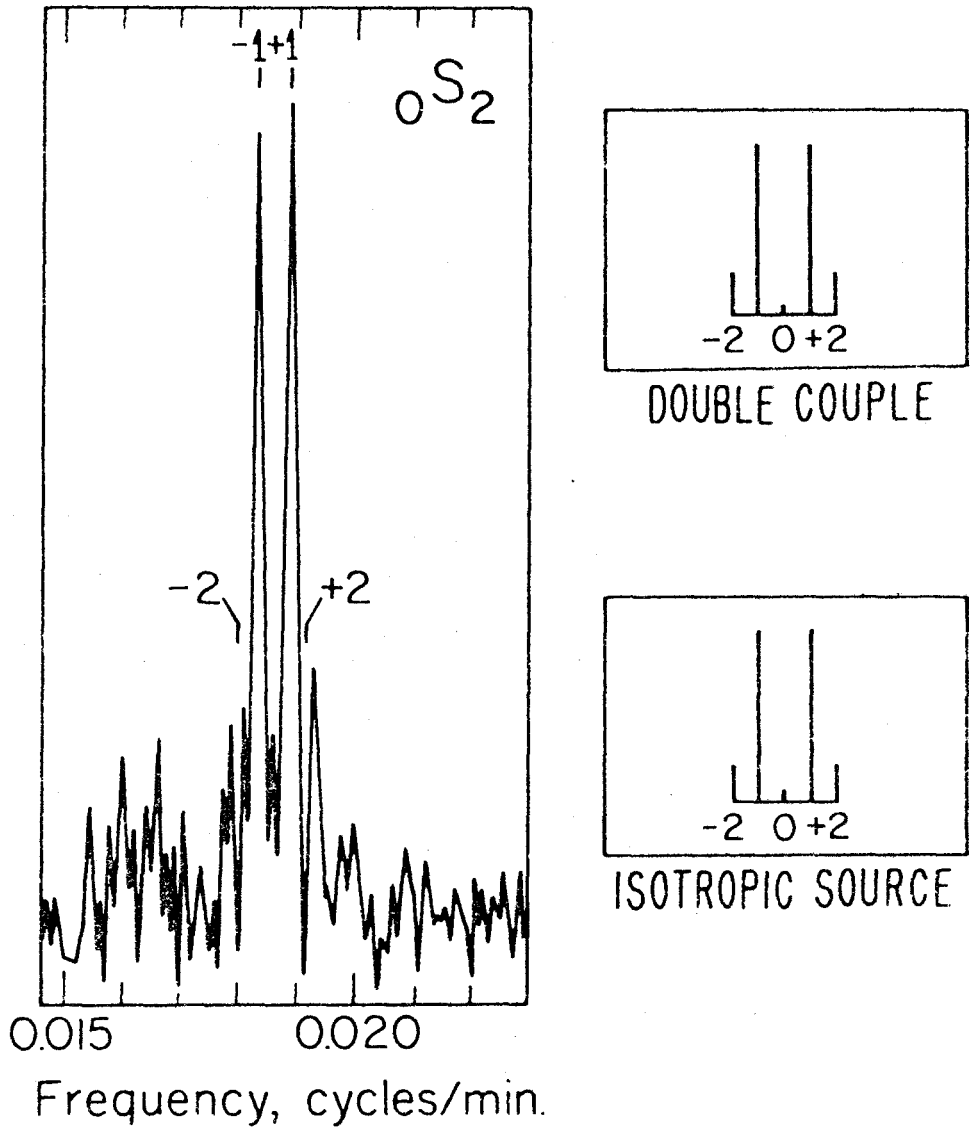

Figure 3.2 - Split spheroidal mode spectra for $_0S_2$ excited by the Alaskan earthquake as observed on a gravity meter at Los Angeles, California by Slichter (1967) after processing by Wiggins and Miller (1972). Details are as in figure 3.1. The finite fault geometry of Kanamori (1970) is used for the double couple source.

DISCUSSION

We have described the reasons for this similarity in some detail in the last chapter, but a briefer explanation will suffice. In the frame of reference of the earthquake source, the radiation patterns of ${}_0S_2$ and ${}_0S_3$ for a double couple are nearly radially symmetric, because the radially symmetric term is much larger than the two-lobed or four-lobed terms. Thus, for these low order spheroidal modes, the radiation pattern of an earthquake nearly always resembles that of an isotropic source, which is completely radially symmetric. This resemblance is maintained when the excitation is transformed into geographic coordinates to calculate the split mode amplitudes. The relative spectra of an earthquake will differ significantly from those of an isotropic source only in special cases, e.g. a pure strike-slip fault.

The isotropic and double couple sources can be resolved very simply from the amplitudes of low order torsional modes, since the former would not excite any torsional oscillations. Torsional oscillations are clearly visible for both the Chilean (Benioff et al., 1961) and Alaskan (Smith, 1966) earthquakes. In addition, long period Rayleigh wave (spheroidal oscillations) and Love wave (torsional oscillations) data are consistent with a double couple source, but not an isotropic source, up to periods of several hundred seconds (Kanamori, 1970; Kanamori and Cipar, 1974). Therefore, the double couple source seems preferable in explaining the very long period free oscillation spectra. It is, of course, possible that an isotropic source component may exist as well as the dominant double couple source. This is a difficult

issue to resolve. Further study seems warranted; the observation of splitting for higher spheroidal models and for torsional modes could be useful in determining the mechanisms of these earthquakes, and others as well, at long periods.

For example, the theoretical singlet amplitudes of double couples depend strongly on fault geometry for spheroidal modes with $\ell > 4$ and in general differ from those of an isotropic source. Thus, if splitting of these modes could be observed, it would be possible to test whether the fault mechanism determined from surface waves is appropriate for much longer period free oscillations. Furthermore, once the mechanism has been determined, the absolute spectral amplitudes may be used to determine the moment at these much longer periods.

An alternate approach, which is used in the next chapter, is to study time domain records of these earthquakes, for the lowest angular order modes. We demonstrate in the next chapter that modes ($_0S_4$, $_0S_5$, $_0T_3$, $_0T_4$) for which splitting is difficult to observe in the frequency domain show the effects of splitting in the time domain. By computing synthetic seismograms for different fault geometries, we can obtain additional information about the source.

Kanamori (1977) has summarized evidence showing that the interplate slip rates inferred from long period surface waves are considerably smaller than those determined from magnetic anomalies. In view of the observations (Kanamori, 1972; Shimazaki and Geller, 1977) that in several cases the earthquake moment was still increasing at periods of several hundred seconds, it seems desirable to use low order free

oscillations to determine the moment at periods of almost one hour. Such determinations would allow us to distinguish between earthquake deformation having a time constant of one hour and longer period aseismic slip which might involve large portions of the lithosphere. For past great earthquakes (e.g. Chile and Alaska), poorly determined instrument calibrations and the small number of long period records present difficulties in determining absolute spectral amplitudes. The new long period network (Agnew et al., 1976) should allow much more reliable very long period moment determinations.

REFERENCES

Agnew, D., J. Berger, R. Buland, W. Farrell and F. Gilbert (1976). International deployment of accelerometers: a network for very long period seismology, EOS, Trans. Am. Geophys. Un., 57, 180-188.

Backus, G. and F. Gilbert (1961). The rotational splitting of the free oscillations of the earth, Proc. Nat. Acad. Sci. US, 47, 362-371.

Benioff, H., F. Press and S. Smith (1961). Excitation of the free oscillations of the earth by earthquakes, J. Geophys. Res., 66, 605-619.

Burridge, R. and L. Knopoff (1964). Body force equivalents for seismic dislocations, Bull. Seism. Soc. Am., 54, 1875-1888.

Dahlen, F. A. (1968). The normal modes of a rotating, elliptical earth, Geophys. J., 16, 329-367.

Kanamori, H. (1970). The Alaska earthquake of 1964: Radiation of long period surface waves and source mechanism, J. Geophys. Res., 75, 5029-5040.

Kanamori, H. (1972). Mechanism of tsunami earthquakes, Phys. Earth Planet. Interiors, 6, 346-359.

Kanamori, H. (1977). Seismic and aseismic slip along subduction zones and their tectonic implications, AGU Monograph (Ewing volume), in press.

Kanamori, H. and D. L. Anderson (1975). Amplitude of the earth's free oscillations and long period characteristics of the earthquake

source, J. Geophys. Res., 80, 1075-1078.

Kanamori, H. and J. J. Cipar (1974). Focal process of the great Chilean earthquake, May 22, 1960, Phys. Earth Planet. Interiors, 9, 128-136.

Ness, N., J. Harrison, and L. Slichter (1961). Observations of the free oscillations of the earth, J. Geophys. Res., 66, 621-629.

Pekeris, C. L., Z. Alterman, and H. Jarosch (1961). Rotational multiplets in the spectrum of the earth, Phys. Rev., 122, 1692-1700.

Saito, M., (1967). Excitation of free oscillations and surface waves by a point source in a vertically heterogeneous earth, J. Geophys. Res., 72, 3689-3699.

Shimazaki, K. and R. J. Geller (1977). Source process of the Kurile Islands tsunami earthquake of June 10, 1975, to be presented at 1977 Spring Annual Meeting of Am. Geophys. Un.

Slichter, L. B. (1967). Spherical oscillations of the earth, Geophys. J., 14, 171-177.

Smith, S. W. (1961). An investigation of the earth's free oscillations, Ph. D. Thesis, California Institute of Technology.

Smith, S. W. (1966). Free oscillations excited by the Alaskan earthquake, J. Geophys. Res., 71, 1183-1193.

Wiggins, R. A. and S. P. Miller (1972). New noise-reduction technique applied to long-period oscillations from the Alaskan earthquake, Bull. Seism. Soc. Am., 62, 471-479.

Chapter 4

TIME DOMAIN OBSERVATION AND SYNTHESIS OF SPLIT SPHEROIDAL AND TORSIONAL FREE OSCILLATIONS OF THE 1960 CHILEAN EARTHQUAKE

ABSTRACT

The rotationally and elliptically split normal modes of the earth are observed for the 1960 Chilean earthquake by analysis in the time domain. One hundred and fifty hours of the Isabella, California strain record are narrow band filtered about the central frequency of each split multiplet to isolate the complex waveform resulting from the interference of the different singlets. Synthetic seismograms are computed using the theoretical results in chapter 2, which show the dependence of the amplitude and phase of the singlets on source location, depth, mechanism and the position of the receiver. By comparing these synthetics to the filtered record, the splitting of modes whose splitting had not been previously resolved is demonstrated: torsional modes (${}_0T_3$, ${}_0T_4$) and spheroidal modes (${}_0S_4$, ${}_0S_5$). The splitting of ${}_0S_2$ and ${}_0S_3$ is reconfirmed. Good agreement is obtained between the synthetics and the filtered data for a source mechanism (previously determined from long period surface waves) of thrust motion on a shallow dipping fault.

Several different methods for estimating the Q of split normal modes are discussed. It is shown that techniques which do not explicitly consider the splitting give seriously inaccurate Q estimates. Of

frequency domain. It is shown that splitting is present for modes for which it has not been previously resolved, including torsional modes.

DATA AND ANALYSIS

Figure 4.1 shows one hundred and fifty hours of the network strain record (filtered electronically to reduce the tidal amplitudes) from Isabella, California (Benioff et al., 1961) for the great 1960 Chilean earthquake. The record (top) was processed to remove tides by twice subtracting three hour running averages. The resulting record (bottom) was tapered at both ends and then filtered to resolve individual low angular order modes. The resulting narrow band filtered data are shown in the upper traces in Figures 4.2 through 4.7 for four spheroidal and two torsional modes. All these waveforms show the general ($e^{-\omega t/2Q}$) attenuation of the entire mode superimposed on a complicated pattern which results from the interference of the split singlets.

The narrow band filter had zero phase shift and an amplitude response decaying exponentially from 1 at the center of the passband to e^{-1} at either end. Outside the passband the filter response was identically zero. The selection of bandwidth was empirical. Widening the window shortens the transient response time of the filter, but also allows more noise to pass. In practice it was found that pass-bands about twice as wide as the splitting interval represented a good compromise between minimizing signal distortion and minimizing noise

techniques which do include splitting effects, comparison of time domain synthetics to narrow band filtered data appears to be an extremely promising method.

Uncertainties in the instrumental response curve for the Isabella strainmeter make it difficult to obtain accurate absolute amplitudes, and thus moment values. However, by comparing the strain records of the Chilean earthquake to the 1964 Alaskan earthquake, the long period moment for Chile is found to be 3.26 times larger than for Alaska. If the effective moment for Alaska is constant from 300 sec to almost one hour, then the moment of the Chilean earthquake for ${}_0S_2$ is estimated to be 2.4×10^{30} dyne cm, using Kanamori's (1970) value of 7.5×10^{29} dyne cm for Alaska.

INTRODUCTION

Split peaks in the earth's normal mode spectrum were first observed for the 1960 Chilean earthquake. The splitting of ${}_0S_2$ and ${}_0S_3$ was reported by Benioff, Press and Smith (1961) and Ness, Harrison and Slichter (1961). Slichter (1967) observed the splitting of ${}_0S_3$ for the 1964 Alaskan earthquake. Splitting has never been clearly demonstrated for other spheroidal modes or for any torsional modes.

Extensive theoretical efforts (summarized in the last two chapters) have been devoted to the computation of the eigenfrequencies of the $2\ell + 1$ individual singlets into which the multiplet of angular order ℓ (e.g., ${}_nS_\ell$) is split. This frequency splitting of the very long period modes is primarily due to rotation (Pekeris et al., 1961 and Backus and Gilbert, 1961) and ellipticity (Dahlen, 1968). In chapter 2 theoretical results were derived which allowed the calculation of the amplitudes and phases of the split normal modes (or equivalently, their time history) excited by a double couple of arbitrary orientation resulting from slip on a fault plane. These results were applied successfully in chapter 3 to split spectra of the Chilean and Alaskan earthquakes.

In this chapter source models derived from long-period surface wave studies are used to generate synthetic seismograms for six multiplets (${}_0S_2$ - ${}_0S_5$, ${}_0T_3$, ${}_0T_4$). The synthetics are then compared to the time domain record of the Chilean earthquake which is narrow-band filtered to isolate each multiplet. This procedure yields several results which were not obtained by earlier studies in the

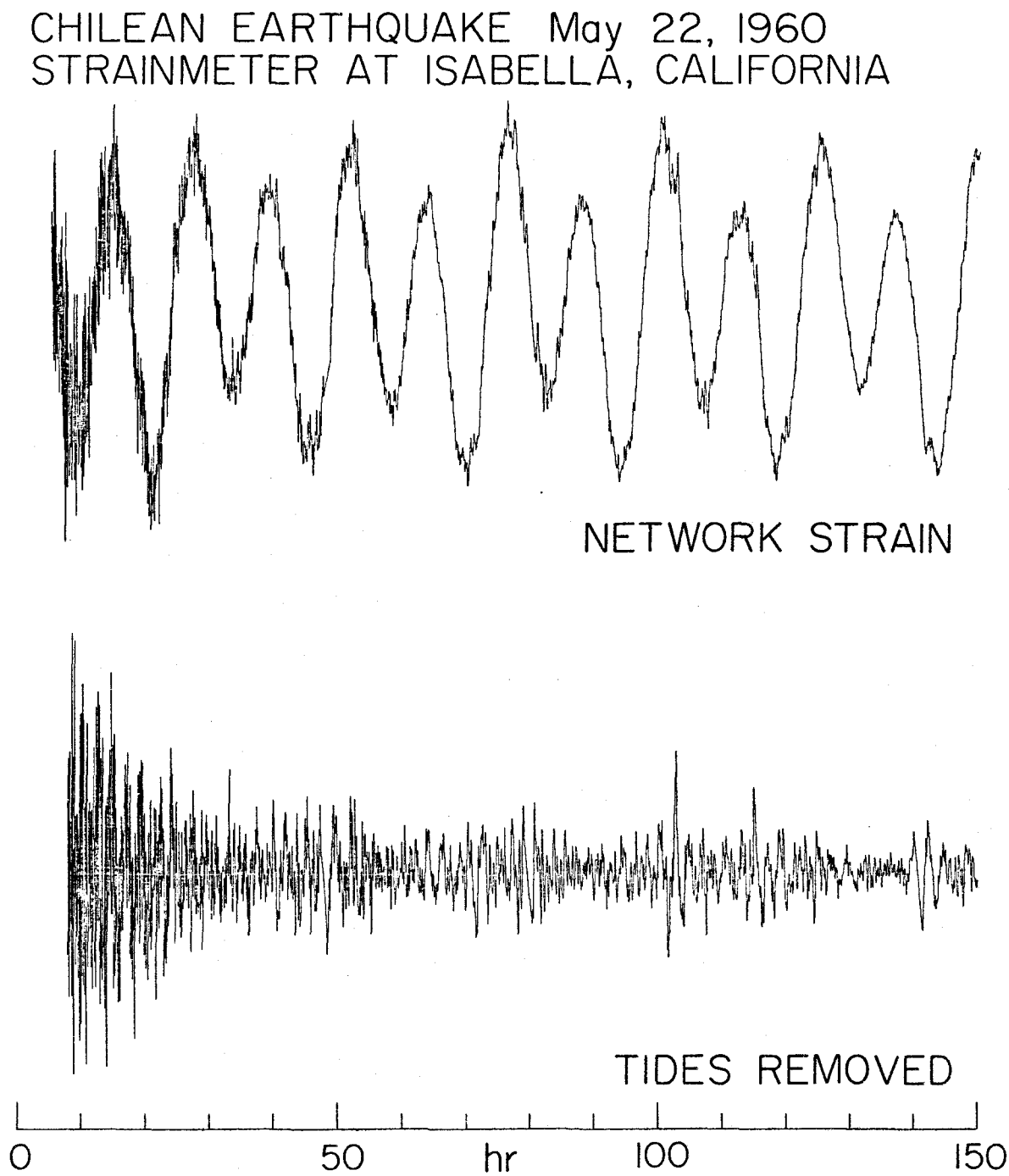

Figure 4.1 - Isabella strain record of the Chilean earthquake (top trace) and the high-passed record with tides removed (bottom trace). The origin time of this figure and all others, is 1911 hrs, 22 May 1960, the origin time of the main shock. The digitized record (top) begins 289 min later, at 0000 hrs, 23 May. The high-passed record (bottom) starts another three hours later.

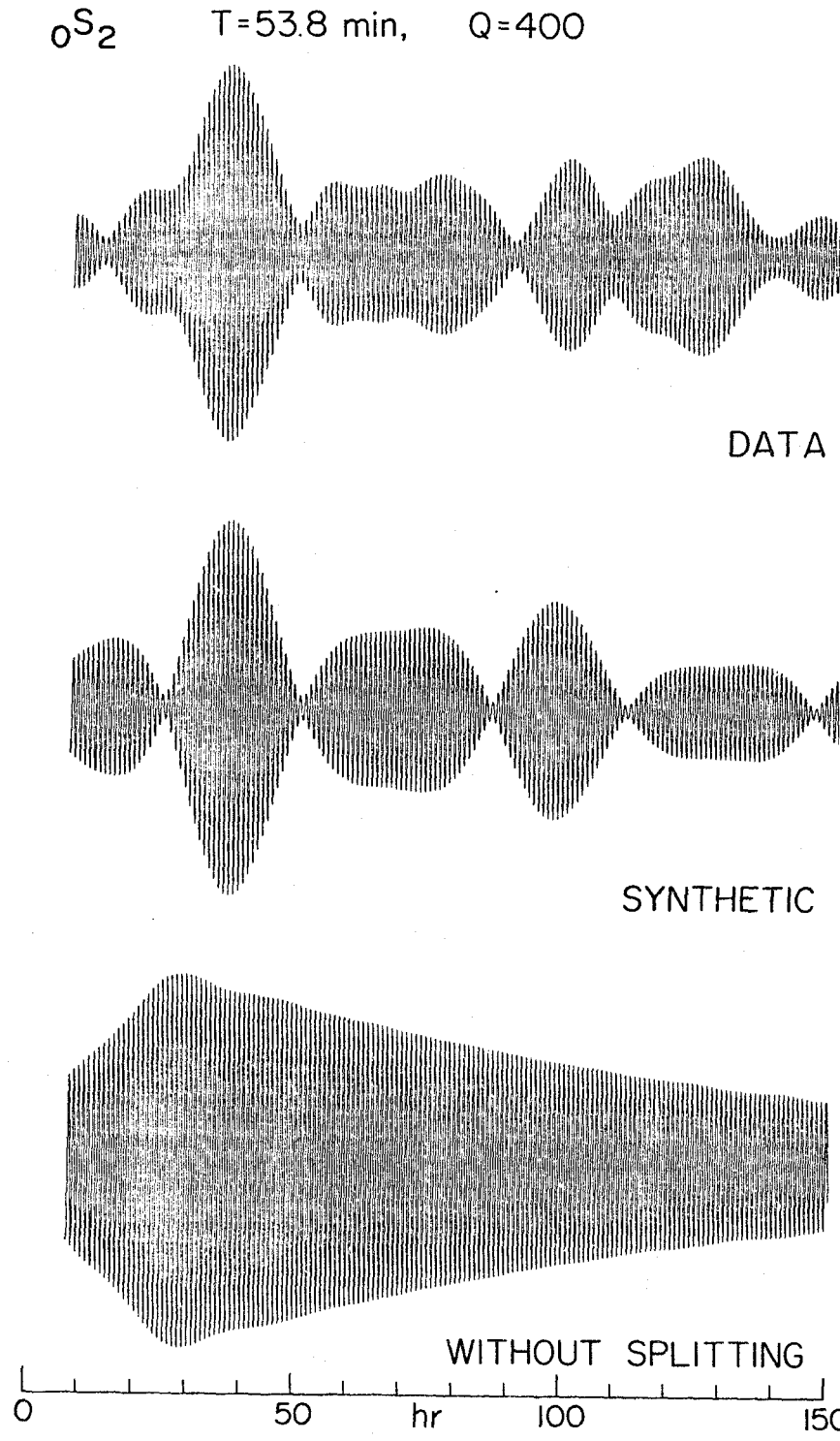

Figure 4.2 - Data and synthetics for $_0S_2$. The top trace is filtered data. The middle trace includes the effects of splitting, and the bottom trace is without splitting. Q = 400 was used for both synthetics. The synthetics are tapered and filtered in the same way as the data.

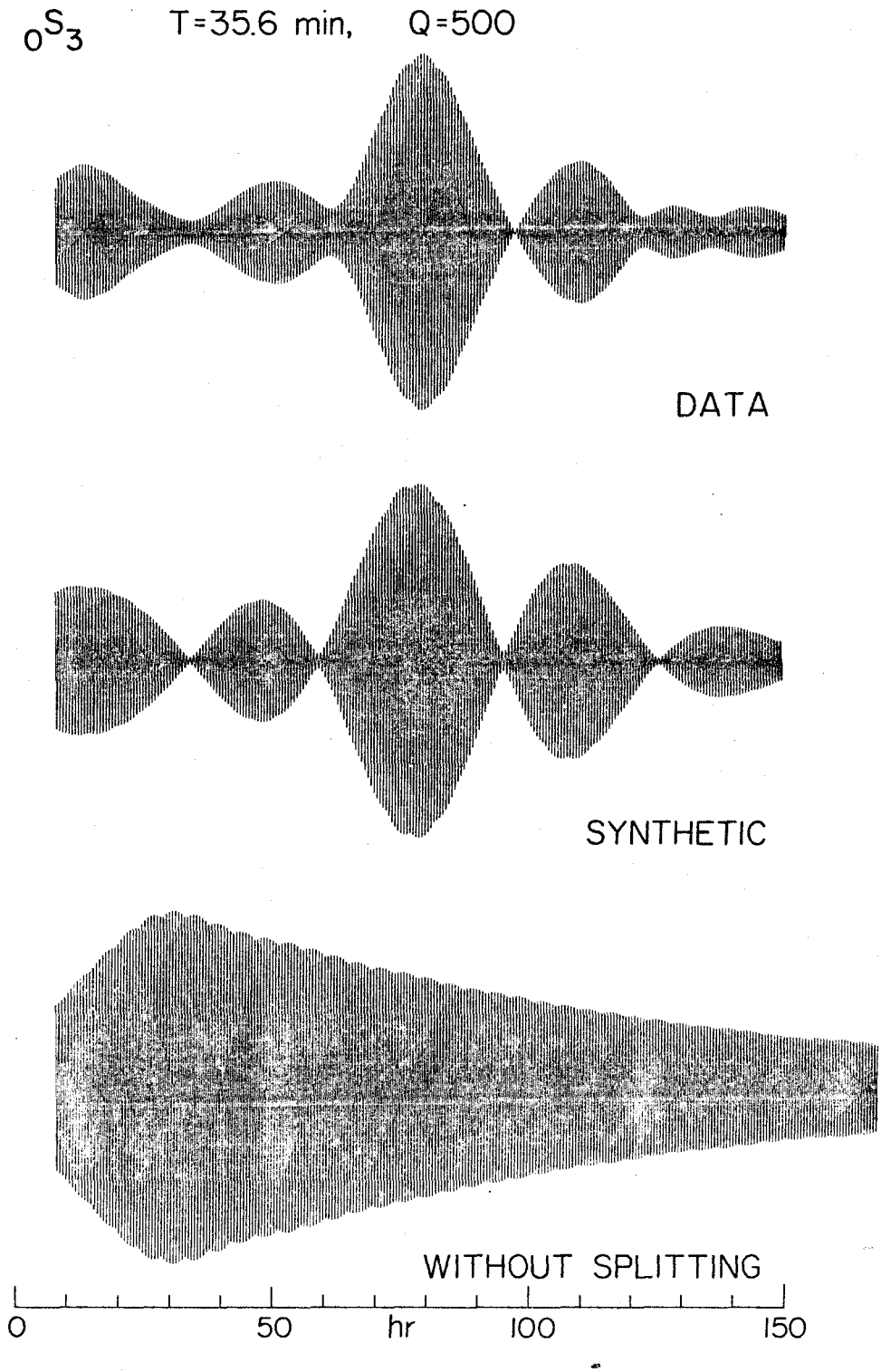

Figure 4.3 - Data and synthetics for $_0S_3$. Q = 500 was used for both synthetics. Other details are as in Figure 4.2.

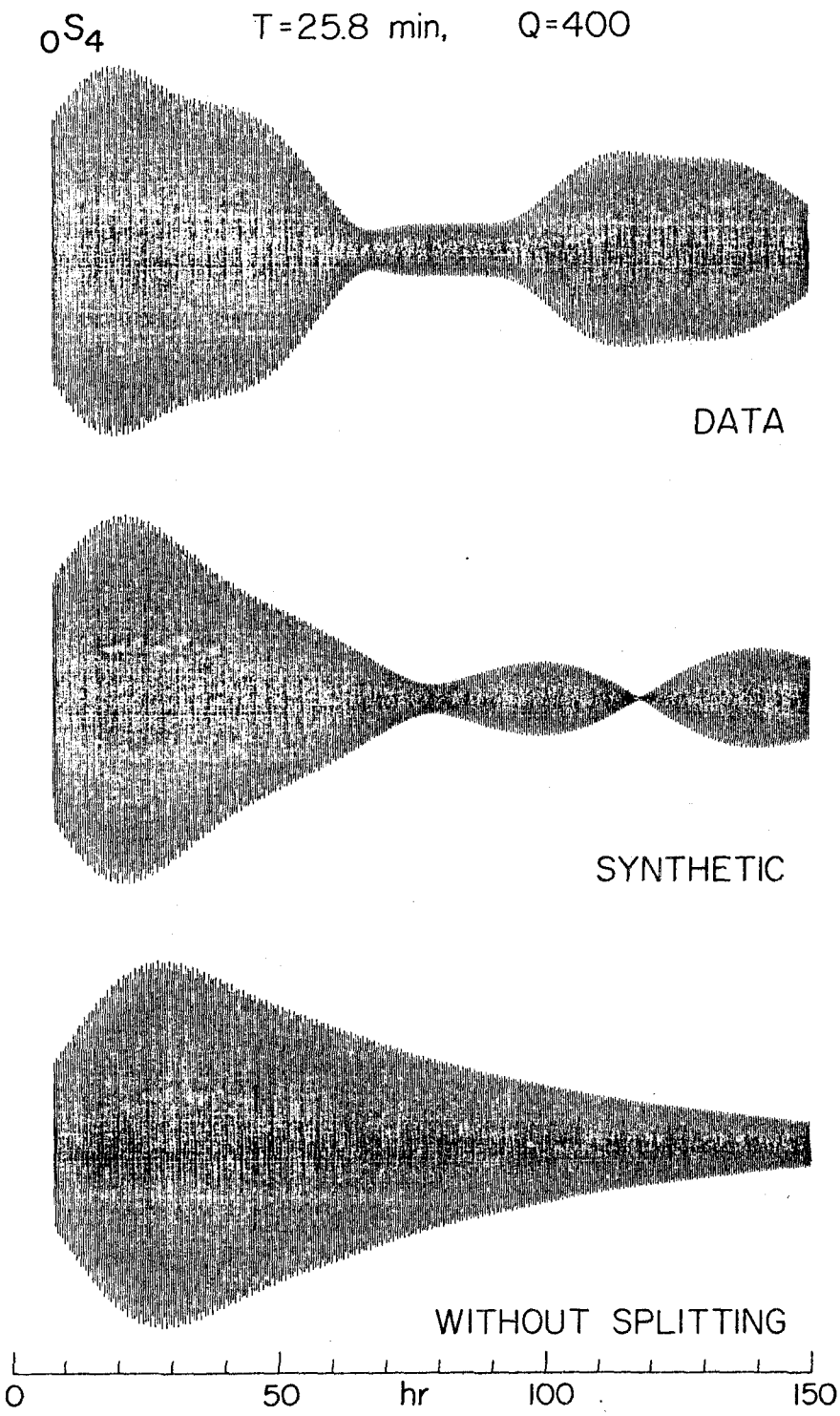

Figure 4.4 - Data and synthetics for $_0S_4$. Q = 400 was used for both synthetics. Other details are as in Figure 4.2.

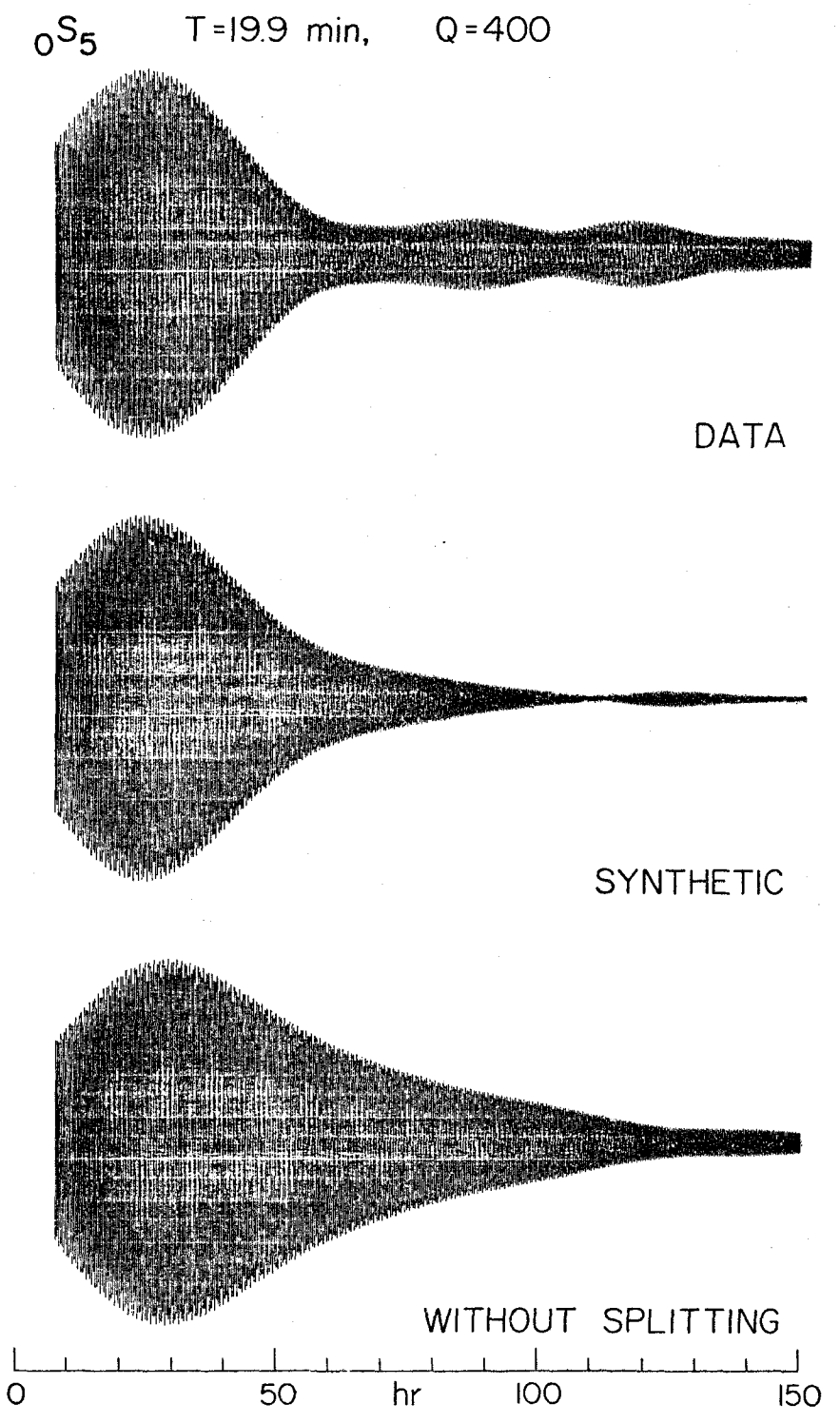

Figure 4.5 - Data and synthetics for $_0S_5$. Q = 400 was used for both synthetics. Other details are as in Figure 4.2.

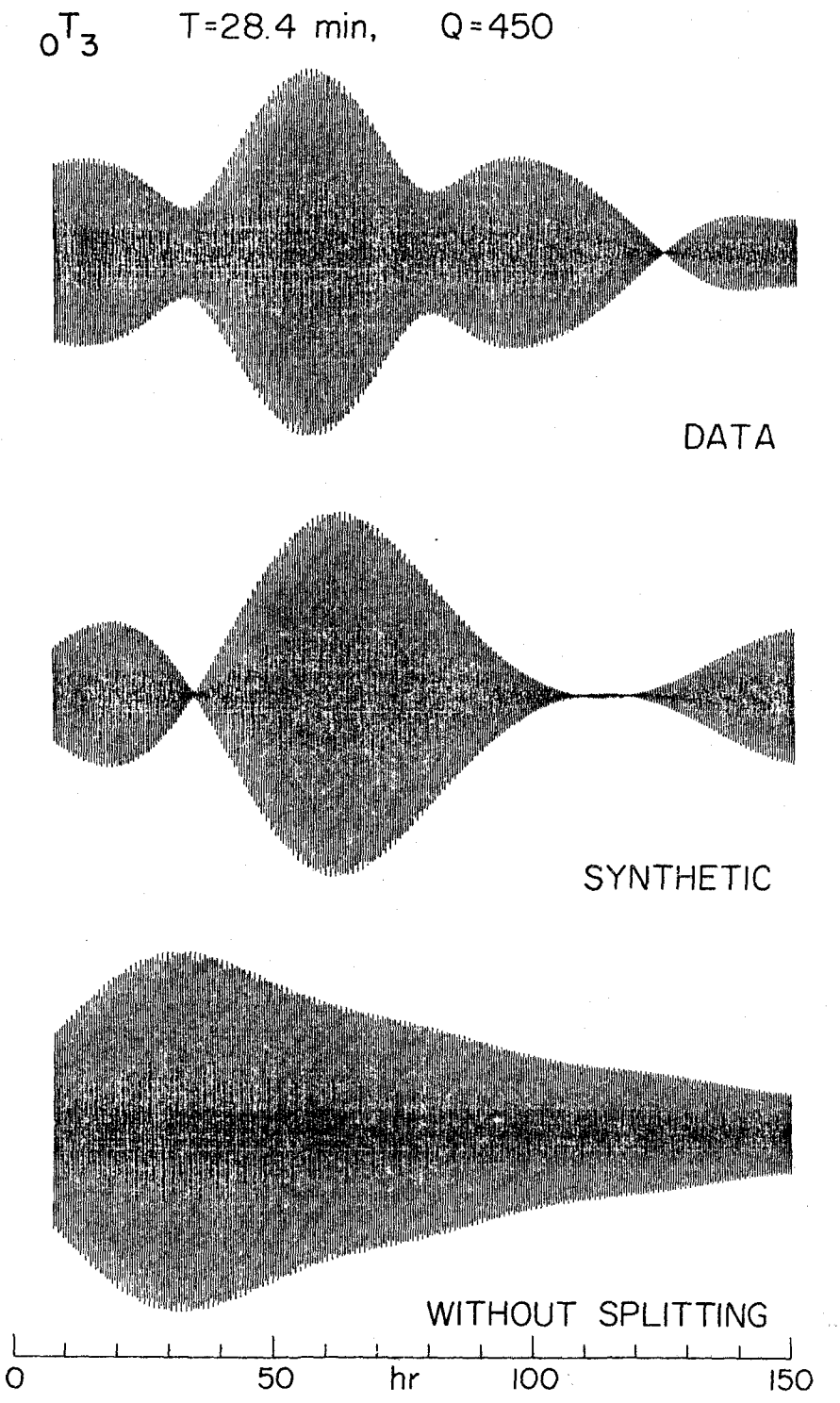

Figure 4.6 - Data and synthetics for $_0T_3$. Q = 450 was used for both synthetics. Other details are as in Figure 4.2.

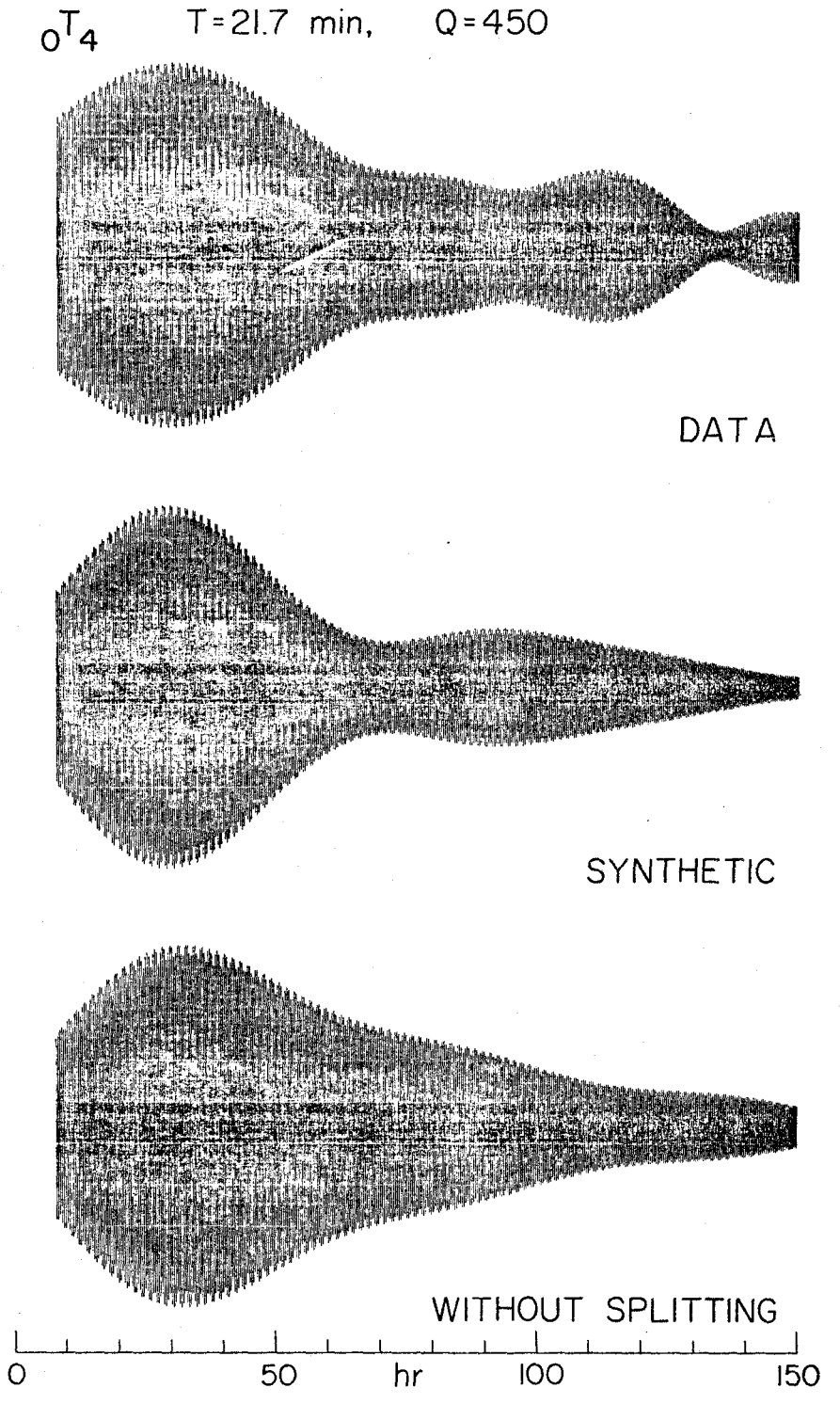

Figure 4.7 - Data and synthetics for $_0T_4$. Q = 450 was used for both synthetics. Other details are as in Figure 4.2.

admittance. The exact passbands used are listed in Table 4.1.

The middle trace of each figure shows a synthetic seismogram for each mode including the effects of splitting. The presence of splitting can be seen by examining the lower traces, which are calculated without splitting. In this case each mode appears as a pure damped harmonic oscillator, since all its singlets have the same frequency. (The synthetic without splitting for ${}_0T_4$ shows some complexity because a relatively wider filter passband is used.) The data are fit far better by the synthetics with splitting than by those without it, and thus splitting is demonstrated.

The eigenfrequency of each singlet is computed using Anderson and Hart's (1977) values for the unperturbed eigenfrequencies and Dahlen's (1968) rotational splitting parameters. Dahlen's elliptical splitting parameters were not used. Woodhouse (1976) has found and corrected an error in the way Dahlen calculated the effect of ellipticity on first order discontinuities within the earth. However, correct values for the low order elliptical splitting parameters are not yet available. When correct elliptical splitting parameters are available, then the fit of synthetics to the data may be significantly improved for ${}_0S_4 - {}_0S_5$ and ${}_0T_3 - {}_0T_4$.

The source mechanism used here was determined by Kanamori and Cipar (1974) from long period surface waves. The rupture was initiated at 38°S, 286.5°E and propagated at 3.5 km/sec to 46°S, 286.5°E, on a fault plane dipping 10° east and striking N10°E. (We approximate the finite source by five point sources at a depth of 55 km). The slip

Table 4.1

FILTER PASSBANDS

Mode	Min. Frequency (cpm)	Max. Frequency (cpm)
$_0S_2$	0.01750	0.01950
$_0S_3$	0.02726	0.02882
$_0S_4$	0.03821	0.03935
$_0S_5$	0.04986	0.05070
$_0T_3$	0.03481	0.03566
$_0T_4$	0.04564	0.04640

angle is 90^{o}, a pure thrust motion. We are also including a precursory slip (Kanamori and Cipar, 1974; Kanamori and Anderson, 1975) at 41.5^{o}S, 285.7^{o}E, with a rise time of 5 min, starting 15 min before the main shock, and with a moment equal to that of the main shock.

Thus the time domain study shows that the fault geometry derived at periods of several hundred seconds is generally consistent with the data at far longer periods, although it certainly is not a unique solution. As we discussed in the previous two chapters, the split singlet amplitudes and phases provide a method for source mechanism studies at very long periods for which splitting is resolvable. (Note that the fault propagation mechanism almost certainly cannot be resolved from studies of very long period modes.)

A prior study of split spectra (Smith, 1961) suggested the possible splitting of ${}_0S_4$, ${}_0T_2$ and ${}_0T_3$, but Smith noted that the data for these modes were marginal. Our synthetics demonstrate the splitting of ${}_0S_4$, ${}_0S_5$, ${}_0T_3$ and ${}_0T_4$.

APPARENT Q OF SPLIT MODES

We study the attenuation of split modes by comparing the data to the synthetics. Splitting is no longer visible when the beat time is longer than the Q decay time. (In the frequency domain this occurs when the broadening of spectral peaks due to attenuation is much greater than the frequency separation of singlets resulting from rotation and ellipticity.) Figures 4.5 and 4.7, respectively, show that splitting is barely detectable for ${}_0S_5$ and ${}_0T_4$, because the

synthetics with and without splitting are much more similar than those for the longer period modes.

Although the effect of the splitting of ${}_0S_5$ is barely visible in figure 4.5, the effect of the splitting on estimates of the Q is substantial. The split synthetic (middle trace) appears to decay more rapidly than the unsplit synthetic (bottom trace); actually both traces were computed using the same Q, 400. The split synthetic decays more rapidly because of the destructive interference of the singlets. Thus neglecting the splitting could easily cause an underestimate of the modal Q value.

The Q values shown in the figures yield acceptable results, but the uncertainty of these values is still rather large. Only the first 150 hours of record are used for these preliminary results. In a forthcoming paper, Geller and Stein (1977) use all 500 hours of available record to obtain well-constrained Q values. Even at the present stage of the study, certain broad limits may be placed on the modal Q values.

Figure 4.8 shows the effect of varying the Q of synthetics for ${}_0S_3$. Three synthetics are calculated with the same source, earth model and receiver, but with Q ranging from 1000 to 250. All of the synthetics have been filtered in the same way as those in Figure 4.3 and are plotted on a common amplitude scale. The effect of the variation in Q can clearly be seen in the changes in both amplitude and waveform. A comparison of the observed record of ${}_0S_3$ in figure 4.3 to the three synthetics in figure 4.8 shows that the actual modal

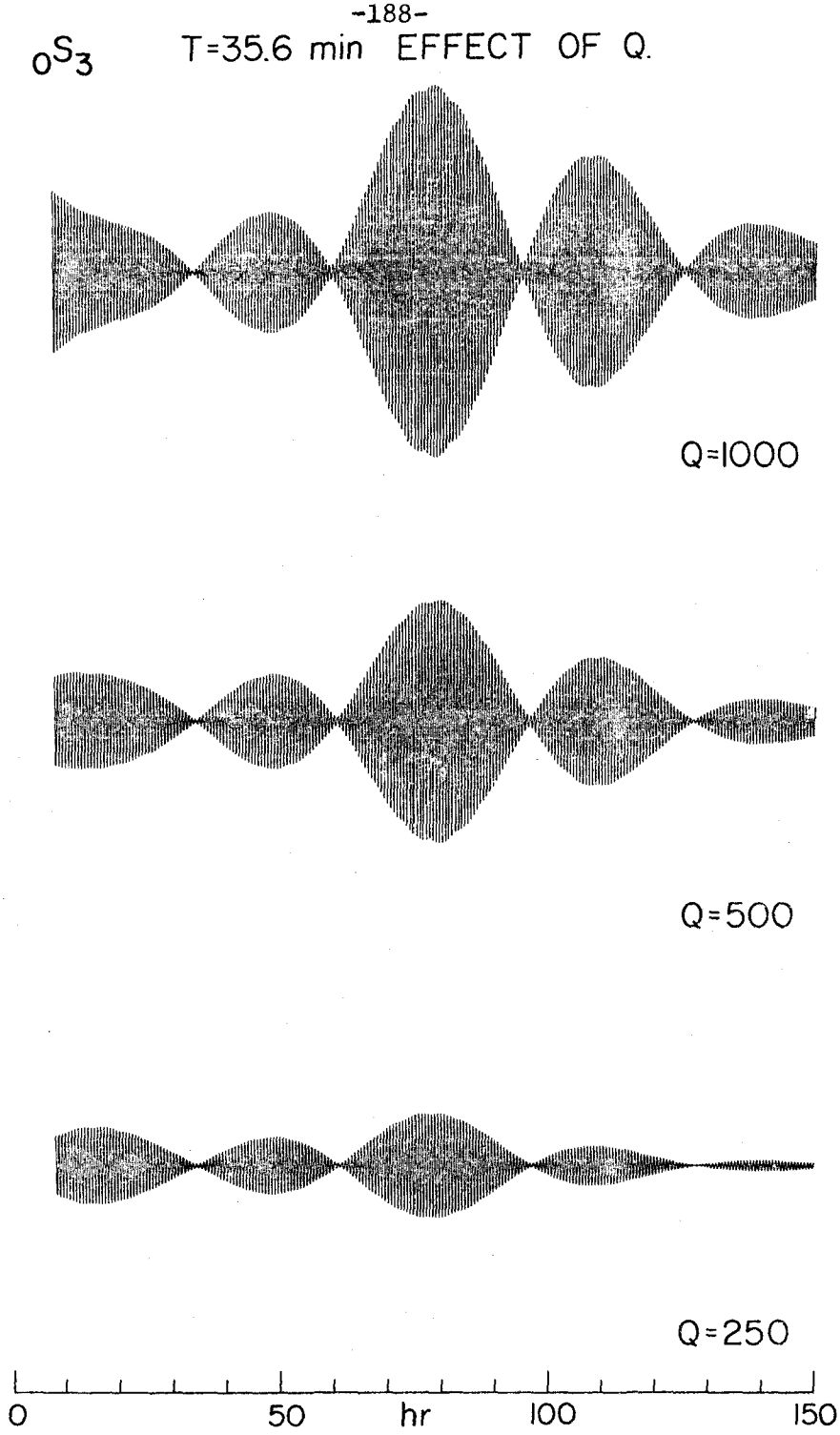

Figure 4.8 - Three synthetics for $_0S_3$ which are calculated in exactly the same way and plotted at the same scale. Since all other parameters are identical, the effect of different Q's is apparent from a comparison of the three traces.

Q is probably bracketed by 250 and 1000, and is fit fairly well by a Q of 500. This value is still preliminary and will be refined by further study.

In this study we have relied on visual fitting of the synthetics to the data to obtain preliminary estimates of the apparent Q of each mode. In the forthcoming research, in which the entire 500 hour record will be used, the visually obtained Q will be used as the starting point for a more rigorous Q determination. Q will be constrained further by cross-correlation of the synthetic envelopes with the data envelope for a suite of Q values clustered around the starting point. The amplitude data will be used as a check on the Q values obtained by cross-correlation.

COMPARISON OF TIME DOMAIN AND FREQUENCY DOMAIN ANALYSES

The technique outlined in this chapter for determining the Q of split modes represents a new approach to this problem. Nearly all previous studies of modal Q's have been conducted in the frequency domain, using the amplitude spectrum. (Even studies of attenuation in the time domain (e.g. Smith, 1972) use the decay of narrow-band filtered data to estimate the Q, rather than calculating synthetics in the time domain.)

As will be seen below, many problems result from using only the amplitude spectrum, and ignoring the information contained in the phase spectrum. This agrees with what would be expected intuitively: the splitting is manifested in the time domain as a beat effect, and

the phase spectrum determines the precise arrangement of the beats. Therefore, if the phase spectrum is not considered, this is equivalent to discarding the information in the beat patterns.

George Backus (personal communication) points out that if both the phase and amplitude spectrum are used, then all of the independently available data for a multiplet are given by very few numbers in the frequency domain (the Fourier transform - amplitude and phase - in the relatively narrow frequency range which contains nearly all of the energy for the multiplet). The same information in the time domain requires many more numbers (the values of the displacement or strain at sufficiently closely spaced points in time).

Nonetheless, it is still desirable to work in the time domain to demonstrate the splitting of modes which were not previously known to be split, confirm the splitting of ${}_0S_2$ and ${}_0S_3$ and measure the Q of each multiplet. All of these goals are related to overall properties of the split multiplets, rather than details of the split singlets which are unnecessary for our purposes. We must know the source mechanism, which controls the relative excitation of the individual singlets, well enough to calculate a reasonable synthetic before we can determine the modal Q. It is well known that all estimation methods require a tradeoff between stability and resolution. A frequency domain analysis will yield a large number of independent data, but will not provide much stability. (Small changes in the windowing, tapering, filtering, etc., or noise randomly present in the data, can substantially affect spectral estimates, especially phase

estimates.) The time domain analysis will be much more stable than the frequency domain analysis in the presence of noise. The price we pay for this is the inability to resolve individual singlets; we can resolve only the overall features of the splitting. However, it is precisely those overall features which are most of interest, and thus the time domain analysis seems preferable for this study.

Ideally, we want to use the spectral amplitude and phase of each singlet to study the earthquake source mechanism. However, there are several problems which arise when we set out to use frequency domain analysis in practice. These problems are demonstrated by comparisons of three different amplitude spectra for the same record of the same event.

Figure 4.9 shows the spectra for ${}_0S_2$ obtained by Benioff et al. (1961) and Smith (1961) for the Isabella strain record of the 1960 Chilean earthquake. The spectrum in figure 4.9a from Benioff et al. was computed using the first 267 hours (16000 min) of the Isabella record, while windows of 318 hours (19100 min) and 636 hours (38200 min) were used for the spectra in Figure 4.9b. It can be seen that as the record length becomes longer, the amplitude of the middle peak ($m = 0$) increases substantially compared to that of the $m = \pm 1$ peaks. There are several reasons for the differences. Although Benioff et al. (1961) and Smith (1961) both used the same strain record, the record was independently digitized for each study. Also, the windowing, smoothing and power spectral analysis were carried out separately in each study. The major point, however, is that three

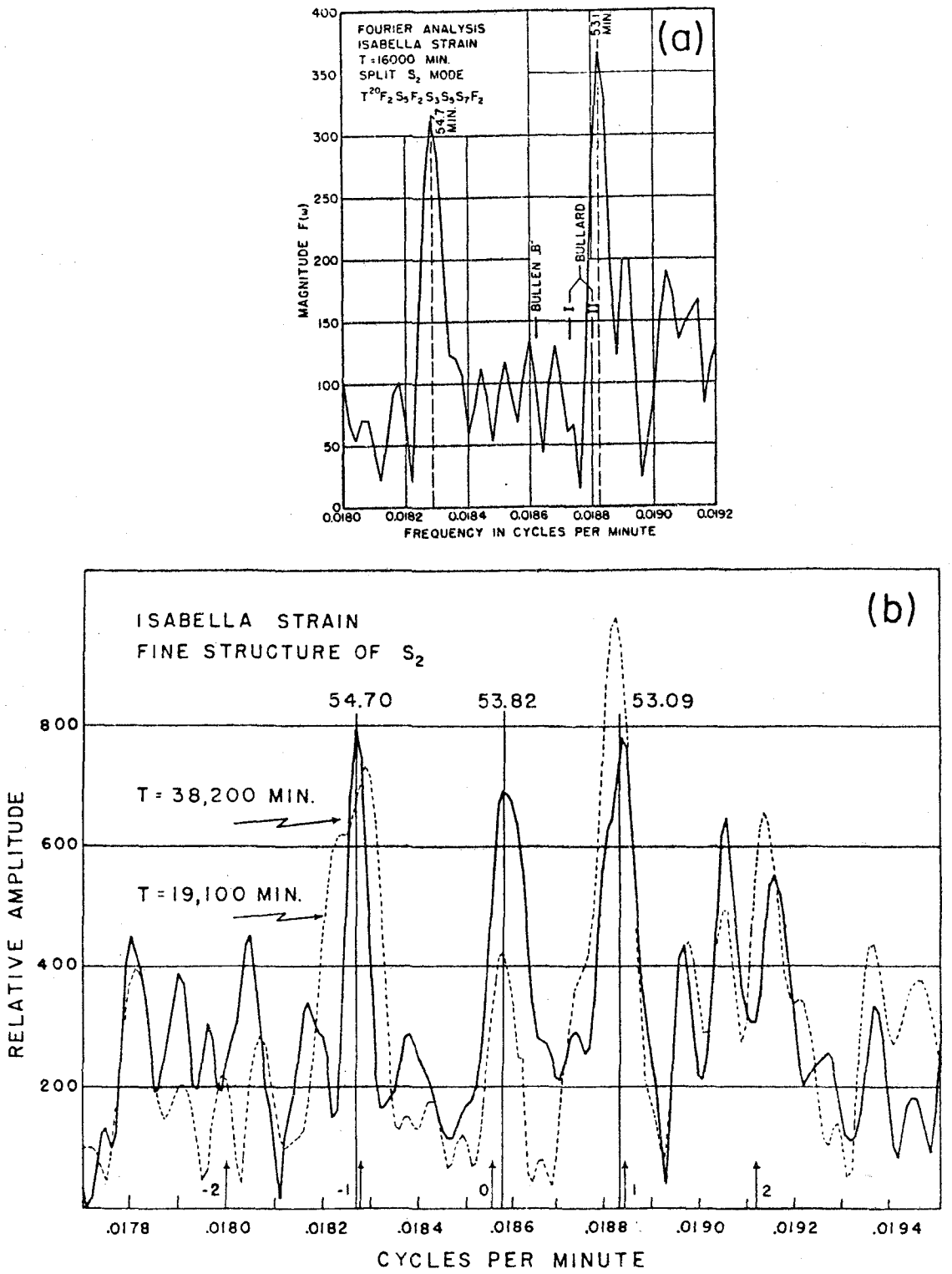

Figure 4.9 - a) High resolution spectrum for ${}_0S_2$ obtained by Benioff et al. (1961). b) High resolution spectra for ${}_0S_2$ obtained by Smith (1961).

different power spectra for the same record of the same earthquake produced spectra which are basically similar, but differ very substantially in their details.

The Chilean earthquake is the largest event for which free oscillations have ever been observed, and both the studies by Benioff et al. and Smith were carried out very carefully. If we attempted to use the spectra in figure 4.9 for detailed analyses, e.g. determining the Q of a singlet from peak width and half-height or determining the relative excitation of singlets from the relative amplitudes of spectral peaks, we would get drastically different results depending on which spectrum we used. Figure 4.10, showing the spectra obtained by Benioff et al. and Smith for ${}_0S_3$ demonstrates an even more spectacular instability. The peak for the m = +2 singlet is present for both the Benioff et al. spectrum and the shorter of Smith's two spectra, but disappears completely from Smith's longer spectrum.

The instability of the spectra is inherent in the attempt to obtain high resolution of the singlets. Small amounts of noise will cause relatively large changes in the fine structure of the singlets. Furthermore, it is almost impossible to get any precise estimates of how the noise has affected the spectrum. In contrast, as Smith (1972) noted, time domain inspection of narrow band filtered normal modes allows a determination of when the signal has decayed to the general background noise level. The time domain analysis thus allows the effects of noise to be seen much more clearly than in the frequency domain analysis.

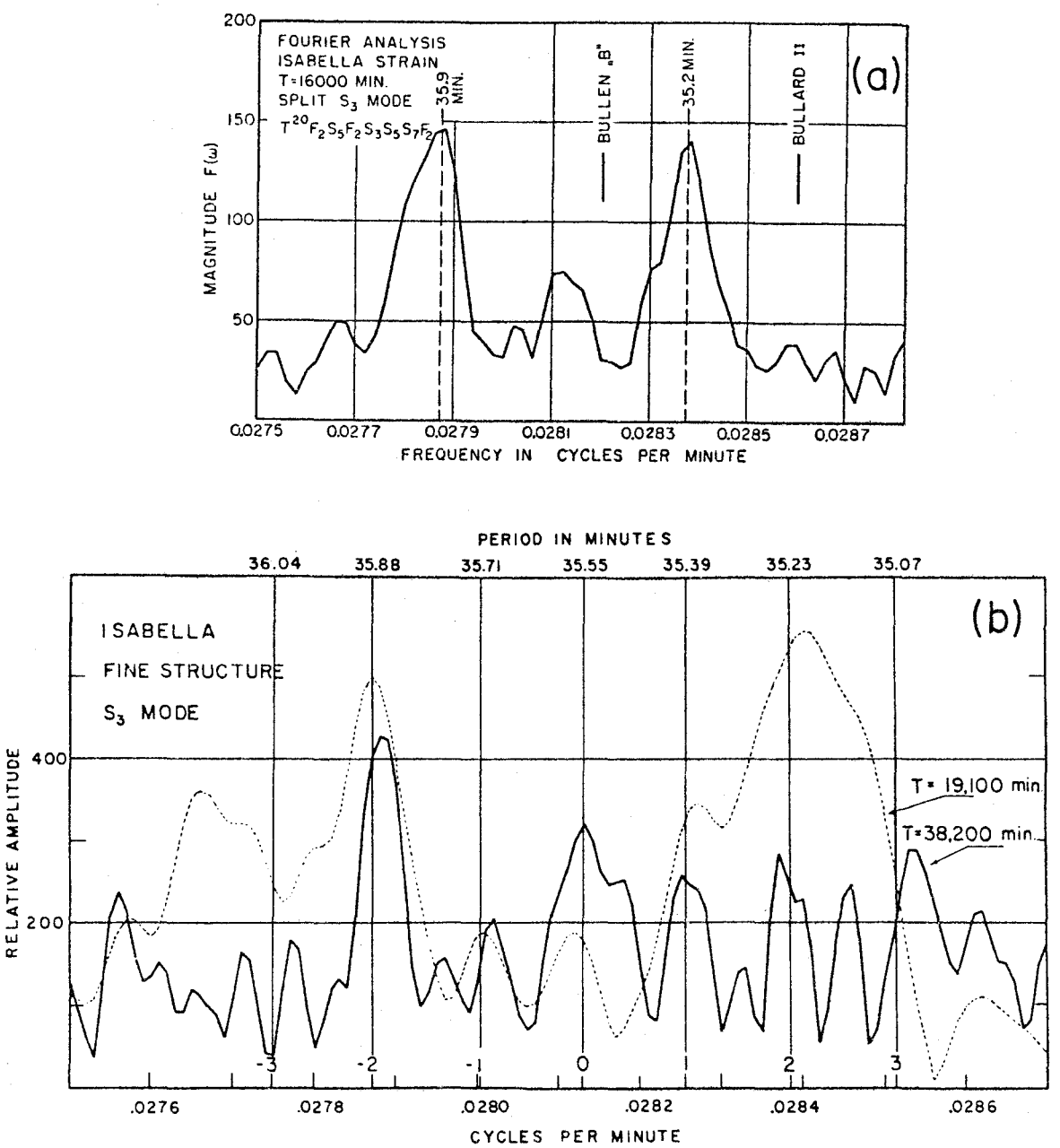

Figure 4.10 - a) High resolution spectrum for ${}_0S_3$ obtained by Benioff et al. (1961). b) High resolution spectra for ${}_0S_3$ obtained by Smith (1961).

COMPARISON OF DIFFERENT Q MEASUREMENT TECHNIQUES

Measurements of the modal Q values may be carried out in either the frequency domain or the time domain. The frequency domain approaches may be grouped into three categories: i) use of peak half-height and width, ii) decay of peak spectral amplitude in successively windowed intervals and iii) decay of total spectral energy in successively windowed intervals. Time domain techniques for modal Q determination may be classed as either i) direct measurements of envelope decay or ii) fitting filtered multiplet data by synthetics. Q measurements based on height and half-width are now considered as too unstable to be useful even for unsplit multiplets (Smith, 1972). However, for unsplit multiplets which are well separated in frequency from other nearby modes, either the frequency domain techniques using decay of peak spectral amplitude or total multiplet energy, or the time domain technique using envelope decay all apparently give reliable Q estimates.

All of the techniques for analysis of the Q of unsplit multiplets rely basically on the fact that they have only a single eigenfrequency and are well separated in frequency from other multiplets. This allows the use of analysis techniques for a damped harmonic oscillator. However, for the case of the split modes, the singlets are not individually resolvable with any degree of stability and we can study only the multiplet with confidence. Since we observe the split multiplet as the sum of several, closely spaced, interfering, singlets, the usual techniques for Q determination break down. This is analogous

to the breakdown of phase equalization techniques for surface waves composed of several interfering overtone branches (Fukao and Abe, 1971). Some of the problems associated with Q determinations for split multiplets are discussed by Gilbert and Backus (1965).

The most common technique for frequency domain Q determination is apparently the use of the decay of successively windowed peak spectral amplitudes. The successive peaks method cannot be used to get reliable Q values when splitting is present. To demonstrate this we will conduct a numerical experiment of the validity of the successive peak method in a case where we exactly know the Q - namely displacement or strain synthetics calculated from equation (4.1):

$$U_\ell(t) = \sum_{m=-\ell}^{\ell} (F_{\ell m}\, e^{i\omega_{\ell m} t} + F^*_{\ell m}\, e^{-i\omega_{\ell m} t}) \cdot \exp(-\omega_\ell t/(2Q_\ell)). \qquad (4.1)$$

$F_{\ell m}$ is the displacement or strain amplitude calculated using the methods in chapters 2 and 3. All singlets have the same Q_ℓ as long as lateral heterogeneity is not present (Gilbert and Backus, 1965) and the attenuation factor is included to zeroeth order. For, positive ω, the Fourier transform of (4.1) is

$$U_\ell(\omega) = \sum_{m=-\ell}^{\ell} F_{\ell m} \left. \frac{e^{i\omega_{\ell m} t - i\omega t - \omega_\ell t/2Q}}{i\omega_{\ell m} - i\omega - \omega_\ell/2Q_\ell} \right|_{T_1}^{T_2} \qquad (4.2)$$

where T_1 and T_2 are the start and end of the windows.

We conduct a numerical experiment for ${}_0S_3$, using the modal amplitudes, F_{3m}, for our source model of the Chilean earthquake and a receiver at Isabella. We use equation (4.2) to obtain the spectrum for any particular time window, and then evaluate the spectral amplitude numerically to find the peak spectral amplitude. In order to guard against the possibility that our result is an artifact of some particular window length, we make runs with two different window lengths, 20 hours and 10 hours. Both runs conclusively demonstrate that the Q estimates made from the decay of peak spectral amplitude are extremely unreliable and scattered when splitting is a significant effect.

The results of the numerical experiment are shown in Figure (4.11). For all cases, Q = 500 is used. The top plot shows the trial with a 20 hour window. The peak spectral amplitude for each 20 hour interval (e.g. 0 - 20 hours, 20 - 40, etc.) is plotted at the center of the interval. Two cases were considered. When there is no rotational splitting (Equations 4.1 and 4.2 are still applicable, but now all the singlets have the same eigenfrequency, $\omega_{\ell m} = \omega_\ell$), the peak amplitudes (the open circles) are well behaved, falling exactly on the line for Q = 500. On the other hand, the peak amplitudes for the case of split modes (closed circles) are very badly scattered and do not even decay monotonically. Even though the peak spectral amplitudes are exactly calculated, with no noise, and the Q is set exactly to 500 in equation (4.2), it is completely impossible to recover the Q from the peak amplitudes. The same is true of the 10 hour window (bottom of Figure 4.11).

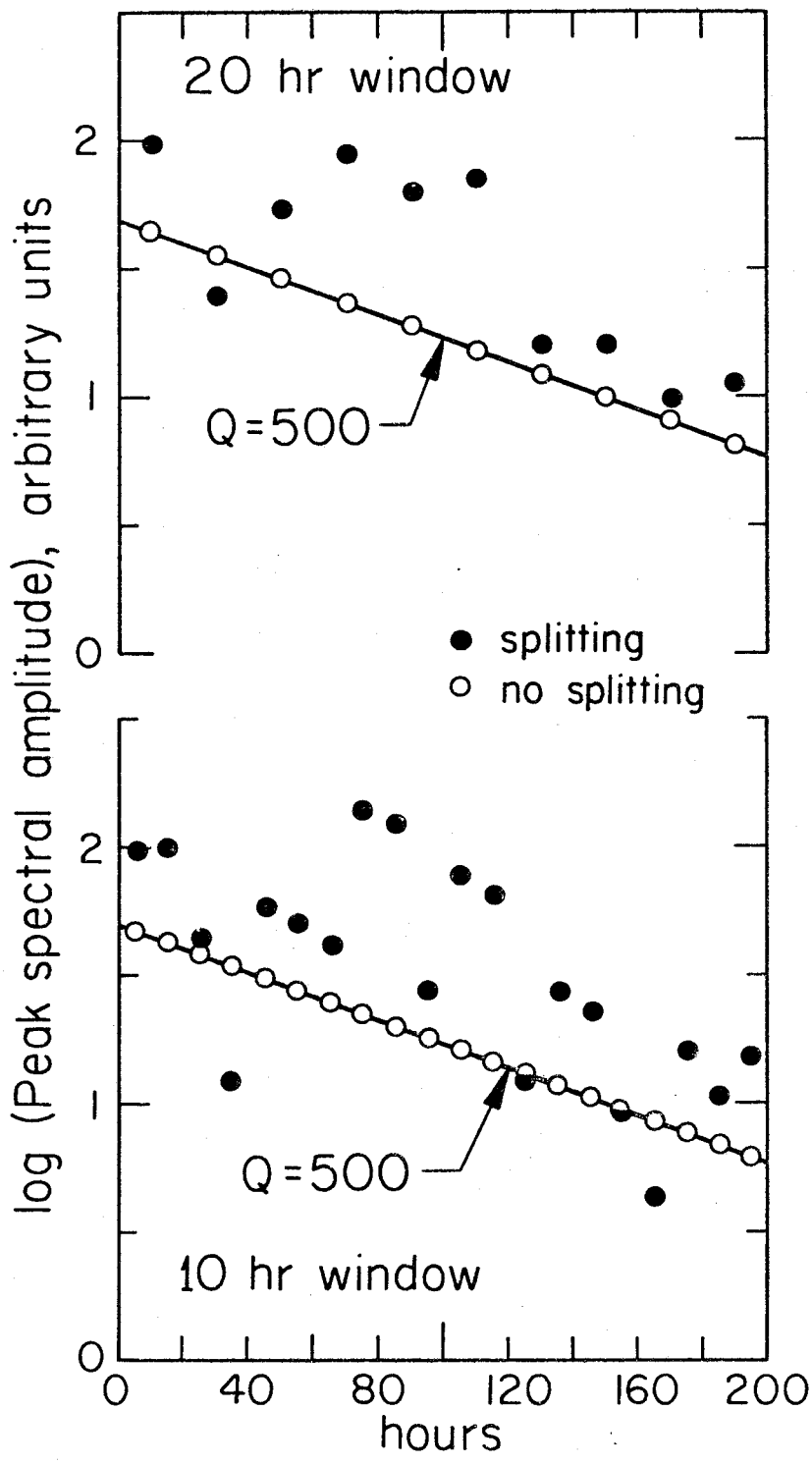

Figure 4.11 - Results of a numerical test of Q estimation by decay of successive windowed peaks. When there is no splitting (open circles) good results are obtained, but when splitting is present (closed circles) extremely poor and scattered spectral peaks result.

Again, although the peak spectral amplitudes for the unsplit modes lie exactly on the Q = 500 curve, in the split case the peak spectral amplitudes are very badly scattered and unusable for a reliable Q determination.

This experiment, and actual experience, show that Q estimates from successive windowed peaks are extremely unreliable when splitting is an important factor. On the other hand, the technique of calculating time domain synthetics for the split modes and varying the Q to produce the best overall agreement apparently gives accurate and stable Q measurements.

Although a similar numerical experiment has not been conducted to test the validity of estimates of Q obtained from the decay of total spectral energy in successively windowed intervals, similar results are expected. This can be seen by an application of the digital equivalent of Parseval's theorem to the data for ${}_0S_3$ shown in figure 4.3. In practice, estimates of the spectral energy of a particular multiplet are made by finding the energy in a finite bandwidth which contains nearly all of the energy. The spectral energy is almost exactly equal to the energy estimate which would be obtained in the time domain by summing $X^2(t)$ at each sampling point. Figure 4.3 clearly shows that if we sum $X^2(t)$ in successive intervals we will not get a monotonically decaying function. Thus the decay of spectral amplitudes will not provide useable Q determinations for split multiplets.

The peak spectral amplitudes are generally related to the spectral

energy in successively windowed data, so a similar argument explains the failure of peak spectral amplitude as a reliable Q estimator. Similarly, the time domain envelope decay will not provide reliable Q estimates. The failure of all these methods may be traced back to a common cause: they all are applicable only to a single, isolated, damped harmonic oscillator, while the split multiplets consist of several interfering harmonic oscillators. Because of the instability which occurs when high resolution spectral techniques are applied we cannot reliably isolate individual singlets. Therefore the only way we can reliably study the Q of split normal modes using the present dataset is by using time domain synthetics.

The focal mechanism, in principle, affects the beat pattern of the filtered seismograms. Therefore, the accuracy of the Q determination from time domain synthetics seems to depend on the accuracy of the focal mechanism determination. However, as was demonstrated in the previous two chapters, the azimuthally symmetric term dominates the radiation pattern of the low order spheroidal modes for all fault geometries except vertical and horizontal fault planes or exactly strike-slip dislocations. Since split normal modes are excited only by great earthquakes which almost invariably occur on shallow angle thrust faults, the split spheroidal mode beat patterns will be almost completely insensitive to small errors in the source mechanism. Although the torsional modes are more sensitive to the fault geometry, their beat patterns generally are smoothly varying functions of focal mechanism. Thus Q estimates from time domain synthetics are probably

not very sensitive to small errors in the focal mechanism.

In the future if good records of a great earthquake ($M_o \sim 10^{30}$ dyne cm) are obtained at many stations on the IDA array (Agnew et al., 1976), it may prove possible to achieve high resolution by spectral stacking techniques. The present lack of sufficient instrumental records for very low order modes makes such stacking impossible at present.

MOMENT OF THE 1960 CHILEAN EARTHQUAKE

Reliable absolute amplitude calibration of the Isabella strain recording system at the time of the Chilean earthquake is very difficult to obtain. Although calibration tests were performed, it is not clear how accurate the results are. Also, topographic effects at the instrument site could cause large and, at the present time, unknown changes in the amplitudes (Beaumont and Berger, 1976). For these reasons, we estimate the moment of the 1960 Chilean earthquake in two stages. First, the Isabella records of the Chilean earthquake and the 1964 Alaskan earthquake are used to obtain the ratio of the moments of the two earthquakes. Then Kanamori's (1970) determination of the moment of the Alaskan earthquake from long period surface waves is used, together with the moment ratio, to find the moment of the Chilean earthquake.

It is also desirable to use the Chilean earthquake data directly to find the relative moment of each mode. If the effective moment is essentially constant for all of the split modes from ${}_0S_2$ to ${}_0T_4$

(periods from about 53 to 20 minutes) this would suggest that the finite propagating rupture and the slow precursory source account for nearly all of the slip associated with the Chilean earthquake. On the other hand, if the effective moment increases with increasing period, this strongly suggests that the coseismic slip and precursory source do not account for all of the fault offset. In the latter case, an "accelerated creep" with a time constant of several hours, possibly involving a slip of the entire lithosphere, is required.

It should be noted that any study of the observed amplitudes to find the moment of each mode is dependent on the source model. In this particular study, we assume the finite source geometry, rupture propagation and precursory source found by Kanamori and Cipar (1974) and Kanamori and Anderson (1975). The parameters for this source model are listed above. It is assumed that the moment of the precursory source is equal to the moment of the mainshock, since that is the general conclusion reached by Kanamori and Cipar and Kanamori and Anderson.

The evidence for the existence of the precursor seems conclusive. Kanamori and Cipar present definite instrumental evidence for body wave arrivals from the precursor on the Pasadena strain instrument. Kanamori (personal communication) has also observed precursors to G2 from the main shock, also on the Pasadena strain record. Kanamori and Anderson inferred the existence of the precursor from spectral holes in the Isabella strain and UCLA gravity spectra.

Although the existence of the precursor seems well established,

its moment relative to that of the main shock is much less constrained. Kanamori and Cipar estimated the precursor moment using synthetic seismograms from a very simple model, while Kanamori and Anderson used amplitude spectral data. These studies show that the precursor moment must be of the same order of magnitude as that of the main shock, but further work seems needed to obtain a more accurate value. On the basis of our present knowledge of the precursor, we set the precursor moment equal to the main shock moment.

In finding the relative moment of the Chilean and Alaskan earthquakes, we wish to use the longest period amplitude data which are available. The amplitudes of ${}_0S_2$ and ${}_0S_3$ for the Chilean earthquake are almost completely unaffected by the details of the precursor. Because ${}_0S_2$, as is shown by Figure 4.2 and by Figure 1 of Benioff et al. (1961), stands out well above the noise, we use its peak-to-peak amplitude for the relative moment calculation. Unfortunately for the Alaskan earthquake the lowest order multiplet which is clearly resolved is ${}_0S_4$ (Smith, 1966, Figure 4). However, no evidence has been reported suggesting that a slow dislocation might have accompanied the seismic slip for the Alaskan earthquake. Therefore the peak-to-peak amplitude of ${}_0S_4$ should be a good measure of the long period moment. The observed amplitudes must be corrected for the instrument response curve, which is different for Chile and for Alaska (Smith, 1966, Figure 3). (The relative instrument calibration is assumed to be reliable.) The moment ratio is then given by

$$R = \frac{\text{Data } ({}_0S_2 - \text{Chile})}{\text{Counts/Strain } ({}_0S_2 - \text{Chile})} \times \frac{\text{Counts/Strain } ({}_0S_4 - \text{Alaska})}{\text{Data } ({}_0S_4 - \text{Alaska})}$$

$$\times \frac{(\text{Synthetic} - {}_0S_4 - \text{Alaska})}{(\text{Synthetic} - {}_0S_2 - \text{Chile})} \qquad (4.3)$$

A digitized record (not shown here) of the Isabella record of the Alaskan earthquake is used and a peak-to-peak amplitude of 72.2 counts (digital units) is obtained. The card deck for the Chilean data is labeled 1" = 400 counts, and the card deck for Alaska, which is not labeled, is assumed to have the same scale. The peak-to-peak amplitude of ${}_0S_2$ for Chile is 27.0 counts. The ${}_0S_2$ Chile strain synthetic has P-P amplitude of 1.24×10^{-13}. The ${}_0S_4$ Alaska synthetic (not shown), which was calculated using Kanamori's (1970) finite source model, has P-P strain amplitude of 4.32×10^{-13}. Taking the response curve from Smith's (1966) Figure 3, we get

$$R = \frac{27.0}{1.4 \times 10^{12}} \times \frac{3.5 \times 10^{12}}{72.2} \times \frac{4.32 \times 10^{-13}}{1.24 \times 10^{-13}} = 3.26 \qquad (4.4)$$

If we use Kanamori's (1970) value of 7.5×10^{29} dyne cm as the moment of the Alaskan earthquake, the moment of the Chilean earthquake is then

$$\begin{aligned} M_o(\text{Chile}) &= 3.26 \times 7.5 \times 10^{29} \\ &= 2.4 \times 10^{30} \text{ dyne cm.} \end{aligned} \qquad (4.5)$$

This value is about half that obtained by Kanamori and Anderson (1975), 4 to 5 x 10^{30} dyne cm, but is well within the range of experimental uncertainty associated with this type of single station measurement.

RELATIVE MOMENTS OF SPLIT MODES FOR THE CHILEAN EARTHQUAKE

The total moment may be independently estimated from the amplitude of each of the split modes. Because of the uncertainty of the absolute calibration of the instrument, only the relative moment for each mode is considered. If the relative moment increases with increasing period, then an "accelerated creep" process can be inferred. Constant relative moment will imply that all of the slip is accounted for by our source model.

The observed P-P amplitudes for each of the split modes is listed in Table 4.2. The instrument response curve, as given in Figure 4 of Benioff et al. (1961), is assumed to give the correct relative amplitude response. The relative amplitudes of the instrument response for each mode are listed in Table 4.2; the normalization is arbitrary. The peak-to-peak amplitudes of the strain synthetics are given for a total moment of 10^{27} dyne cm. The data amplitudes are then divided by the instrument factor and the synthetic amplitudes to obtain the relative moment. The confidence limits are nominal, and serve only to indicate the relative uncertainty. These values are calculated by converting a nominal scatter of ±1 digital unit into the equivalent range of relative moment.

Table 4.2

RELATIVE MOMENT

Mode	Peak-to-Peak Amplitude			Relative
	Data (counts)	Strain Synthetic (x 10^{14})	Instrument (x 10^{9} in/strain)	Moment
${}_0S_2$	27.0	12.4	2.02	1.08 ± 0.04
${}_0S_3$	24.8	12.6	2.02	0.97 ± 0.04
${}_0S_4$	9.66	1.18	2.02	4.05 ± 0.42
${}_0S_5$	11.7	1.76	1.97	3.29 ± 0.29
${}_0T_3$	5.99	3.58	1.97	0.85 ± 0.14
${}_0T_4$	4.61	7.55	1.95	0.31 ± 0.07

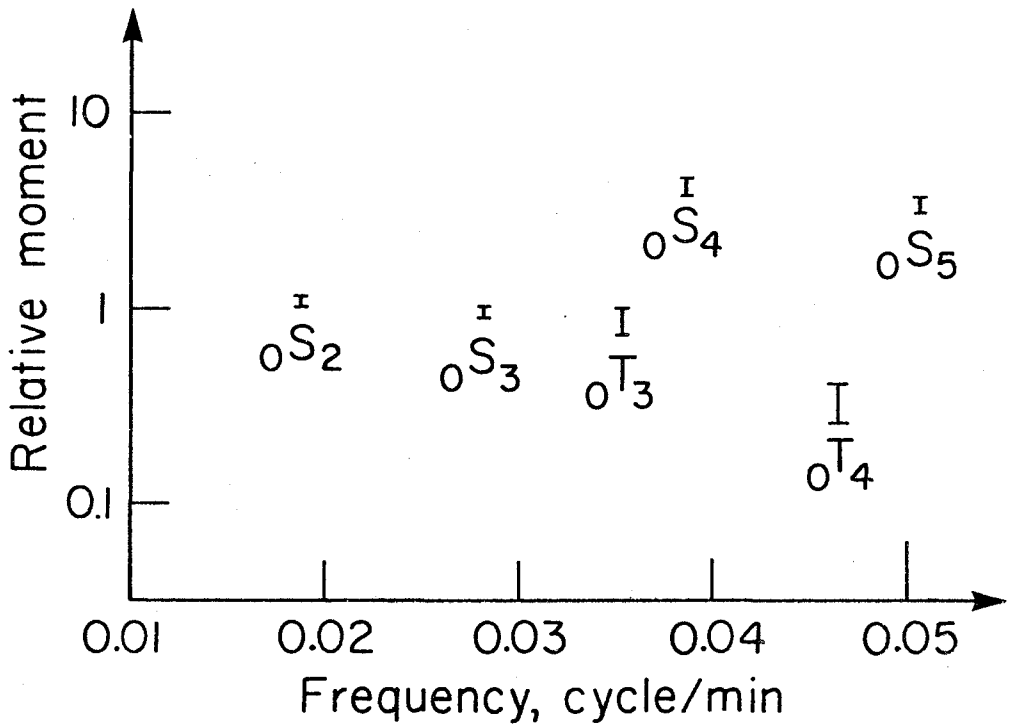

Figure 4.12 - Relative moment of the Chilean earthquake as a function of frequency. Error bars are relative and correspond to one count (digital unit) for each mode.

The relative moment values from Table 4.2 are plotted in figure 4.12. These amplitudes are somewhat scattered for modes ${}_0S_4$ - ${}_0S_5$ and ${}_0T_4$, but these modes are noisier and more affected by lateral heterogeneity than ${}_0S_2$, ${}_0S_3$ or ${}_0T_3$. The amplitudes are generally consistent with the source model used in this study, which has a shallow angle thrust mechanism and a precursor with the same moment as the main shock. This mechanism is not unique, but probably lies in a broad range of acceptable solutions.

The major constraint on the source mechanism obtained from split normal modes is provided by the ratio of torsional to spheroidal amplitudes. The low angular order spheroidal singlet amplitudes themselves are not sensitive to the source mechanism, except for pathological source geometries. Although the torsional singlet amplitudes do vary with source geometry, until the torsional splitting parameters are better known, the detailed excitation patterns cannot be used to study source mechanisms.

CONCLUSIONS

By applying the theoretical techniques developed in Chapter 2, synthetic seismograms of the split normal modes are calculated for the 1960 Chilean earthquake. These synthetics, for ${}_0S_2$ - ${}_0S_5$ and ${}_0T_3$ - ${}_0T_4$ are in agreement with the observed data. The splitting of ${}_0S_2$ and ${}_0S_3$ is confirmed, and the splitting of ${}_0S_4$ - ${}_0S_5$ and ${}_0T_3$ - ${}_0T_4$ is demonstrated for the first time. The agreement of the synthetics for the higher angular order modes is expected to improve when correct

eilipticity splitting parameters are used.

Different techniques for determining the Q of split modes are compared. It is shown that techniques which implicity treat the split mode data as the output from a single damped harmonic oscillator do not give meaningful Q estimates. Q can be estimated from either time or frequency domain techniques which explicitly include splitting effects. However, the amplitude and (especially) phase spectra are very unstable, in the presence of noise; changes in window, filter response, etc. can also substantially affect the spectrum. Because of the instability of frequency domain measurements, Q measurements from comparison of time domain synthetics to data seem much more stable and reliable.

By comparing the amplitude of ${}_0S_2$ for Chile to ${}_0S_4$ for Alaska, after normalizing each by the synthetic amplitude, the moment of the Chilean earthquake is estimated to be 2.4×10^{30} dyne cm. However, because of the wide scatter of the relative moments (shown in Figure 4.2) and the uncertainty in the source geometry and the precise nature of the precursor, this value should be considered as preliminary.

Time domain analysis of split normal modes is a powerful new tool for data analysis. Future applications of this technique will result in more accurate Q determinations and better knowledge of earthquake source mechanisms at very long periods.

REFERENCES

Agnew, D., J. Berger, R. Buland, W. Farrell and F. Gilbert (1976). International deployment of accelerometers: a network for very long period seismology, EOS, Trans. Am. Geophys. Un., 57, 180-188.

Anderson, D. L. and R. S. Hart (1977). The Q of the Earth, J. Geophys. Res., submitted.

Backus, G. and F. Gilbert (1961). The rotational splitting of the free oscillations of the Earth, Proc. Nat. Acad. Sci. U. S., 47, 362-

Beaumont, C. and J. Berger (1976). An analysis of tidal strain observations from the United States of America II. The inhomogeous tide, Bull. Seism. Soc. Am., 66, 1821-1846.

Benioff, H., F. Press and S. Smith (1961). Excitation of the free oscillations of the earth by earthquakes, J. Geophys. Res., 66, 605-619.

Blackman, R. B. and J. W. Tukey (1958). The Measurement of Power Spectra, Dover, New York.

Dahlen, F. A. (1968). The normal modes of a rotating, elliptical Earth, Geophys. J., 16, 329-367.

Fukao, Y. and K. Abe (1971). Multimode Love waves excited by shallow and deep earthquakes, Bull. Earthq. Res. Inst. Tokyo Univ., 49, 1-12.

Gilbert, F. and G. Backus (1965). The rotational splitting of the free oscillations of the Earth, 2, Rev. Geophys., 3, 1-9.

Geller, R. J. and S. Stein (1977). Source mechanism and attenuation studies using split normal modes, in preparation.

Kanamori, H. (1970). The Alaska earthquake of 1964: Radiation of long-period surface waves and source mechanism, J. Geophys. Res., 75, 5029-5040.

Kanamori, H., and D. L. Anderson (1975). Amplitude of the earth's free oscillations and long period characteristics of the earthquake source, J. Geophys. Res., 80, 1075-1078.

Kanamori, H. and J. J. Cipar (1974). Focal process of the great Chilean earthquake, May 22, 1960, Phys. Earth. Planet. Interiors, 9, 128-136.

Ness, N., J. Harrison and L. Slichter (1961). Observations of the free oscillations of the earth, J. Geophys. Res., 66, 621-629.

Pekeris, C. L., Z. Alterman, and H. Jarosch (1961). Rotational multiplets in the spectrum of the Earth, Phys. Rev., 122, 1692-1700.

Slichter, L. B. (1967). Spherical oscillations of the earth, Geophys. J., 14, 171-177.

Smith, S. W. (1961). An investigation of the earth's free oscillations, Ph. D. Thesis, California Institute of Technology, Pasadena, California.

Smith, S. W. (1966). Free oscillations excited by the Alaskan earthquakes, J. Geophys. Res., 71, 1183-1193.

Smith, S. W. (1972). The anelasticity of the mantle, Tectonophysics, 13, 601-622.

Woodhouse, J. H. (1976). On Rayleigh's principle, Geophys. J., 46, 11-22.